Technische Universität München
Lehrstuhl für Botanik

Role and regulation of the TRAPPII protein complex in protein sorting during cell division

Raksha Ravikumar

Vollständiger Abdruck der von der TUM School of Life Sciences der Technischen Universität München zur Erlangung einer

Doktorin der Naturwissenschaften

genehmigten Dissertation.

Vorsitzende: Prof. Dr. Caroline Gutjahr

Prüfer der Dissertation:
1. Prof. Dr. Farhah Assaad-Gerbert
2. Prof. Dr. Joop Vermeer
3. Prof. Dr. Brigitte Poppenberger-Sieberer

Die Dissertation wurde am 20.10.2021 bei der Technischen Universität München eingereicht und durch die TUM School of Life Sciences am 07.02.2022 angenommen

Abstract

The trans-Golgi-network (TGN) is the hub for the flow of information to and from various cellular compartments. Secretory, endocytic and vacuolar sorting pathways intersect at the TGN. Two proteins residing at the TGN: TRAPPII (Transport protein particle II) protein complex and ECHIDNA have both been reported to regulate key functions at the TGN involving protein sorting decisions. The TRAPPII complex is well characterized in yeast and metazoans as a tethering factor as well as a Rab GEF. ECHIDNA on the other hand, initially characterized in poplar plants, plays a role in cell elongation and secretion. However, it remains unclear whether these two players act in concert or in parallel to fulfill their functions. In the initial portion of the study, role and relationship between these two proteins were explored. Genetic and physical interactions between TRAPPII and ECHIDNA were assessed via a combination of double mutant, quantitative imaging and localization studies. Taken together, these findings imply that TRAPPII and ECHIDNA have overlapping basal or housekeeping TGN functions such as exocytosis and maintenance of TGN structure, but distinct specialized functions such as cell plate biogenesis during cytokinesis and cell elongation.

In the second section of this study, a subunit of the TRAPPII complex was characterized. AtTRS33 is a shared component of TRAPPII and TRAPPIII complexes in yeast and metazoans. Its homologue in yeast is necessary for TRAPPII complex assembly. Double mutant analysis of a double knockout mutant - *trs33-1club-2*, where *club-2* is the null allele of CLUB (TRAPPII-specific subunit), revealed a functional link between them. Furthermore, this study demonstrated the role of AtTRS33 in TRAPPII membrane association using localization analyses. Overall, the experiments attributed AtTRS33 as a part of the TRAPPII complex and its necessity for proper localization dynamics of the TRAPPII complex.

The third portion of the thesis attempted to determine whether the TRAPPII complex acts as Rab GEF in plants. The role of the TRAPPII complex as a guanine

nucleotide exchange factor (GEF) for Rab GTPases, is well studied in other eukaryotes. However, it is still unclear whether it retains its GEF activity in plants. A previous study hinted that it may perhaps be acting upstream of Rab-A GTPases in *Arabidopsis*. Using quantitative imaging and utilizing different mutant versions of Rab-A GTPases, I demonstrated the function of the TRAPPII complex as a putative Rab-A GEF.

In the fourth and final part of this thesis, post-translational regulatory mechanisms of the TRAPPII complex was elucidated. *in vitro* kinase assays coupled with mass spectrometry revealed that GSK3 kinases phosphorylate the AtTRS120 subunit of the TRAPPII complex on distinct amino acid positions. The phosphorylation status of AtTRS120 impacted its membrane and cytosolic associations. Taken together, the results indicate that the phosphorylation of AtTRS120 by GSK3 kinases is necessary for the regulation of its membrane dynamics in the cell. Lastly, my data confirmed a link between a membrane trafficking component and the environmental regulatory networks in plants.

The trans-Golgi-network (TGN) is the hub for the flow of information to and from various cellular compartments. This study determined whether two TGN resident proteins: TRAPPII protein complex and ECHIDNA act in concert or in parallel to fulfill their functions. Additionally, a subunit of the TRAPPII complex was characterized and a new role of the TRAPPII complex as a Rab GEF in plants was established. Finally, post-translational regulatory mechanisms of the TRAPPII complex were elucidated.

Zusammenfassung

Basierend auf verschiedenen cell biologieschen Fragestellungen, kann die vorliegende Arbeit in vier Abschnitte unterteilt werden. Im ersten Teil wurden die Rolle von zwei Proteinkomplexen, die sich im Trans-Golgi-Netzwerk (TGN) befinden und deren Beziehung zueinander untersucht. Das TGN ist ein wichtiger Knotenpunkt um den intrazellulären Informationsfluss von und zu verschiedenen zellulären Kompartimenten zu erhalten. Am TGN treffen mehrere Signalwege aufeinander, der sekretorische-, der endozytäre- und der vakuoläre Sortierweg. Bisher wurde von zwei, am TGN befindlichen Schlüsselproteinen berichtet, dem Transportproteinpartikel II-Proteinkomplex (TRAPPII)Transportproteinpartikel II-Proteinkomplex und ECHIDNA, dass diese wichtigen Funktionen bezüglich der Proteinsortierung im TGN regulieren. Der TRAPPII-Komplex ist ein Proteinkomplex mit mehreren Untereinheiten, der in Hefe und Metazoen sowohl als Tethering-Faktor als auch als Rab GEF gut charakterisiert ist. ECHIDNA hingegen ist an der Zellelongation und Sekretion beteiligt, jedoch ist unklar, ob diese beiden Akteure gemeinsam oder parallel agieren, um ihre Funktionen auszuführen. In dieser Arbeit wurden die genetischen und physikalischen Interaktionen zwischen TRAPPII und ECHIDNA durch eine Kombination aus Doppelmutation, quantitativer Bildgebenden Verfahren und Lokalisierungsanalysen untersucht. Die Ergebnisse der Studie legen nahe, dass TRAPPII und ECHIDNA überlappende basale oder haushaltende TGN-Funktionen wie Sekretion und Aufrechterhaltung der TGN-Struktur haben, aber unterschiedliche spezialisierte Funktionen wie Zellplatten-Biogenese und Zelldehnung.

Im zweiten Teil dieser Studie wurde eine Untereinheit des TRAPPII-Komplexes charakterisiert. Dabei konzentrierte ich mich auf AtTRS33, dass eine gemeinsame Komponente von TRAPPII und TRAPPIII in Hefe und Metazoen ist; sein Homolog ist in der TRAPPII-Komplex-Assemblierung in Hefe involviert. Eine Doppelmutantenanalyse der Null-Mutante *trs33-1* mit der Null-Mutante der TRAPPII-spezifischen Untereinheit *club-2* zeigte eine funktionelle Verbindung

untereinender. Zusätzlich zeigte die Studie die Notwendigkeit von AtTRS33 in der TRAPPII-Membranassoziation durch Lokalisationsanalysen. Insgesamt wiesen die Experimente nach, dass AtTRS33 als Teil des TRAPPII-Komplexes ist und seine Notwendigkeit für die richtige Lokalisationsdynamik des TRAPPII-Komplexes.

Der dritte Teil der Studie versuchte zu klären, ob der TRAPPII-Komplex als Rab GEF in Pflanzen fungiert. Die Rolle des TRAPPII-Komplexes als Rab GEF ist in anderen Eukaryoten gut untersucht. Es ist jedoch noch unklar, ob der TRAPPII-Komplex seine GEF-Aktivität in Pflanzen beibehalten hat. Mittels quantitativen Bildgebenden Verfahren, unter Verwendung verschiedener mutierter Versionen einer Rab-A GTPase, konnte ich die Funktion des TRAPPII als putatives Rab-A GEF nachweisen.

Im vierten und letzten Teil dieser Arbeit wurden die posttranslationalen Regulationsmechanismen des TRAPPII-Komplexes aufgeklärt. Mit Hilfe eines *in vitro* Kinase-Assays, gekoppelt mit Massenspektrometrie wurde gezeigt, dass GSK3-Kinasen die AtTRS120-Untereinheit des TRAPPII-Komplexes an spezifischen Aminosäurepositionen phosphorylieren. Der Phosphorylierungsstatus von AtTRS120 wirkte sich auf seine Membran- und zytosolischen Verbindungen aus. Zusammengenommen deuten die Ergebnisse darauf hin, dass die Phosphorylierung von AtTRS120 durch GSK3-Kinasen für die Regulierung seiner Membrandynamik in der Zelle notwendig ist. Schließlich bestätigten meine Daten eine Verbindung zwischen einer Komponente des Membranverkehrs und den Umweltregulationsnetzen in Pflanzen

Acknowledgement

First and foremost, I would like to extend my sincere gratitude to Prof. Dr. Farhah Assaad for giving me the opportunity to work in your lab. I am very grateful for your supervision, support, advice and also opportunities to visit various collaborators, to learn new techniques during my PhD. You have trained me to become a professional academic.

I would like to thank both the members of the panel Prof. Joop Vermeer and Prof. Brigitte Poppenberger for accepting to be a part of my thesis committee panel. I am grateful to Prof. Joop Vermeer for mentoring me and being supportive whenever I reached out to you.

I am thankful for all the help and assistance received in the lab from my colleagues and friends. It was a pleasure to work in the lab because of all of you. It was always nice to quickly catch-up during lunches, making my stressful work days a bit better. I also would like to thank everyone in the department of Botany, for being so friendly and kind. And would additionally like to acknowledge Beate Seeliger and Ulrike Schuberth for helping out with the administrative tasks since the beginning.

I am indebted to all the collaborators. Thank you, Prof. Dr. Ramon Angel Torres Ruiz, for your help and patience in teaching me embryo analyses and also helping out when problems arose at the Leica SP8 microscope. Thanks to Prof. Gerhardt Wanner and Dr. Eva Facher, at the Ludwig Maximilians Universität, for performing scanning electron microscopy on my samples. I enjoyed my time there always and the cherry on top was visiting the botanical gardens. I would like to thank Prof. Rishikesh Bhalerao and Dr. Delphine Gendre for being so friendly and kind during my visit in the cold Swedish winter. A special thanks to Dr. David Ehrhardt for teaching me spinning disk microscopy, it blew my mind. I am very appreciative for your encouragement and trust in letting me use the microscope as long as I wanted. I am grateful to Dr. Christina Ludwig and her lab for their help with proteomics data.

I would like to thank Deutsche Forschungsgemeinschaft for funding my PhD research.

I really appreciate the mentoring sessions with Doro and want to continue this tradition forever. A big thanks to all my friends who were empathetic, encouraging and caring; you are my family away from home.

Last but not the least, I would like to thank my people, the foundation that has sustained me and made me who I am today. Thank you Appa, Amma, Rakesh and my dear Vinay. You all are my towers of strength and for that, I am eternally grateful.

List of figures

List of tables

Abbreviations

°C	Degree Celsius
AGP	Arabinoglycans
APS	Ammonium persulfate
attB	Attachment site B
BIN2	Brassinosteroid insensitive 2
BSA	Bovine Serum Albumin
CAA	chloroacetamide
CLSM	Confocal laser scanning microscopy
Co-IP	Co-Immunoprecipitation
Col	Columbia ecotype
CPAM	Cell plate assembly matrix
DAPI	4',6-diamidino-2-phenylindole
DMSO	Dimethyl sulfoxide
DNA	deoxyribonucleic acid
DTT	dithiothreitol
ECH	ECHIDNA
EDTA	Ethylenediaminetetraacetic acid
ER	Endoplasmic reticulum
FA	formic acid
g	grams
GEF	Guanine nucleotide-exchange factor
GDP	Guanosine diphosphate
GFP	Green Fluorescent Protein
GSK3	Glycogen synthase kinase 3
GTP	Guanosine triphosphate
GST	Glutatione S-Transferase
IPTG	beta-D-1-thiogalactopyranoside
kb	Kilobase
kDa	Kilodalton
LB	Luria-bertani
LC-MS/MS	Liquid-Chromatography coupled with tandem mass spectrometry

M	Molar
MAP	Microtubule-associated protein
MES	2-morpholinoethansulfone acid
MTOC	Microtubule organizing center
ml	Milliliter
mM	Millimolar
MS	Murashige and Skoog
MTSB	Microtubules stabilizing buffer
nm	nanometer
OD	Optic density
PBS	Phosphate buffered saline
PCR	polymerase chain reaction
PPZ	propiconazole
PPB	Pre-prophase bands
Rab	Ras-related in brain
rcf	Relative Centrifugal Force
rpm	Revolutions per minute
SDS-PAGE	Sodium dodecyl sulfate Polyacrylamid gel electrophoresis
SEM	Scanning electron microscopy
SNARE	Soluble N-ethylmaleimide-sensitive factor
SOC	Super Optimal broth with Catabolite repression
TEMED	N,N,N,N'-tetramethylethylene diamine
TGN	Trans Golgi network
TRAPP	Transport protein particle
V	Voltage
WT	wild-type
Y2H	Yeast two-hybrid
µl	Microliter

Table of contents

1. Introduction

1.1 Membrane trafficking

Eukaryotic cells, unlike the prokaryotes, are compartmentalized. This means that every organelle is surrounded by a membrane and each organelle has a separate composition, chemical property and carries out specific functions. Communication or exchange of macromolecules between these compartments and the plasma membrane occurs through different mechanisms, membrane trafficking being one such process. Communication between organelles is essential, for example in transmitting cell cycle cues or in environmental responses. Membrane trafficking ensures that a correct complement of proteins and lipids are transported to the right cellular compartment.

The trafficking process from the donor to the target membranes or compartments can be split into five main steps. First, the cargo or the macromolecule to be transported is surrounded by specific coat proteins that recognize a cytosolic sorting signal (Aridor & Traub, 2002; Aridor, Weissman, Bannykh, Nuoffer, & Balch, 1998; Barlowe, 2003). The total set of coat proteins, cargo and other regulatory elements are referred to as a vesicle. After the vesicle is formed, it is then mechanically 'pinched off' by deforming the donor membrane to enable vesicle budding. In the next step, the vesicles are actively transported to their destination to reach the target membrane with the help of microtubules. Upon reaching their destination, even though the vesicle does not directly interact, it forms an initial connection with the membrane. The first indirect contact of the vesicle with its target membrane is called as tethering and this comprises the third step of trafficking. This step brings donor vesicles and the target membrane in close proximity (300 –2000 Å). Two classes of proteins confer specificity to the tethering step: Rabs, which are regulatory GTPases and tethering factors. The next step is docking where the cargo/ macromolecule comes into contact with the target membrane. The final step is fusion with the target membrane. After vesicle fusion, the cargo often undergoes further processing by either getting refolded, post-translationally modified or glycosylated.

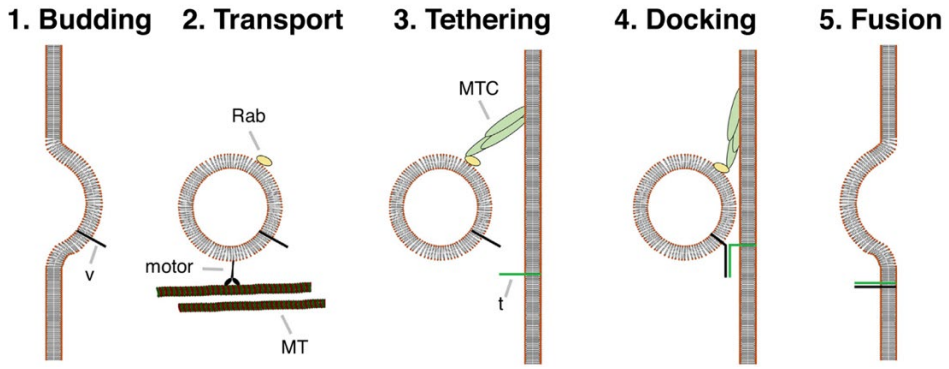

Figure 1: Five major steps in membrane traffic.

Budding: a vesicle buds off a donor membrane. Transport: the vesicle, depicted as moving along microtubules (MT) with the help of a motor protein (motor), is delivered to the target membrane. Tethering: the vesicle is tethered to the target membrane by virtue of an interaction between a Rab GTPase (Rab) on the vesicle and a tethering molecule or complex (MTC) on the acceptor membrane. Docking: the tethered vesicle becomes tightly docked when the v- (v) and t (t) - SNAREs form a SNARE pin, or a trans-SNARE complex. Fusion: The vesicle and target membranes fuse as a cis-SNARE complex zippers and pulls them together, thereby delivering vesicle cargo to the target compartment. Illustration and caption by Alexander Steiner (Ravikumar et al. 2017).

Proteins, which are synthesized at the endoplasmic reticulum (ER) are transported via secretory trafficking to their target destination. The newly synthesized proteins are added to vesicles as cargo and are transported via anterograde trafficking from the ER to the Golgi. They can also be transported further to the trans-Golgi network (TGN). From there, proteins are sorted to the plasma membrane (exocytosis), lysosomes, vacuoles, the extracellular space (Griffiths & Simons, 1986), the cell plate (Ravikumar et al., 2018, 2017) and even to the edges of the cells during interphase (Kirchhelle et al., 2016). Via retrograde trafficking, proteins can be sent back to the ER (Hua & Graham, 2003). Additionally, membrane trafficking can be divided into biosynthetic and degradative pathways. In the former, vesicles are transported to the target membrane to carry out their functions. On the contrary, in degradative pathways, macromolecules and often even organelles are destroyed. Autophagy is a very good example of a degradative pathway where the molecules are broken down and recycled. The ability of the TGN to regulate transfer of proper cargo to the

right complement clearly indicates that the TGN acts as a hub in the flow of information to and from the different locations in the cell.

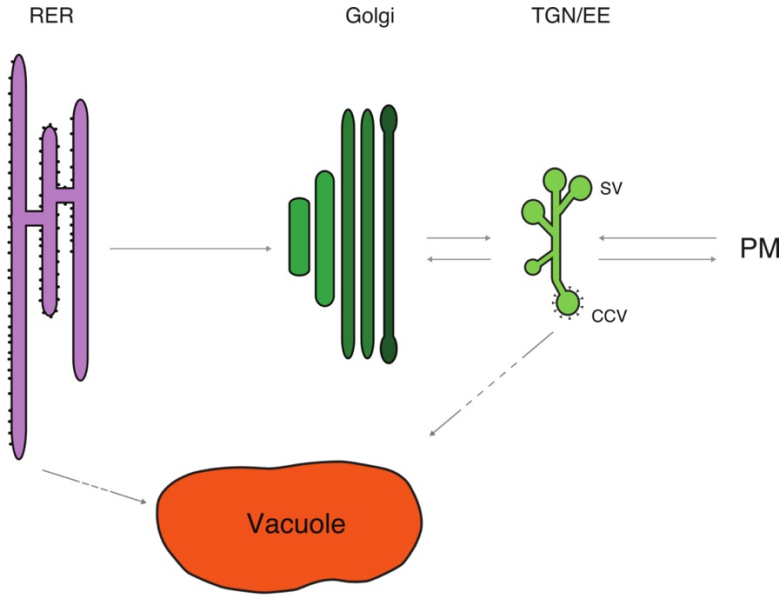

Figure 2: Trafficking routes in the cell.
Based on the direction of vesicle movement in the cell, membrane trafficking can be categorized as endocytosis or exocytosis. Additionally, membrane trafficking is also classified into biosynthetic and degradative pathway. In the biosynthetic pathway, trafficking occurs at the target membrane where the cargo is utilized to carry out the necessary cellular functions. In degradative pathways, the vesicles are transported to be dispersed away. Autophagy, where the transported molecules are degraded is one such example of a degradative pathway. Illustration by Miriam Abele (Kalde et al., 2019).

1.2 Membrane tethering

Tethering of vesicles is a highly specific stage of the membrane trafficking pathway. Only the right vesicle at the proper destination is able to tether to the membrane. Coat proteins, Rab-GTPases (Rabs), tethering factors and SNAREs confer specificity to this process.

Rabs only function in their active GTP-bound form and cycle between active (GTP-bound) to inactive form (GDP-bound) by interacting with including guanine nucleotide exchange factors (GEFs) and GTPase-activating proteins (GAPs). There are 57 Rab GTPases encoded by the *Arabidopsis thaliana* genome, categorized into eight clades (Rutherford & Moore, 2002), with some of the clades

significantly larger than the Rab subclasses in other systems. The Rabs act upstream of tethers, where they engage various tethering factors and SNAREs to their associated membranes (Novick et al., 2006; Siniossoglou & Pelham, 2001) and therefore are important for endomembrane compartment identity and also for pathway specificity (Elliott, Moore, & Kirchhelle, 2020).

Tethering factors are categorized into two groups based on their quaternary protein structure: multisubunit tethering complexes (MTCs) that consist of multiple subunits, and coiled-coil proteins, mostly consisting of homodimers. Tethering factors function primarily as bridges for membranes, but they are also responsible for the SNARE complex assembly, cargo selection, coating events and signaling (Sztul & Lupashin, 2006). They bring donor and acceptor membranes into a proximity of ~ 300–2000 Å. Ten diverse MTCs are known in eukaryotes, where they partake in biosynthetic as well as degradative pathways. Each tethering complex resides on specific cellular compartments. All known eukaryotic MTCs are also encoded by plant genomes but not all of them have been characterized. Information of a few of the MTCs show that they function similar to those in yeast (Ravikumar et al., 2018).

After the tethering factors initiate contact with the vesicles, SNAREs take over and are involved in the docking and fusion of the vesicles (Söllner, Bennett, Whiteheart, Scheller, & Rothman, 1993). SNAREs bring the membranes to ~140 Å proximity. There are three types of SNAREs: vesicle (v-) SNAREs, target (t-SNAREs) and syntaxins, all helical in structure. They interact with each other forming a quaternary protein complex called as a trans-SNARE complex or SNAREpin. Every vesicle and target membrane has a characteristic v- and t-SNARE respectively, therefore SNAREs along with tethering factors play an important role in bestowing specificity to the vesicle docking and fusion stage (Söllner et al., 1993).

1.3 Rab GTPases

Rab GTPases belong to the Ras superfamily of regulatory GTPases and are one of the main regulators involved in targeting specificity in membrane trafficking.

They are present in all eukaryotes, and interestingly, Rab-like proteins are also suggested to be present in some prokaryotes (Elliott et al., 2020; Surkont & Pereira-Leal, 2016). They are known to regulate the activity of tethering factors as wells as SNARE complexes in yeast and metazoans. Additionally, interactions between vesicles and the cytoskeleton during vesicle transportation step is also mediated by some Rabs (Lazar, Götte, & Gallwitz, 1997; Segev, 2001; Zerial & McBride, 2001).

Rab GTPases cycle between an active state (GTP-bound membrane-associated) and an inactive state (GDP-bound cytosolic), mediated by several regulatory factors, such as guanine nucleotide exchange factors (GEFs), GTPase-activating proteins (GAPs), Rab GDP dissociation inhibitor (GDI) etc. Every Rab GTPase family member is recruited from the cytosol onto their assigned membrane domain where they are firstly, activated by specific GEFs. GEFs catalyze in the removal of GDP from the GTPases, which then allows for the subsequent binding of GTP. This GTP bound and activated Rab GTPase is then able to employ particular downstream Rab effectors to the membrane. Rab effector proteins bind only to the GTP-bound state and so are recruited to only those membranes, on which the Rab is active. Membrane-associated Rab GTPases can recruit a myriad of effectors involved in compartment: motility (motor proteins), docking (tethering factors), fusion (SNAREs) as well as the upstream GEF for the next Rab GTPase in the pathway. ‘Rab cascades’, in which one Rab GTPase recruits the GEF for the subsequent Rab GTPase, are essential for the spatiotemporal self-organization of membrane identity and pathway specificity (Grosshans, Ortiz, & Novick, 2006; Markgraf, Peplowska, & Ungermann, 2007). One of the best examples to illustrate this is the conversion of Rab-5-positive early endosomes (or TGN) to Rab-7-positive late endosomes and lysosomes. Rab-5, which is present at the early endosomes, accumulates at the said location until a definite threshold, after which is rapidly substituted by Rab-7 causing a transfer of the cargo to the late endocytic pathway (Barr, 2013; Del Conte-Zerial et al., 2008).

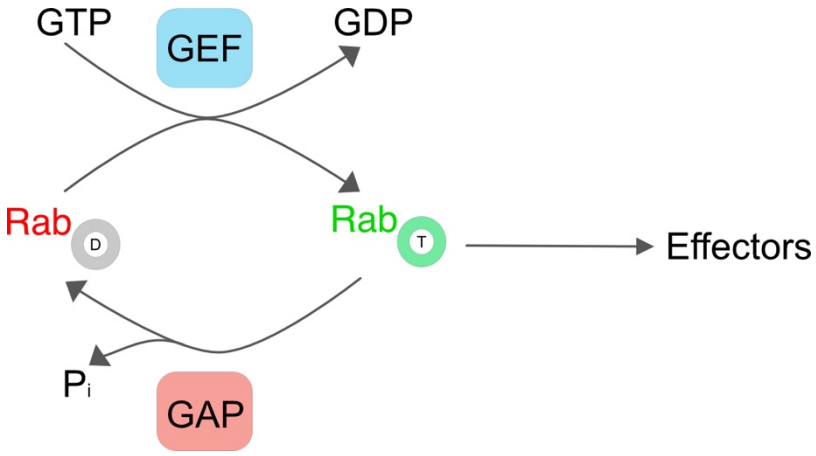

Figure 3: Overview of the Rab GTPase activation.

Rab GEFs are involved in the activation of the Rab GTPases by exchanging a GDP with a GTP. The GTPases are converted from its inactive state (GDP, grey box with D) to an active state (GTP, green box with T) to carry out their functions in vesicle trafficking.

Saccharomyces cerevisiae encodes 11 Rab GTPases, which are divided into eight functionally distinct subclasses. Interestingly, humans have at least 60 different Rab proteins that are assigned to about 40 different functional subclasses. In *Arabidopsis*, 57 Rab GTPases are currently classified into eight different groups (Table 1; Rab A to Rab H). The Rab A branch constitutes the biggest group, with 26 different Rab-A GTPases and six subclasses (Table 1; Rab A1 to Rab A6). In yeast, this class encompasses two members, referred to as Ypt31/32; while the human genome codes for three members, named as Rab11 (Elliott et al., 2020; Rutherford & Moore, 2002). This shows a dramatic, lineage-specific diversification of the Rab-A family in plants, indicating that there might be plant-specific functions involved. Different classes and subclasses of the Rab GTPases are associated with different membrane compartments, contributing to discrete membrane identity, which in turn controls the specificity and directionality of membrane trafficking pathways (Table 1; Zhen and Stenmark, 2015).

Since Rab-GTPases along with the TRAPPII tethering complex, are two of the major players impacting spatial and temporal specificity during membrane trafficking, one of the objectives of this thesis is to understand how they work together to achieve this function. Previous works have demonstrated a link between the Rab-A class of Rab-GTPases and the TRAPPII complex (Qi, Kaneda,

Chen, Geitmann, & Zheng, 2011; Qi & Zheng, 2011); however, the dynamics of this linkage is still unclear. Additionally, it would be interesting to evaluate if other members of the Rab-A subclade are also working in concert with the TRAPPII complex to mediate the trafficking processes in the cell.

Table 1: Overview of the Rab GTPase family in *Arabidopsis*.

The 57 Rab GTPases of *Arabidopsis thaliana* fall into eight clades named Rab-A to Rab-H.

Rab GTPase clade	Subclade	Localization	Suggested trafficking function
Rab-A (related to Rab11)	Rab-A1 (9 members)	TGN/EE and PM	De novo secretion from TGN/EE to PM? Recycling from TGN/EE to PM (non-basal and basal?) Cell plate biogenesis
	Rab-A2 (4 members)	TGN/EE and PM	De novo secretion fromTGN/EE to PM? Non-basal recycling fromTGN/EE to PM Cell plate biogenesis
	Rab-A3	TGN/EE	
	Rab-A4 (5 members)	TGN/EE	De novo secretion fromTGN/EE to PM FLS2 endocytosis from the PM
	Rab-A5 (5 members)	Cell edge compartments (and TGN/EE)	De novo secretion fromTGN/EE to PM? Cell plate biogenesis
	Rab-A6 (2 members)	TGN/EE?	FLS2 endocytosis from the PM
Rab-B (related to Rab2)	Rab-B1 (3 members)	Golgi?	ER-to-Golgi trafficking
Rab-C (related to Rab18)	Rab-C1 Rab-C2 (2 members)	Uncertain - Golgi/post-Golgi compartments?	Unknown
Rab-D (related to Rab1)	Rab-D1 Rab-D2 (3 members)	Golgi and TGN/EE	ER-to-Golgi trafficking
Rab-E (related to Rab8)	Rab-E1 (5 members)	Golgi, TGN/EE and PM	Golgi-to-PM trafficking
Rab-F (related to Rab5)	Rab-F1 Rab-F2 (2 members)	TGN/EE subdomain and LEs	TGN/EE-to-LE trafficking LE-to-PM trafficking
Rab-G (related to Rab7)	Rab-G1 Rab-G2 Rab-G3 (6 members)	LEs and Tonoplast	LE-to-vacuole trafficking and possibly autophagous trafficking
Rab-H (related to Rab6)	Rab-H1 (5 members)	Golgi (and TGN/EE)	Golgi-to-PM? Required for properexocytosis of CSCs

Table is adapted from Elliott, Moore and Kirchhelle, 2020.

In my study, I have utilized the Rab-A2a GTPases of the Rab-A clade to assess if the TRAPPII complex behaves as a RAB GEF for the Rab GTPases and/or as a downstream tethering factor in membrane trafficking. Members of the Rab-A clade primarily localize to the TGN (Table 1; which also functions as an early endosome). They are recruited to the cell plate during cytokinesis, which is a TGN derived compartment (Chow et al. 2008). They are present at the center of the cell plate during cell plate biogenesis and later re-organize to the leading edge of the cell plate during cell plate expansion and maturation.

In order to investigate whether the TRAPPII complex acts as tether and/or as a GEF, I utilized the GDP- and GTP- locked versions of Rab-A GTPase constructs (previously described by Chow et al. 2008) in the TRAPPII complex-specific mutant: *trs33-1*. The experiments make use of a GDP-locked version S26N Rab-A GTPase variant, which stabilizes the inactive state or GTPase-deficient and GTP-locked version Q71L Rab-A GTPase variant, which stabilizes the GTP-bound active state (Kotzer et al., 2004; Olkkonen & Stenmark, 1997; Ueda et al. 2001; Zheng et al., 2005). For the sake of convenience, they are termed as YFP:A2a-DN (GDP-bound S26N Rab GTPase) and YFP:A2a-CA (GTP-bound Q71L Rab GTPase) in the current study. In my image analysis, YFP:A2a-DN was recruited to the cell plate and at least partially relocalized to its leading edges at the end of cytokinesis. However, YFP:A2a-CA labelled wild-type cell plates in a more uniform manner than YFP:RAB-A2a showing no relocalization to the leading edges. The results from my experiment shed light on the possible function of the TRAPPII complex as an upstream GEF for the Rab-A GTPases in plants.

1.4 The TRAPP complexes

The TRAPP complexes are major regulators of the membrane trafficking process. The TRAPP complex was originally identified in yeast as a tethering factor acting in endoplasmic reticulum (ER) to Golgi trafficking. Protein purification at the lowest salt concentration allowing for the release of TRAPP subunits from membranes uncovered two TRAPP complexes: TRAPPII and TRAPPIII (Thomas, Joiner, & Fromme, 2018). The TRAPPII subunit AtTRS120 was found to act as a putative tether for COPI vesicles during the transport from early endosomes to the

late Golgi (H. Cai, Zhang, Pypaert, Walker, & Ferro-Novick, 2005). TRAPPII complex mediates intra-Golgi traffic as well as post-Golgi trafficking (Thomas et al., 2018; Zou et al., 2013). ER to Golgi, medial/late Golgi, endosomes as well as autophagy or vacuolar trafficking is mediated by the TRAPPIII complex (Thomas et al., 2018). Trafficking from the trans-Golgi to the plasma membrane is mediated by the TRAPPII and the EXOCYST complexes.

The two complexes share six common or shared subunits, which are then combined in a modular fashion along with complex-specific subunits to form the different complexes (Table 2; Sacher et al., 2019). The TRAPPII complex was proposed to exist as a dimer with the TRAPPII-specific subunits sandwiched between two anti-parallel shared subunits (J. J. Kim, Lipatova, Majumdar, & Segev, 2016; Yip, Berscheminski, & Walz, 2010). Metazoan TRAPP complexes contain homologs of both yeast TRAPP complexes but have also evolved additional subunits and rearrangements in complex composition (Table 2,Bassik et al., 2013). The compositions of the metazoan TRAPP complexes were also identified using Tandem Affinity Purification with two-step purifications allowing for stable binding partners (Riedel, Galindo, Muschalik, & Munro, 2018). Just like in yeast cells, TRAPPII and TRAPPIII complexes share a common heptameric core and additional complex-specific subunits, which are specific for TRAPPII or for TRAPPIII (Bassik et al., 2013; Riedel et al., 2018). Previous studies in metazoans and in yeast also postulate the structures for TRAPPII and TRAPPIII complexes, including a crystal structure for a core-TRAPP subcomplex (J. J. Kim, Lipatova, & Segev, 2016; Tan et al., 2013; Yip et al., 2010).

Table 2: TRAPP complex organization in yeast and metazoans.

Yeast TRAPP	Metazoan TRAPP	
Subunit	Complex	Subunit
Bet5	Shared	TRAPPC1
Trs20	Shared	TRAPPC2
Bet3$^{(2x)}$	Shared	TRAPPC3
Trs23	Shared	TRAPPC4

Trs31	Shared	TRAPPC5
Trs33#	Shared	TRAPPC6 (A, B)
Tca17	Shared	TRAPPC2L
Trs120	II	TRAPPC9
Trs130	II	TRAPPC10
-	-	-
Trs65#	III	TRAPPC13
Trs85	III	TRAPPC8
-	III	TRAPPC11
-	III	TRAPPC12

Shared subunits are colored in blue, TRAPPII-specific subunits in green and TRAPPIII-specific in orange. 2x = 2 copies of Bet3 (Thomas et al. 2019). # = necessary subunits for assembly of TRAPPII-specific subcomplex onto core TRAPP to generate TRAPPII. (A, B) two homologues of TRAPPC6 is present in the humans (Borner et al., 2014).

Most tethering proteins act downstream of Rab GTPases as Rab effectors. However, in yeast and metazoans, it has been established that in addition to the role of tethering, the TRAPP complex also acts as an upstream Rab GEF. In yeast, TRAPPII acts as a GEF for Ypt31/32 (Rab-11 in metazoans, Rab-A in *Arabidopsis*) and TRAPPIII has Rab GEF activity for the Ypt1 Rab GTPase (Rab-1, Rab-D) (Lynch-Day et al., 2010; Morozova et al., 2006; Tan et al., 2013; Thomas et al., 2018, 2019). In metazoans, TRAPPII acts as a GEF for both Rab-1 (Rab-D) and Rab-11 (Rab-A) while TRAPPIII only having activity on Rab-11 (Rab-D) (Jenkins et al., 2020; Riedel et al., 2018).

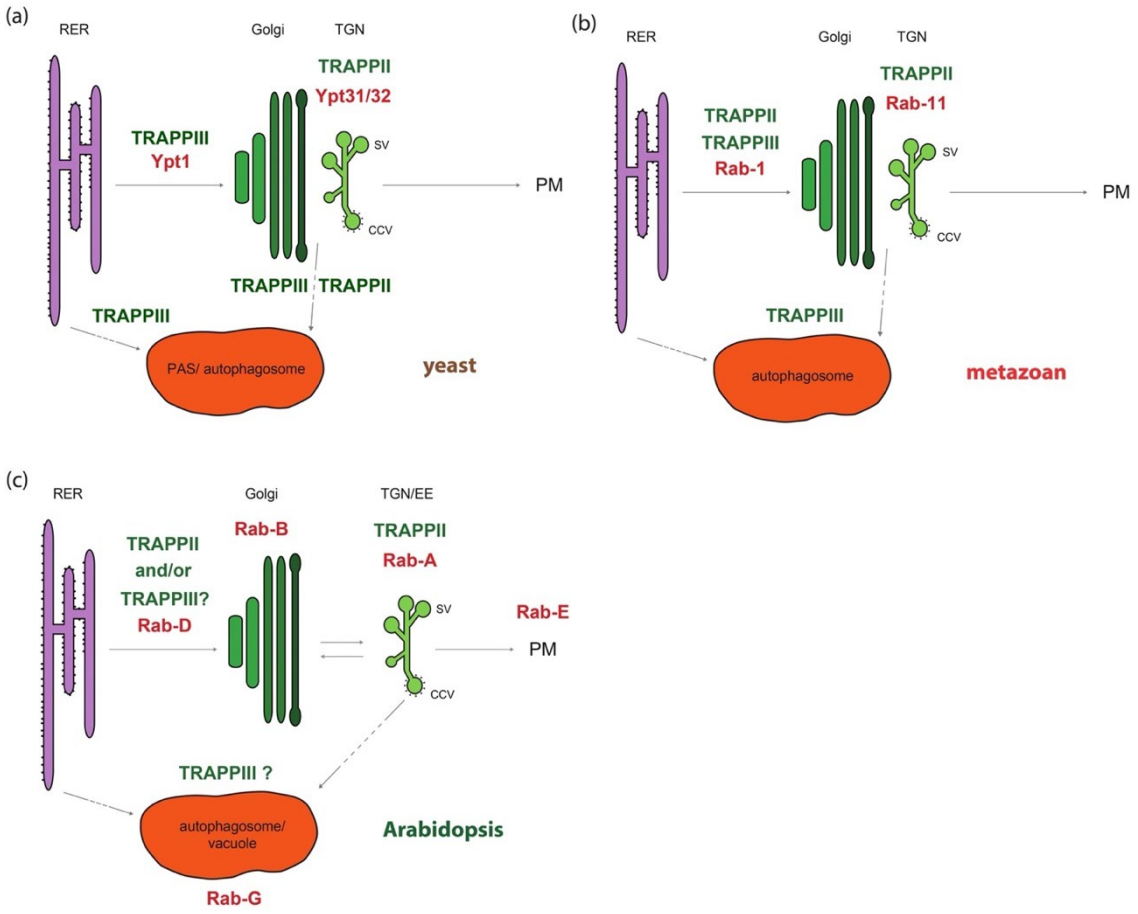

Figure 4: TRAPP complexes and Rab GTPases in membrane trafficking.

(a). Two TRAPP complexes are found in yeast: TRAPPIII acts as a GEF for Ypt1 and TRAPPII as a GEF for Ypt31/32 (Morozova et al., 2006; Thomas et al., 2018). TRAPPII acts at the TGN to mediate secretion and has also been implicated in autophagy (Thomas et al., 2018; Zou et al., 2013). TRAPPIII is involved in ER-Golgi traffic, in autophagy, and in trafficking between the medial/late Golgi and endosomes (Morozova et al., 2006; Thomas et al., 2018). PAS: phagophore assembly site or pre-autophagosomal structure. The dashed arrow does not distinguish between medial/trans Golgi and the TGN and does not depict endosomes along post-Golgi trafficking routes.

(b). Two TRAPP complexes are known in metazoans. TRAPPII possesses GEF activity for both Rab-1 and Rab-11 (Riedel et al., 2018). The TRAPPIII possesses GEF activity for Rab-1 and is thought to play a role in ER-Golgi traffic, COPII recruitment to ER and autophagy (Bassik et al., 2013; Lamb et al., 2016; Scrivens et al., 2011; C. Zhang et al., 2002; Zhao et al., 2017). The dashed arrow does not distinguish between medial/trans Golgi and the TGN and does not depict endosomes along post-Golgi trafficking routes.

(c). In plants, TRAPPII resides at the TGN/EE and is a putative GEF for the Rab-A clade of Ypt31/Rab-11 orthologues. Clades: Rab D, B, A and E were identified in the TRAPPII IP-MS (Assaad lab), these are on a biosynthetic trafficking route. Rab-F or Rab-G clades were not robustly identified in the CLUB/AtTRS130 interactome. Kalde et al., 2019 postulated the existence

of a plant TRAPPIII complex that resembles metazoan TRAPPIII. Based on preferrential binding to the vacuolar Rab-G, which is required for autophagy (Kwon, Cho, Kim, & Park, 2013), and on orthology TRAPPIII was tentatively placed on an autophagy and/or vacuolar trafficking route. Whether *Arabidopsis* TRAPPII or III play a role in ER-Golgi traffic remains to be determined. The dashed arrow does not does not depict late endosomes/multivesicular bodies along post-Golgi trafficking routes.
RER: rough endoplasmic reticulum; TGN: trans-Golgi network; SV: secretory vesicles; CCV: clathrin coated vesicles. Image panel and captions by Miriam Abele (Kalde et al., 2019).

In *Arabidopsis*, the TRAPPII complex is present at the TGN. Its subunits – CLUB and AtTRS120, which were identified in forward and reverse genetic screens for cytokinesis-defective mutants, have both been indicated to play a role in cell plate biogenesis during cytokinesis. Null mutants of the subunits showed severe defects in cytokinesis; this phenotype is manifested by cell wall stubs, 'floating walls' and bloated cells (Jaber et al., 2010; Qi & Zheng, 2011; Ravikumar et al., 2018, 2017; Rybak et al., 2014; Thellmann, Rybak, Thiele, Wanner, & Assaad, 2010). Both AtTRS120 and CLUB localize to the cytosol and TGN endomembrane compartments in interphase cells; in cytokinetic cells they localize to the cell plate and later re-organize to the cell plate edges (Ravikumar et al., 2018; Rybak et al., 2014). TRAPPII complex also plays a role in the housekeeping functions of the TGN such as exocytosis, endocytosis and protein sorting (Luo et al., 2015; Ravikumar et al., 2018; Rosquete, Davis, & Drakakaki, 2018). Due to the presence of untethered vesicles in the cells of the *trappii* mutants, it is postulated that TRAPPII might act as a tethering factor in plants (Jaber et al., 2010; Ravikumar et al., 2018, 2017).

One of the primary objectives of my thesis was to determine the role of the TRAPPII tethering complex during protein sorting. I carried out extensive live-cell imaging with different membrane marker to elucidate the function of the TRAPPII complex in sorting these markers during cytokinesis.

We know that the TRAPP complexes are well conserved across kingdoms and homologs of all the TRAPP complex subunits are present in *Arabidopsis* (Koumandou, Dacks, Coulson, & Field, 2007). Previous work from the Assaad

group has already identified six of the thirteen potential *Arabidopsis* TRAPP subunits through IP-MS that had co-purified with CLUB and AtTRS120 (Rybak et al., 2014; Steiner, Rybak, et al., 2016). Recently, along with a collaborator's lab, the Assaad lab could identify all of the thirteen subunits in an IP-MS with CLUB:GFP as well as Rab A2a GTPase as baits. Also, the subunit composition and topology of the TRAPP complexes were elucidated (Figure 5; Kalde et al., 2019). I aimed to identify the function of the various TRAPPII-specific subunits. To address this goal, I set out to characterize a subunit of the TRAPP complex: AtTRS33, demonstrated to be necessary for the TRAPPII complex assembly in yeast (Tokarev et al., 2009) and *Aspergillus* (Pinar, Arias-Palomo, de los Ríos, Arst, & Peñalva, 2019). I wanted to verify if this is conserved in *Arabidopsis*. I determined the localization dynamics of AtTRS120 in the absence of AtTRS33 and also carried out double mutant analysis with AtTRS33 and another TRAPPII-specific subunit: CLUB to test if they could interact. All of these results provided new insights about the organization and function of the TRAPPII complex in *Arabidopsis*.

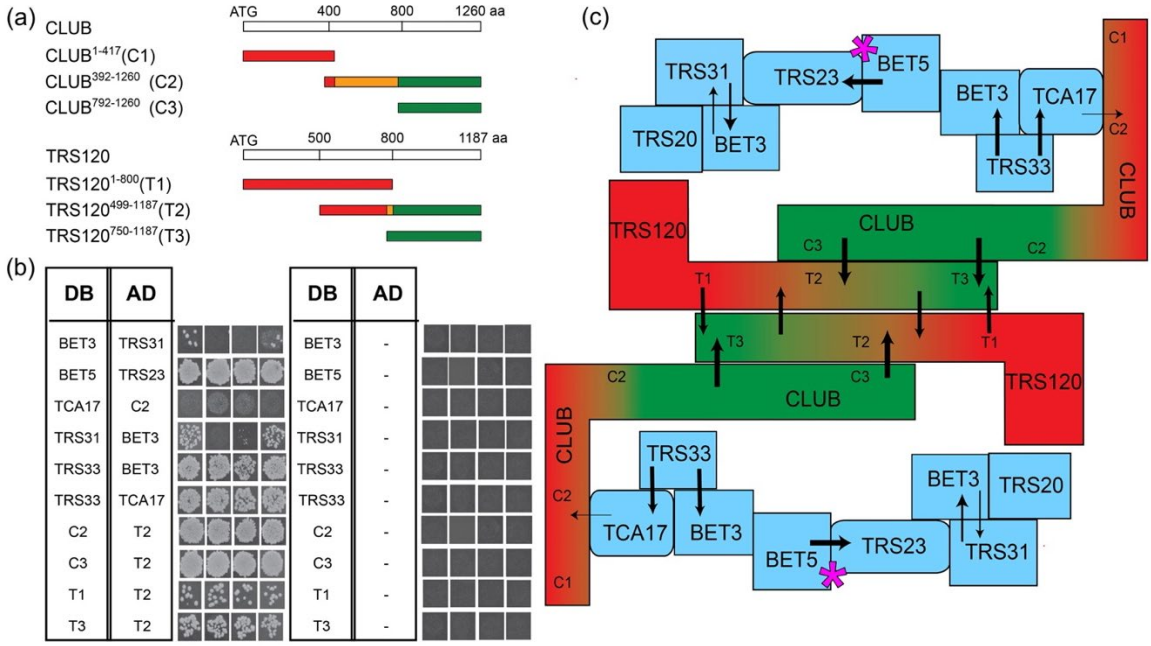

Figure 5: Binary interactions between TRAPP subunits

(a). TRAPPII truncations used for binary interaction assays. Segments colored in red are conserved across kingdoms, while ones in green are plant-specific. The orange moiety of the C2 segment is poorly conserved across kingdoms. The T2 middle segment corresponds to sequences found to interact with the exocyst in a yeast two-hybrid screen (Rybak et al., 2014).

(b). Yeast two-hybrid experiments; the panels are spliced together from different plates. Four independent replicate experiments are shown. Note positive interactions between the plant-specific C3_DB CLUB/AtTRS130 truncation and AtTRS120 T2_AD, and between CLUB C2_DB and T2_AD. A weak interaction was observed between TCA17_DB and C2_AD. T2_DB is an auto activator, as evidenced by colony growth with the empty AD vector, and this precludes our ability to determine whether AtTRS120_T2 interacts with any TRAPP subunit.
(c). A dimerization model best explains all the binary interactions reported by Kalde et al., 2019. This is based on the crystal structure of a core sub-complex (Kim et al., 2006) and on the TEM micrographs of the TRAPPII complex (Taussig, Lipatova, & Segev, 2014; Yip et al., 2010). Arrows represent the binary interactions in the DB to AD orientation and the thickness of the arrow depicts the strength of the interaction. Note that the TRS120-T3 truncation is included in TRS120-T2. TRAPPII-specific subunit segments colored in red are conserved across kingdoms, while ones in green are plant-specific (see a.). Subunits common to TRAPPII and TRAPPIII are in blue. The pink asterisk depicts the approximate location of the putative GEF catalytic site, based on yeast models (Cai et al., 2008; Thomas et al., 2019). Image panel and captions by Miriam abele (Kalde et al., 2019).

It is still ambiguous whether the TRAPP complex has GEF activity. But previous studies have shown that the TRAPPII complex colocalizes and is also functionally linked to Rab-A GTPases. One study demonstrated that expression of a constitutively active Rab-A1 but not a Rab-D2 subclade, partially rescues the phenotype of a *trs130* null allele (Qi et al. 2011; Qi & Zheng, 2011). In our recent study, differential IP-MS with Rab-A2a GTPases demonstrated that TRAPPII is a putative Rab-A GEF (Kalde et al., 2019). With the help of live-cell imaging and further quantitative analyses, I was able to verify the differential IP-MS results and could provide another line of evidence for the putative function of the TRAPPII complex as a RAB-A GEF in *Arabidopsis*.

1.5 Two master regulators at the TGN: ECH and TRAPPII complex

ECHIDNA (ECH) was initially identified as an evolutionary conserved protein within *A. thaliana*, hybrid aspen and budding yeast. It is also a TGN localized protein crucial for TGN function similar to the TRAPPII complex. *ech* mutants have been shown to have a dwarf phenotype with severely reduced stature and bushy appearance, implying that it plays a role during cell elongation. Although *ech* mutants are viable and fertile, male fertility was considerably reduced in the

mutants due to decreased anther size, pollen viability, reduced amounts of pollen and impaired pollen tube growth, as well as anther opening (Fan et al., 2014).

Even though, both ECH and TRAPPII tethering complex are involved in exocytosis, they seem to mediate overlapping yet different pathways. From previous works, it has been shown that ECH is needed for the proper secretion of cell wall polysaccharides, which form a major part of the mucilage secretory cells of the *A. thaliana* seed coat epidermis (Gendre et al., 2013; McFarlane et al., 2013) but mucilage secretory defects have not been observed in *trs120-4* and *club-2* seeds (Assaad, unpublished). Secreted green fluorescent protein (secGFP) is a secretory variant of GFP, which is synthesized in the ER and transported via the Golgi to the cell wall. Surprisingly, secretion of secGFP, unlike the cell wall polysaccharides, is impaired in both *ech* and *trappii* mutants (Gendre et al., 2011; Qi et al., 2011).

Protein sorting to the proper destination is very important post-Golgi and TGN function. Interestingly, in *ech* and *trappii* mutants mislocalization of proteins that are normally present at the TGN, plasma membrane, vacuole, cell plate could be observed. ECH has been shown to be required for proper localization of TGN proteins and *ech* mutants exhibited mislocalization of TGN proteins to vacuolar and cell plate compartments (Gendre et al., 2013, 2011). ECH has also been shown to be necessary for the proper sorting of the auxin influx carrier AUX1 but not for the auxin efflux carrier PIN2, PIN3 and BRI1 (Boutté et al., 2013; Gendre et al., 2011). Similarly, both AtTRS120 and CLUB are required for polar localization of PIN2 but not PIN1 and AtTRS120 is needed for correct AUX1 localization (Qi et al., 2011; Qi & Zheng, 2011). In *ech* mutants, the vacuolar marker γ-TIP-GFP was localized to unique multilamellar structures in addition to the localization at the tonoplast (McFarlane et al., 2013). However, in the *club-2* mutants, an artificial vacuolar marker SecN-Rm-2A was correctly sorted (Qi et al., 2011). These observations highlight the sophistication of the plant endomembrane trafficking network. Diverse cargoes that are destined to the same target destination are transported by different pathways, using different sets of vesicular trafficking machinery and/or targeting motifs. The current study therefore unravels

how these three major players – ECH, CLUB and AtTRS120 might be regulating and coordinating the diverse functions of the plant TGN.

1.6 GSK3 kinases

The glycogen synthase kinase 3 (GSK3) or *Arabidopsis thaliana* Shaggy-like kinase (AtSK) family consists of ten isoforms that are further divided into four clades. They are important integrators of versatile signaling pathways. Even though the name suggests that it is a kinase regulating metabolism in eukaryotes, it is also involved in a wide array of cellular events. For example, evidence shows that plant GSK3s are involved in a variety of processes, such as flower development, brassinosteroid signaling, salt stress and wound responses (Jonak & Hirt, 2002). Interestingly, the substrates phosphorylated by GSK3s have a common motif: Ser/Thr-X-X-X-Ser/Thr. Additionally, many of the substrates that are phosphorylated by GSK3s must first be primed, i.e., phosphorylated by another protein kinase, at a priming phosphorylation site that is four amino acids C-terminal to the site of GSK-3 phosphorylation (Dajani et al., 2001; Frame, Cohen, & Biondi, 2001; Ter Haar et al., 2001) .

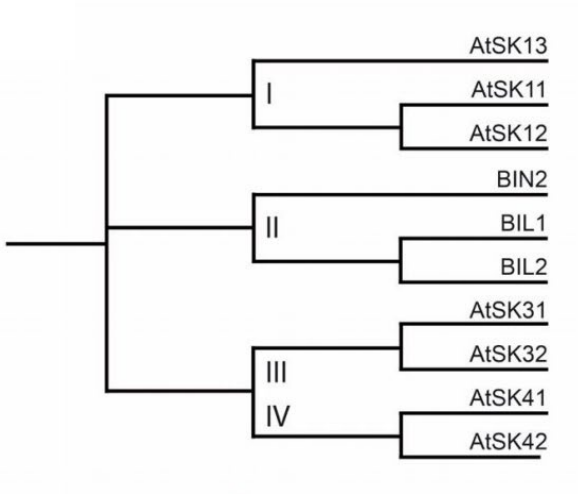

Figure 6: The GSK3 kinase family in plants.
The family is divided further into four subclades. Illustration by Miriam Abele.

One of the most characterized proteins of the GSK3 kinases is the BRASSINOSTEROID INSENSITIVE 2 (BIN2) kinase. BIN2 is a serine/threonine protein kinase and is a negative regulator of the brassinosteroid signaling

pathway, and plays a key role in phytohormone signaling pathways. Brassinosteroids (BR) are a class of steroid hormones that are important regulators and antagonist of light signaling. They suppress light-induced genes and promote skotomorphogenesis in the dark. Additionally, they are also known to play a role in cell elongation, cell division and differentiation, in abiotic and biotic stress responses, and also in plant reproductive development (Clouse, 2011; Wang, Zhu, & Sae-Seaw, 2013).

BR response pathway is an intricate pathway with dynamic phosphorylation and dephosphorylation events of key players in response to the various environmental signals. Phosphorylation of BIN2 seems to prevent the BZR1 and BRI-EMSSUPPRESSOR 1 (BES1 / BZR2) transcription factors from binding to DNA that is in turn involved in the expression of various genes involved in BR response. As negative feedback, when BR levels increase, BIN2 is dephosphorylated by BSU1 and further degraded. A protein phosphatase 2A (PP2A) is the BIN2 complement. It readily dephosphorylates BZR1 and BES1, thus promoting BR signaling (Clouse, 2011; Wang et al., 2013).

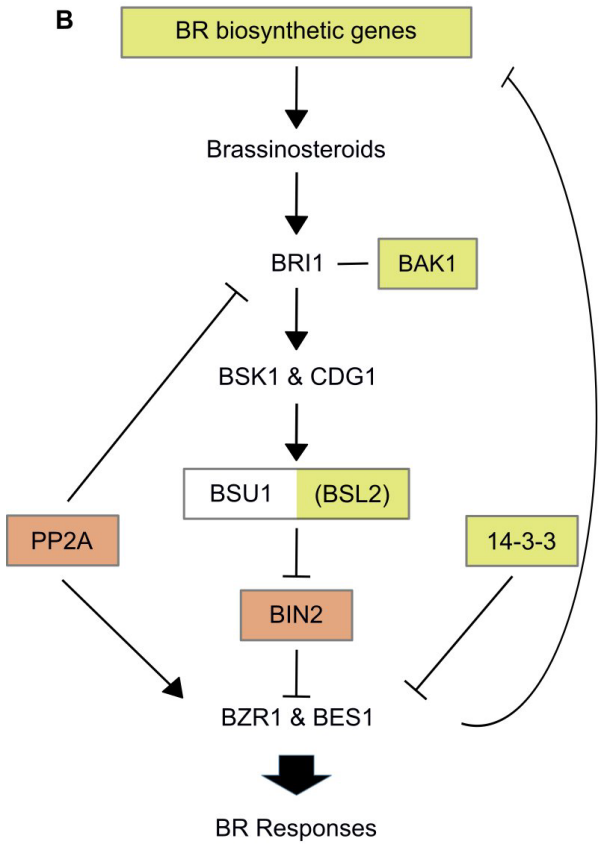

Figure 7: The Brassinosteroid signaling pathway.

Initially, brassinosteroids (BRs) are synthesized from the precursor Campesterol and bind to an extracellular domain of a BR receptor, BRI1. BRI1 then starts a signaling cascade, inducing the expression of BR responsive genes. BR signaling components that are found to interact with TRAPPII subunits in IP-MS (yellow) and Y2H (orange). Experiment and illustration by the lab of Prof. Farhah Assaad (unpublished).

An important objective of this thesis was to assess whether the TRAPPII complex is regulated by post-translational modifications such as phosphorylation. To elucidate this, the lab attempted to detect binary interactions with the TRAPPII-kinase interactions via yeast two-hybrid (Y2H). Y2H was carried out with truncations of the TRAPPII-specific subunits AtTRS120 and CLUB/AtTRS130 (Figure 5a), which have been shown to interact with conserved and plant-specific subunits of the TRAPPII complex (Garcia et al., 2020; Kalde et al., 2019). In a large scale Y2H screen including 2400 pair-wise tests, an interaction was detected between a TRS120$^{499\text{-}1187}$ (or TRS120-T2) truncation and the shaggy-like kinase BIN2 (Figure 6;Figure 8). No other TRAPPII-kinase interactions were identified in the Y2H screen. This data prompted me to determine the BIN2 target sites on

AtTRS120 and also to elucidate the nature of this interaction. I carried out *in vitro* kinase assays and yeast-2 hybrid experiments (Y2H) to identify the BIN2 target sites on AtTRS120 and also to understand the nature of interaction of the BIN2 kinase on its substrate: AtTRS120. Finally, I tested if the phosphorylation status of AtTRS120 affected its localization pattern *in planta*. The data from my experiments provide a novel link between the brassinosteroid signaling pathway and the post-translational regulation of a membrane trafficking component.

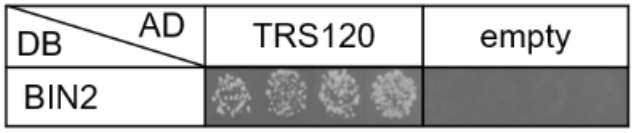

Figure 8: BIN2 and TRS120 are binary interactors.

Large scale Y2H screening in the Assaad lab showed that BIN2-TRS120 interact. This interaction was exclusive, since BIN2 was the only kinase that interacted with any of the subunits of the TRAPPII complex. Experiment and figure panel curtesy of Melina Altmann (unpublished data from the laboratories of Prof. Farhah Assaad and Prof. Falter Pascal-Braun).

2. Objectives

The primary aim of my thesis was to identify the role of the TRAPPII complex and ECH in the regulation of protein sorting decisions at the TGN. Based on previous works that have characterized these proteins (Gendre et al., 2013, 2011; Rybak et al., 2014), the hypothesis was that they might have distinct roles at the TGN. To test this, the Assaad lab tested whether TRAPPII – ECH interacted physically. Furthermore, I determined whether the two proteins interact genetically by performing double mutant analysis of a null allele of ECH and a hypomorphic allele of a TRAPPII subunit. I carried out immunostaining with antibodies against various cell wall polysaccharides to examine whether the secretory function was still intact in these double mutants. And together with the Assaad lab, the cell elongation phenotype was investigated in the double mutants. We also elucidated and quantitatively analyzed the impact on endocytosis and the TGN structure in *ech* and *trappii* mutants. Finally, the localization dynamics of different markers as well as that of the two proteins themselves was ascertained in both *ech* and *trappii* mutants.

Structure and subunit composition of the TRAPP complexes has been well studied and characterized in yeast and metazoan systems (J. J. Kim, Lipatova, & Segev, 2016; Riedel et al., 2018). In *Arabidopsis*, CLUB and AtTRS120 (two TRAPPII complex-specific subunits) have been previously identified and well characterized as being a part of the TRAPPII complex and necessary for cell plate biogenesis during cytokinesis (Jaber et al., 2010; Rybak et al., 2014; Thellmann et al., 2010). However, explicit information regarding the subunit composition and modularity of the different TRAPP complexes in plants is still unclear. Therefore, I attempted to characterize a TRAPP complex subunit: AtTRS33 and understand its role in TRAPPII complex function. Based on previous knowledge from other systems, I hypothesized that AtTRS33 could be a subunit of the TRAPPII complex in plants and might be necessary for the TRAPPII complex assembly. To this end, I performed double mutant analysis between a double knockout of AtTRS33 (*trs33-1*) and a mutant of a TRAPPII-specific subunit (*club-2*), to determine whether they

were part of the same complex. Additionally, localization dynamics of another TRAPPII-specific subunit: AtTRS120 in the absence of AtTRS33 was assessed.

Another interesting feature of the TRAPPII complex is that, in addition to its role as a tethering factor during membrane trafficking, it also behaves as a guanine nucleotide exchange factor (GEF) for Rab GTPases. Evidence for its function as a Rab GEF is found in yeast, humans, *Drosophila* and *Aspergillus* (Lipatova, Hain, Nazarko, & Segev, 2015; Pinar et al., 2015; Pinar & Penãlva, 2020; Riedel et al., 2018; Thomas et al., 2019). Based on previous works by other colleagues, it was hypothesized that *Arabidopsis* TRAPPII complex might be acting as an upstream GEF to Rab-A GTPases. Additionally, Rab-A GTPases were functionally linked to the TRAPPII complex (Qi & Zheng, 2011). Therefore, to test this hypothesis, firstly differential IP-MS studies were carried out in the Assaad lab using Rab-A GTPases as well as the different Rab-A GTPase variants to assess the nature of interaction of the TRAPPII complex with the Rab-A GTPases. Secondly, I quantified the localization dynamics of Rab-A GTPases in the *trappii* mutants. And finally, performed quantitative imaging analyses using different Rab-A GTPase GTP-locked variants in *trs33-1* mutants to shed light on the putative function of the TRAPPII complex as a Rab-A GEF in plants.

The final aim of the thesis was to elucidate the post-translational regulatory mechanisms of the TRAPPII complex during cell division. Earlier works in eukaryotes including plants, mainly focused on the structure and functions of the TRAPP complexes. However, the upstream regulatory mechanisms / components of the TRAPPII complex are still vastly unknown. As a preliminary cue, a distinct binary interaction between BIN2 (a member of the GSK3 kinase family) and AtTRS120 was observed in a large Y2H screen conducted in the Assaad lab. This observation strongly suggested that BIN2 kinase, as well as the other GSK3 kinase family members might be putative upstream regulators of the TRAPPII complex. To test this hypothesis, firstly, an *in vitro* kinase assay coupled to mass spectrometry was developed by the lab. Protein expressions and purifications of the different GSK3 kinases and the substrate – AtTRS120 were performed. They were then utilized in the kinase assay in a time and concentration dependent

manner to determine the presence of phosphorylated substrates of AtTRS120 and also to pin down on the GSK3 target sites. Next, the Assaad lab performed IP-MS analysis to assess the interactome of the various AtTRS120 phosphovariants. Thirdly, a Y2H analysis with BIN2 and various AtTRS120 phosphovariants was carried out to assess the mechanism of interaction between the two proteins. Finally, the localization dynamics of the AtTRS120 phosphovariants was elucidated using confocal laser scanning microscopy (CLSM).

3. Materials and methods

3.1. Equipment and instruments

Table 3: Microscopes used in the study

Microscope	Model	Company
Confocal Laser Scanning Microscope	SP8 Hyvolution, Fluoview FV1000	Leica, Olympus
Digital Microscope	KEYENCE VHX 700FM	KEYENCE
Dissecting Microscope	KL 1500 LCD	Zeiss
DIC Microscope	BX61	Olympus
Spinning disk Microscope	Olympus OSR with Yokogawa CSU-W1	Olympus, Yokogawa

Table 4: Miscellaneous devices used in the study

Device	Model	Company
Centrifuge	Eppendorf 5415D	Eppendorf AG, Hamburg
	Eppendorf 5424R	
	Beckman Avanti J-25	Beckman Coulter Inc., Brea, USA
	Beckman L 7-55 Ultracentrifuge	Beckman Coulter Inc., Brea, USA
Centrifuge rotor	JA-25.50	Beckman Coulter Inc., Brea, USA
	JA-10	Beckman Coulter Inc., Brea, USA
	Type 75Ti	Beckman Coulter Inc., Brea, USA
Chemiluminescence detection system	LAS4000 mini	Fujifilm, FUJIFILM Europe GmbH, Düsseldorf
Electroporator	Eppendorf Eporator	Eppendorf AG, Hamburg
Gel system	Biometra Compact XS/S or Biometra Compact M	Analytic Jena AG (Jena, Germany)
Lab balance	GT2100	Ohaus Corporation
NanoDrop	IMPLEN Nanophotometer	Serva Electrophoresis (Heidelberg, Germany)

PCR-Cycler	Thermocycler ep gradient	Eppendorf
pH-meter	pH 526	WTW GmbH
Pipette (0.2µl-5ml) pipetman	Gilson	Gilson Inc., Middleton, USA
Pure water system	Milli-Q Academic System	Millipore Corporation
SDS-PAGE unit	Mini-PROTEAN Tetra Cell	Bio-Rad Laboratories Inc.
Sample Mixer	HulaMixerTM	Invitrogen
Thermoshaker	Thermomixer 5355 4 VWR	Eppendorf
UV/Visible Spectrophotometer	Ultrospec 2000	Pharmacia Biotech Inc. (USA)
Voltage source		Pharmacia Biotech
Vortex	MS-1 MiniShaker	IKA-Werke GmbH

Table 5: Software used in the study

Software	Version	Purpose
Affinity designer		Image panel construction
GIMP 2	2.8	Image editing
ImageJ	1.51n	Image processing, colocalization analysis
Imaris		Image editing
Inkscape	0.91.1	Image panel construction
slidebook		Image viewer

3.2. *Escherichia coli* (*E. coli*) strains used in this study

Table 6: List of *E.coli* strains

Strain	Abbreviation	Genotype	Resistance	Company
DH5α	DH5α	gyrA462 endA1 glnV44 *Δ(sr1-recA) mcrB mrr hsdS20(r_B^-, m_B^-) ara14 galK2 lac2Y1 proA2 rpsL20(Sm^r) xyl5 Δleu mtl1*	No resistance	Invitrogen, USA
BL21 (DE3)	BL21	F– ompT $hsdS_B$ (r_B-m_B-) gal dcm (DE3)	Ampicillin	Invitrogen, USA

Rosetta-gami™ (DE3)	RoGa	*Δ(ara-leu)7697 ΔlacX74 ΔphoA PvuII phoR araD139 ahpC galE galK rpsL (DE3) F'[lac+ lacIq pro] gor522::Tn10 trxB pRARE2*	Chloramphenicol, Streptomycin, Tetracycline	Novagen, USA

3.3. Antibiotics used in the study

Table 7: List of antibiotics and working concentrations

All antibiotic stock solutions were stored at -20˚C.

Antibiotic	Working concentration for		Solvent
	bacteria	plants	
Carbenicillin	20 µg/ml	-	ddH_20
Tetracycline	10 µg/ml	-	EtOH
Chloramphenicol	25 µg/ml	-	EtOH
Spectinomycin	20 µg/ml	-	ddH_20
Kanamycin	25 µg/ml	50 µg/ml	ddH_20
Gentamycin	20 µl/ml	-	ddH_20
Ampicillin	100 µl/ml	-	ddH_20

3.4. Chemicals and kits

Unless otherwise indicated, chemicals were ordered from Carl Roth GmbH, Wacker Chemie AG, Merck KGaA or Sigma-Aldrich Chemie GmbH.
Template sequencing were carried out by Eurofins Genomics.

Table 8: Ready to use kits used in the study

Kit	Company
Gateway® BP and LR Clonase™ II enzyme mix	Thermo Fisher Scientific
Phire Plant Direct PCR Kit	Thermo Fisher Scientific (F-130WH)
Mix2SeqKit	EurofinsGenomics
QIAprep® Spin Miniprep Kit	Qiagen®
QuikChange® Site-Directed Mutagenesis Kit	Stratagene

3.5. Bacterial vectors used in this study

Table 9: List of bacterial vectors used in the study

Vector	Characteristics	Antibiotic resistance	Company
pDONR207	attP1/attP2	Gentamycin	Thermo Fisher Scientific
pDEST15	GST-tag; attR1/attR2	Ampicillin	Thermo Fisher Scientific
pDEST AD	Gal4 activation domain	Ampicillin	Thermo Fisher Scientific
pDEST DB	GAL4 DNA-binding domain	Ampicillin	Thermo Fisher Scientific

3.6. Plant material

All the *Arabidopsis thaliana* insertion lines were in the Columbia ecotype (Col-0) background and used as wild type control. Seed stocks were obtained from the Nottingham *Arabidopsis* Sock Centre (NASC; http://arabidopsis.info; Scholl et al., 2000), *Arabidopsis* Biological Recourse Center (ABRC; https://abrc.osu.edu), GABI (https://www.gabi-kat.de; Rosso et al., 2003) or Salk Institute Genomic Analysis Laboratory (SIGnal, http://signal.salk.edu/).

3.7. Primers

All Primers used in the study were ordered from MWG Operon (Ebersberg) as lyophilized salt-free or HPLC purified stocks. Primer3 and Oligo Calc: Oligonucleotide Properties Calculator online software's were used to design primers for genotyping and cloning/sequencing, respectively. Cloning primers for the phosphomutants are listed in Table 14 and primers used for T-DNA genotyping are listed in Table 15.

3.8. Molecular markers

3.8.1. DNA markers

GeneRuler™ 100bp DNA Ladder and GeneRuler™ 1kb DNA Ladder (Fermentas, Thermo Scientific) were used as DNA markers in agarose gels.

3.8.2. Protein markers

PageRuler™ Prestained Protein Ladder (Fermentas, Thermo Scientific) was used as the protein marker in western blots.

3.9. Media used in the study

For the production of Murashige & Skoog (MS) medium, measured amounts of MES-monohydrate, macro- and micronutrient stocks (according to) were dissolved in milliQ water and the pH adjusted to 5.7 by titrating with 5 M KOH. Without any further addition, this mixture was called MS (or ½MS) liquid medium. To produce solid MS 1.2 % agarose and 1 % sucrose was added additionally. After autoclaving the mixture and cooling it a little bit, the B5 vitamins were added under sterile conditions.

Table 10: Constituents of MS media

Name	Chemical Component	Volume [mg/L]
10 x Macronutrients	NH_4NO_3	1650
	KNO_3	1900
	$MgSO_4 \cdot 7 H_2O$	370
	KH_2PO_4	170
	$CaCl_2 \cdot 2 H_2O$	440
1000 x Micronutrients	Na_2EDTA	37.3
	$FeSO_4 \cdot 7 H_2O$	27.8
	$MnSO_4 \cdot H_2O$	16.9
	H_3BO_3	6.2
	$ZnSO_4 \cdot 7 H_2O$	8.6
	KI	0.83
	$NaMoO_4 \cdot 2 H_2O$	0.25
	$CuSO_4 \cdot 5 H_2O$	0.025
	$CoCl_2 \cdot 6 H_2O$	0.025
B5 vitamins	Myo-inositol	100
	Nicotinic acid	10
	Pyridoxine hydrochloride	1
	Thiamine hydrochloride	1

For the preparation of LB medium and SOC medium, the measured ingredients were added (according to) to milliQ water and autoclaved. For solid LB medium, 1.5% of LB agar was added before autoclaving.

Table 11: Media preparation protocol

Name	Chemical Component	Volume
½ MS medium	MES-monohydrate 10 x Macronutrient stock 1000 x Micronutrient stock ddH_2O B5 vitamins	0.49 g 100 ml 1 ml 2 L 2 ml pH 5.7
½ MS medium + kanamycin	½ MS medium kanamycin	 50 mg/L pH 5.7
1 MS medium	MES monohydrate 10 x Macronutrient stock 1000 x Micronutrient stock ddH_2O B5 vitamins	0.49 g 100 ml 1 ml 1 L 2 ml pH 5.7 with KOH
1 MS medium + sucrose	1 MS medium sucrose	 1% pH 5.7 with KOH
LB medium	Yeast extract Trypton NaCl ddH_20	5 g 10 g 10 g 1 L
LB agar	LB medium LB-agar	 1.5 %

SOB medium	Yeast extract Trypton NaCl KCl $MgCl_2$ Glucose ddH_20	5 g 10 g 0.5 g 25 mM 10 mM 50 mM 1 L pH 7.0

3.10. Mutant lines used

Table 12: Overview of the mutant lines used in the study

Allele	AGI gene identification	Polymorphism	Intron/ Exon	Nature of the allele	Reference
club-2 (attrs130[b])	At5g54440	SALK_ 039353	Intron	Null; sdlg[a] lethal	(Jaber et al., 2010)
trs120-4[c]	At5g11040	SAIL_1285_ D07	Intron	Null; sdlg[a] lethal	(Thellmann et al., 2010)
trs120-5	At5g11040	SALK_015227	promoter	Hypomorph; viable	(Qi et al., 2011)
trs33-1	At3g05000	SALK_ 109244	Exon	Null; sdlg[a] lethal	(Thellmann et al., 2010)
echidna	At1g09330	SAIL_163_E09	Intron	Null; viable	(Gendre et al., 2011)

a: Seedling (abbreviated “sdlg”)- lethal lines were propagated as hetero- or hemizygotes. b: Note that *club-2* is referred to as *attrs130* in Qi et al., 2011. c: This is distinct from the hypomorphic allele later named *trs120-4* by Qi et al., 2011.

3.11. Marker constructs used in the study

Table 13: Overview of marker lines used in the study

Construct	AGI gene identification	Promotor	Reference
TRS120:GFP	At5g11040	Native	(Rybak et al., 2014)
TRS120:mCherry	At5g11040	Ubiquitin	(Rybak et al., 2014)
EXO84b:GFP	At5g49830	Native	(Fendrych et al., 2010)

KEULE:GFP	At1g12360	Native	(Steiner, Müller, et al., 2016)
SYP121:GFP	At3g11820	Native	(Collins et al., 2003)
VHAa1:GFP	At2g28520	Native	(Dettmer, Hong-Hermesdorf, Stierhof, & Schumacher, 2006)
SYP61:CFP	At1g28490	Native	(Drakakaki et al., 2012)
RabA2a:YFP	At1g09630	Native	(Chow et al., 2008)
RabA2a:YFP-CA	At1g09630	Native	(Chow et al., 2008)
RabA2a:YFP-DN	At1g09630	Native	(Chow et al., 2008)

3.12. Agrobacterium-mediated transformation of *Arabidopsis thaliana*

All constructs were introduced into Agrobacterium tumefaciens strain GV3101::pMP90. A simplified floral dip method of Agrobacterium-mediated transformation was carried out (Clough & Bent, 1998). *A. tumefaciens* strain carrying gene of interest on a binary vector was cultivated in 400 ml of LB medium containing a selective antibiotic. *A. tumefaciens* culture was centrifuged (6000 x g) for fifteen minutes at 4°C. The pellet was resuspended in 5% sucrose (w/v). Silvet L-77 was added to a concentration of 0.05% (v/v). Above-ground parts of plant were dipped in Agrobacterium solution for 2-3 seconds, with gentle agitation. Afterwards, plants were covered with a dome for 24hours to maintain high humidity. The procedure was repeated after five days. T1 plants were selected for transformants on MS-medium agar plates containing 50 µg/ml kanamycin

Phosphomutants of TRS120 were generated using a DpnI-mediated Site-Directed Mutagenesis protocol. Site-directed mutations were introduced into the template construct via polymerase chain reaction using mutagenic primers with the desired mutations (Table 14) and the KOD Hot Start DNA Polymerase (Novagen®) for strand extension. Subsequently, the methylated nonmutated DNA template was digested with the DpnI endonuclease (Thermo Scientific). Mutated vectors were transformed in *Escherichia coli* DH5α for nick repair and amplification of the plasmids. After subsequent purification, the constructs were sequenced to ensure correct mutagenesis. For mutation of two or three phosphorylation sites,

sequential mutagenesis was carried out using already mutated vectors as template.

All the phospho-dead and phosphomimetic TRS120 phosphovariant constructs were generated using the GATEWAY® cloning kit with their respective site-specific primers (Table 14). TRS120-T2 cDNA sequences (spanning amino acids 499-1187; Rybak et al., 2014) were used as the template for protein expression in *E. coli* (kinase assays) and in yeast (Y2H). For *in planta* experiments (confocal microscopy, IP-MS), the full length genomic construct P_{TRS120}::TRS120:GFP (Rybak et al. 2014) was used as the SDM template. TRS120 phosphovariants were introduced into the *trs120-4* segregating mutant line via *Agrobacterium* mediated transformation (Clough & Bent, 1998).

Table 14: List of sites mutated in TRS120-T2 phosphovariants and corresponding primer sequences used for mutagenesis.

Phosphovariant	Amino acid substitutions	Primer sequences
SαA	S923A	fwd: 5'-GCC AAG GAA GAT GAT TCT GCA CCA GTA CAA GAT TCT CCA GAG-3' rev: 5'-CTC TGG AGA ATC TTG TAC TGG TGC AGA ATC ATC TTC CTT GGC-3'
SβA	S971A, S973A, S974A, S975A	fwd: 5'-CCC TCC ACC TGG TGC CCC TGC AGC TGC TAG AAA TCC GAG CTT CTC-3' rev: 5'-GAG AAG CTC GGA TTT CTA GCA GCT GCA GGG GCA CCA GGT GGA GGG-3'
SγA	T1163A, S1165A	fwd: 5'-GTA CTC AGA GCA CGA GCA GGA GCT GCT GCT CCA AAC GAA CCC ATC-3' rev: 5'-GAT GGG TTC GTT TGG AGC AGC AGC TCC TGC TCG TGC TCT GAG TAC-3'
SαβA	S923A, S971A, S973A, S974A, S975A	fwd: 5'-GCC AAG GAA GAT GAT TCT GCA CCA GTA CAA GAT TCT CCA GAG-3' rev: 5'-CTC TGG AGA ATC TTG TAC TGG TGC AGA ATC ATC TTC CTT GGC-3' fwd: 5'-CCC TCC ACC TGG TGC CCC TGC AGC TGC TAG AAA TCC GAG CTT CTC-3'

		rev: 5’-GAG AAG CTC GGA TTT CTA GCA GCT GCA GGG GCA CCA GGT GGA GGG-3’
SαγA	S923A, T1163A, S1165A	fwd: 5’-GCC AAG GAA GAT GAT TCT GCA CCA GTA CAA GAT TCT CCA GAG-3’ rev: 5’-CTC TGG AGA ATC TTG TAC TGG TGC AGA ATC ATC TTC CTT GGC-3’ fwd: 5’-GTA CTC AGA GCA CGA GCA GGA GCT GCT GCT CCA AAC GAA CCC ATC-3’ rev: 5’-GAT GGG TTC GTT TGG AGC AGC AGC TCC TGC TCG TGC TCT GAG TAC-3’
SβγA	S971A, S973A, S974A, S975A, T1163A, S1165A	fwd: 5’-CCC TCC ACC TGG TGC CCC TGC AGC TGC TAG AAA TCC GAG CTT CTC-3’ rev: 5’-GAG AAG CTC GGA TTT CTA GCA GCT GCA GGG GCA CCA GGT GGA GGG-3’ fwd: 5’-GTA CTC AGA GCA CGA GCA GGA GCT GCT GCT CCA AAC GAA CCC ATC-3’ rev: 5’-GAT GGG TTC GTT TGG AGC AGC AGC TCC TGC TCG TGC TCT GAG TAC-3’
SαβγA	S923A, S971A, S973A, S974A, S975A, T1163A, S1165A	fwd: 5’-GCC AAG GAA GAT GAT TCT GCA CCA GTA CAA GAT TCT CCA GAG-3’ rev: 5’-CTC TGG AGA ATC TTG TAC TGG TGC AGA ATC ATC TTC CTT GGC-3’ fwd: 5’-CCC TCC ACC TGG TGC CCC TGC AGC TGC TAG AAA TCC GAG CTT CTC-3’ rev: 5’-GAG AAG CTC GGA TTT CTA GCA GCT GCA GGG GCA CCA GGT GGA GGG-3’ fwd: 5’-GTA CTC AGA GCA CGA GCA GGA GCT GCT GCT CCA AAC GAA CCC ATC-3’ rev: 5’-GAT GGG TTC GTT TGG AGC AGC AGC TCC TGC TCG TGC TCT GAG TAC-3’
SαD	S923D	fwd: 5’-GCC AAG GAA GAT GAT TCT GAC CCA GTA CAA GAT TCT CCA GAG-3’ rev: 5’-CTC TGG AGA ATC TTG TAC TGG GTC AGA ATC ATC TTC CTT GGC-3’
SβD	S971D, S973D,	fwd: 5’-CCC TCC ACC TGG TGA CCC TGA CGA TGA TAG AAA TCC GAG CTT CTC-3’

	S974D, S975D	rev: 5’-GAG AAG CTC GGA TTT CTA TCA TCG TCA GGG TCA CCA GGT GGA GGG-3’
SγD	T1163D, S1165D	fwd: 5’-GTA CTC AGA GCA CGA GCA GGA GAT GCT GAT CCA AAC GAA CCC ATC-3’ rev: 5’-GAT GGG TTC GTT TGG ATC AGC ATC TCC TGC TCG TGC TCT GAG TAC-3’
SαβD	S923D, S971D, S973D, S974D, S975D	fwd: 5’-GCC AAG GAA GAT GAT TCT GAC CCA GTA CAA GAT TCT CCA GAG-3’ rev: 5’-CTC TGG AGA ATC TTG TAC TGG GTC AGA ATC ATC TTC CTT GGC-3’ fwd: 5’-CCC TCC ACC TGG TGA CCC TGA CGA TGA TAG AAA TCC GAG CTT CTC-3’ rev: 5’-GAG AAG CTC GGA TTT CTA TCA TCG TCA GGG TCA CCA GGT GGA GGG-3’
SαγD	S923D, T1163D, S1165D	fwd: 5’-GCC AAG GAA GAT GAT TCT GAC CCA GTA CAA GAT TCT CCA GAG-3’ rev: 5’-CTC TGG AGA ATC TTG TAC TGG GTC AGA ATC ATC TTC CTT GGC-3’ fwd: 5’-GTA CTC AGA GCA CGA GCA GGA GAT GCT GAT CCA AAC GAA CCC ATC-3’ rev: 5’-GAT GGG TTC GTT TGG ATC AGC ATC TCC TGC TCG TGC TCT GAG TAC-3’
SβγD	S971D, S973D, S974D, S975D, T1163D, S1165D	fwd: 5’-CCC TCC ACC TGG TGA CCC TGA CGA TGA TAG AAA TCC GAG CTT CTC-3’ rev: 5’-GAG AAG CTC GGA TTT CTA TCA TCG TCA GGG TCA CCA GGT GGA GGG-3’ fwd: 5’-GTA CTC AGA GCA CGA GCA GGA GAT GCT GAT CCA AAC GAA CCC ATC-3’ rev: 5’-GAT GGG TTC GTT TGG ATC AGC ATC TCC TGC TCG TGC TCT GAG TAC-3’

SαβγD	S923D, S971D, S973D, S974D, S975D, T1163D, S1165D	fwd: 5'-GCC AAG GAA GAT GAT TCT GAC CCA GTA CAA GAT TCT CCA GAG-3' rev: 5'-CTC TGG AGA ATC TTG TAC TGG GTC AGA ATC ATC TTC CTT GGC-3' fwd: 5'-CCC TCC ACC TGG TGA CCC TGA CGA TGA TAG AAA TCC GAG CTT CTC-3' rev: 5'-GAG AAG CTC GGA TTT CTA TCA TCG TCA GGG TCA CCA GGT GGA GGG-3' fwd: 5'-GTA CTC AGA GCA CGA GCA GGA GAT GCT GAT CCA AAC GAA CCC ATC-3' rev: 5'-GAT GGG TTC GTT TGG ATC AGC ATC TCC TGC TCG TGC TCT GAG TAC-3'

3.13. Methods for plant analysis

3.13.1. Seed sterilization and stratification

All the seeds were first washed in 80% ethanol for a few seconds, followed by 15min incubation in the sterilization buffer (10% SDS 12% NACIO). After washing 5 times with sterile ddH_2O, the seeds were incubated in a 0.15% agar solution and stored at 4°C for two days for stratification. After this, they were plated on MS or ½ MS plates depending on the experiments.

3.13.2. Growing conditions for *Arabidopsis thaliana*

Arabidopsis thaliana plants were grown in growth chambers (at the department of Botany and at TUMmesa) under controlled conditions:

Light intensity: 180 µmol/m2s
Photoperiod: 6:00 to 22:00 (16 hours light, 8 hours dark)
Light gradient: Sunrise and Sunset 30 minutes
Temperature: 22°C (@ day), 18°C (@ night)
Day/night humidity: 50% / 60%

Seedlings were grown in the cell culture room with the following settings:
Light intensity: 50 µmol/m^2s

Photoperiod: full day

Temperature: 22°C

3.14. T-DNA Genotyping

Genotyping of T-DNA insertions in seedlings/plants was carried out by PCR. PCR cycling conditions as well as the reaction components were used according to the manufacturer's instructions (PCR cycling conditions table). The PCR products were then separated by 1% agarose gel electrophoresis, supplemented with 0.025% EtBr (Carl Roth GmbH, Karlsruhe) for 20 - 40 mins at 130V. For agarose gel electrophoresis, 4µl PCR product was mixed with 1µl of DNA Loading Solvent (23ml Glycerol, 0.1g Orange G, 80µl 0.5M EDTA, 17ml H_20). 5-15µl of this was then loaded onto the gel. Additionally, 5µl of GeneRuler 1kb Plus DNA Ladder, was also loaded to determine the length of the construct.

Table 15: Primers used for T-DNA genotyping of plants

Target	Primer	Sequence [5' □3']	Tm [°C]
club	fwd	CTC GTC CAA GGA GCG GCA AG	62
	rev	GGC ACG AAC AGG GAC CCA AA	62
trs120-5	fwd	AAA CCG ATC AAC GAT TTC CTC	60.6
	rev	CAC CAA GCA CAA ATT TGA ACC	60.7
trs120-4	fwd	TGA TTG AGC ATG GTT TTC TGG AG	63
	rev	TGT CCA CTT GGG AGG AAT GG	63.3
ech	fwd	TCG TGG GAC CTC GTC ATC TTG TTC	62
	rev	CAT TGA TCT CGT TCC ACC ACC TGA G	61
Left border T-DNA primers	LB3	TAG CAT CTG AAT TTC ATA ACC AAT CTC GAT ACA C	66.5
	LBa1	TGG TTC ACG TAG TGG GCC ATC G	58.6
	LBb1.3	ATT TTG CCG ATT TCG GAA C	58.7

Table 16: Primer combinations to determine homo / heterozygosity of the T-DNA insertions in plants

Mutant	Insertion line	Primer combination	Fragment length (bp)
echidna	SAIL_163_E09	F + R	1132
		R + LB3	~ 700
trs120-4	SAIL_1285_D07	F + R	749
		R + LB3	~ 400
trs120-5	SALK_015227	F + R	1111
		R + LBb1.3	~ 625
club-2	SALK_039353	F + R	999
		R + LBa1	~ 750

3.15. Analysis of endocytosis

Endocytosis studies were performed with FM4-64 as described by Dettmer et al., 2006. For time lapses experiments, five-day-old wild-type and mutant seedlings were firstly, incubated with 4µM FM4-64 (Invitrogen) for five minutes and then placed on microscope slide and imaged via CLSM. Time lapses were measured as a percent of cell, in which FM4-64 positive endocytotic residues were observed at two-minute intervals.

3.16. Methods for microscopy

3.16.1. Scanning electron microscopy

Seedlings were sterilized, stratified for two days and plated on ½ MS agar. They were imaged at day 5 post stratification. All SEM imaging took place at the Faculty of Biology, LMU (Department of systematic botany and mycology) with the assistance of Dr. Eva Facher.

3.16.2. Antibody Stains

Seeds were surface sterilized (493.13.1) and plated on MS plates supplemented with vitamins and 1% sucrose. 5 days old seedlings were fixed in 4% Paraformaldehyde (PFA) in MTSB and vacuum infiltrated (300 – 400 mbar) for an hour. The seedlings were then washed 4 times with sterile ddH_2O for 10min.

8 to 10 seedlings were then placed on SuperFrost®Plus slides (Gerhard Menzel GmbH, Braunschweig) and dried at room temperature overnight. Next day, the roots were encircled with a water repellant PAP pen and rehydrated with MTSB for 10min. Antibodies can only enter the cells if they are permeabilized first. The cell wall was digested by an enzyme mix ordered by Sigma Aldrich GmbH (Driselase). Enzyme powder was dissolved in MTSB (20mg/ml) and spun down for 2 minutes at 10,000 rpm. The supernatant was then spread over the slides. After incubation for 50min at 37°C in a humid chamber, the slides were washed with PBS, for 5min, 4 times. The cell membrane was permeabilized with a permeabilization buffer and incubated at room temperature for 1 hour in a humid chamber. Afterwards, slides were rinsed and washed with PBS for 5 minutes, 6 times. Samples were blocked with 4% BSA/PBS solution by incubating them for 1 hour at 37°C under humid conditions. Then, the primary antibody (Table 18) was spread over the slides and incubated at 4°C overnight in a humid chamber. Before the secondary antibody was added, slides were washed 3 times for 10 minutes with 0.01% Triton diluted in PBS and 3 times for 10 minutes with PBS. Samples were prepared for the secondary antibody staining by washing the samples quickly with 4% BSA/PBS solution. From here, all further steps were carried out in the dark. Secondary antibodies (Table 18) were added to the slides and incubated for 3.5 hours at 37°C in the dark. Samples were washed again with PBS 4 times for 10 minutes and 2 times with ddH_20 to remove residual secondary antibodies. In the next step, DAPI was diluted in water 1:2000 and added to the samples. They were then incubated for 20 minutes at 37°C in a humid chamber. One last time, samples were washed 6 times for 5 minutes with ddH_20. In the end, samples were covered with 3-4 drops of CitiFluor AF1 (Agar Scientific, UK) and the samples stored between a cover glass and the SuperFrost®Plus slides.

Table 17: Buffers and Solutions for Antibody Stains

Buffer name	Components	Concentration/pH
Microtubule-stabilizing buffer (MTSB)	Pipes EGTA $MgSO_4.7H_2O$	50 mM 5 mM 5 mM pH 7.0

Fixation buffer	PFA in MTSB at 60°C After solution cools down	4% pH 11 Readjusted pH 7.0 (H_2SO_4)
Driselase cocktail	Driselese (SIGMA-Aldrich) in MTSB	2%
PBS	NaCl KCl Na_2HPO_4 KH_2PO_4	136 mM 3.67 mM 9 mM 1.7 mM pH 7.4
Blocking solution	BSA in PBS	4% (v/v)
Permeabilization buffer	DMSO Nonidet P40 MTSB	4176 µl 480 µl (cut tips) 144 µl

Table 18: Antibodies used in this work

Primary Antibody	Corresponding secondary Antibody	Dilution Primary / Secondary Antibody
Anti-ECHIDNA (rabbit, Gendre et al., 2011)	Anti-rabbit monoclonal Alexa-m488 (goat, Molecular Probes)	1:600 / 1:600
LM14 (rat monoclonal, Plant Probes)	anti-rat Alexa-m488 (goat, Molecular Probes)	1:10 / 1:100
Anti-GFP (mouse, Abcam ab1218)	Anti-mouse alexa 488 (goat, Life technologies, A11001)	1:1000 / 1:600
Anti-tub (sheep, cytoskeleton, ATN02-A)	Cy3 anti-sheep (immunoresearch)	1:200 / 1:100
Anti-Tubulin (mouse, Sigma, T9026)	Anti-mouse Cy3 (goat, Dianova)	1:2,500 / 1:600
Anti-GFP (rabbit, life technologies, A11122)	Anti-rabbit alexa 488 (goat, life technologies, A11034)	1:200 / 1:400

3.16.3. Confocal Laser Scanning Microscopy (CLSM)

For live-cell imaging, seedlings were first sterilized and stratified for 2 days at 4°C before they were plated on ½ MS supplemented with vitamins and sucrose

or 1 MS supplemented with vitamins and sucrose. The seedlings on plates were grown in the cell culture room. 5 days old seedlings were imaged for CLSM. Confocal microscopes used for imaging were an Olympus (www.olympus-ims.com) Fluoview 1000 confocal laser scanning microscope (CLSM) and a Leica (www.leica-microsystems.com) SP8 Hyvolution CLSM. Cell cycle stages (depicted as described by Smertenko et al., 2017) were determined via TRS120, tubulin, MAP65-3 and/or DAPI stains or localization dynamics, taking into account how membrane markers follow phragmoplast microtubule dynamics (Steiner et al., 2016a). Imaging data were acquired using LAS-X software (Leica). A 63X water immersion 0.9NA objective was used. Quantitative analysis of confocal scans was carried out in ImageJ. Line graphs of mean signal were corrected for photobleaching during the course of a time lapse.

Table 19: Excitation and Emission wavelengths for fluorophores used in this study

Fluorophor	Excitation wavelength [nm]	Emission wavelength [nm]
GFP	488	500-550
YFP	514	525-575
CFP	405	480
mRFP	561	581-754
mCherry	561	580-643
FM4-64	515	640
DAPI	358	461
Alexa Fluor® 488	495	519
Cy3	550	570

3.16.4. Embryo analysis

Embryos were harvested, fixed, infiltrated, embedded and imaged as described (Matthes and Torres-Ruiz, 2016). They were prepared for analyses using fresh siliques at different growth stages, putting them on a glass slide, then covering them with Hoyer's medium (Table 20) and finally the cover slip on top. After few minutes of incubation, the embryo images were captured using differential interference contrast (DIC) optics of an Olympus BX61 microscope. The genotype of the double mutant was confirmed by PCR analysis of both insertion alleles.

Table 20: Components of Hoyer's medium.

Component	Amount
Gum Arabic	15 g
Chloral hydrate	100 g
Glycerol	10 g
mQ water	25 ml

3.17. Protein expression and purification

2 ml of Pre-cultures were inoculated in 1l flasks filled with 200 ml LB medium supplemented with carbenicillin. Carbenicillin was used instead of Ampicillin to avoid hydrolysis of the β-lactam ring. Bacteria were grown to an OD_{600} = 0.6 – 0.8 at 37°C and 200 rpm. The OD_{600} was determined with a spectrophotometer. 100 µl of a 1 M β-D-1-thiogalactopyranoside (IPTG), a non-hydrolysable analog of lactose, was added to the culture to induce the expression of protein of interest. Expression conditions varied for different proteins and are shown in Table 21.

Table 21: Protein expression constructs and their conditions

protein	Vector (resistance)	Expression strain (resistance)	Expression conditions	LB supplementation	Purification
AtTRS120 – T2	pDEST15 (Car)	RoGa (Tet, Chl, Strp)	18 °C, 20 hours	none	GST-tag based
AtSK11	pDEST15 (Car)	RoGa (Tet, Chl, Strp)	25 °C, 20 hours	0.5% glucose+ 0.2mM MgSO4	GST-tag based
BIL2	pDEST15 (Car)	RoGa (Tet, Chl, Strp)	25 °C, 20 hours	none	GST-tag based
SK32	pDEST15 (Car)	RoGa (Tet, Chl, Strp)	25 °C, 20 hours	0.5% glucose + 0.2mM MgSO4	GST-tag based
SK41	pDEST15 (Car)	RoGa (Tet, Chl, Strp)	25°C 20 hours	0.5% glucose+ 0.2mM MgSO4	GST-tag based

After induction, the OD_{600} was measured again to evaluate the growth of bacteria. To avoid deviations from the Lambert-Beersche-law, samples with an OD_{600} higher than 0.8 were diluted with LB medium. Bacteria were centrifuged at 10,000

rpm for 15 minutes at 4°C, the supernatant was removed, and the pellet was stored at -80 °C.

For protein purification, firstly the pellets were thawed on ice for 15 minutes if it was stored at – 80°C. Then, it was suspended with 20 ml lysis buffer (Table 22) and then transferred to a 50 ml Falcon tube. The suspension was incubated on ice in the cold room while gently shaking. To destroy the cell wall, bacteria were sonicated for 7.5 minutes (Settings: 20 % amplitude, 5 x cycle, 20 seconds on, 10 seconds off) with a Sonoplus Homogenisator on ice slurry. Afterwards, cell debris was sedimented by centrifugation at 16,000 rcf for 30 minutes at 4 °C and the supernatant containing the protein of interest was transferred to a fresh Falcon tube. Meanwhile, 600 µl Glutathione Sepharose 4 Fast Flow Beads (GE Healthcare, Chicago USA) were added to an Eppendorf tube. Beads were washed three times with Tris-HCl purification buffer (Table 22). The supernatant was cautiously removed after each centrifugation step (13,000 rpm for 3 minutes). All beads were added to the supernatant from the previous step and incubated for 2 hours in cold room with gentle agitation. Next, beads were spun down at 3,000 rpm for 3 minutes at 4°C with a slow deacceleration mode on. The supernatant was removed, and the beads washed three times with purification buffer. Beads were then added to the purification columns and washed two times with 10 ml purification buffer without letting the columns run dry. 1 ml elution buffer (Table 22) was added to the column and incubated for 10 minutes. The protein was afterwards eluted and concentrated with Amicon Ultra-4 Centrifuge filters by centrifugation (4,000 rpm, 4 °C) until 150 µl remained. This step was repeated one more time and the elute stored separately. In case of AtSK11, the elute was concentrated again with Amicon Ultra-4-Centrifuge filters to remove contaminants.

Table 22: Protein purification buffers.

Buffer name	Components	Volume/ concentration/ pH
Lysis buffer	Tris-Base*	50 mM
	NaCl	150 mM
	PMSF	1 mM

	Inhibitor cocktail Triton X-100	1# 1% pH 7.8
Tris-HCl purification buffer	Tris-Base NaCl	50 mM 150 mM pH 7.8
Elution buffer	Tris-HCl purification buffer Reduced Glutathione	10 ml 10 mM pH 7.8

Tablet for 80 ml buffer

The results of protein expression and purification was analyzed and quantified using SDS PAGE.

3.18. Co-immunoprecipitation

Coimmunoprecipitation experiments were carried out on 3 g of light-grown seedlings, which were harvested at day 7, as described by Park et al. (2012). Seedling lysates were incubated with GFP-trap beads (Chromotek). We supplemented both the lysis and washing buffers with a protease inhibitor cocktail for plants (Sigma-Aldrich P9599) and added 1mM phenylmethanesulfonylfluoride every 45min. An inhibitor of proteasome activity (Sigma-Aldrich C2211) was also added to the lysis buffer. The washing buffer (50mM Tris [pH 7.5] and 0.2% [v/v] Triton X-100) was supplemented with 200mM NaCl. After washing away all non-binding proteins, 70µl 2x NuPAGE LDS + 25mM DTT buffer (ThermoFisher, US) was added and boiled at 70°C for 10min to denature the bait and all interaction partners. The results of the Co-IP were verified on Coomassie blue gels. Further trypsin digestion and LC-MS/MS measurements of Co-IP samples were carried out at the BayBioMS facility.

3.19. Yeast Two-Hybrid (Y2H)

Full length cDNA clones obtained from the RIKEN Bioresource Center (Seki et al., 2002) were used as templates for all clones used in binary interaction assays. Y2H pairwise tests were performed as described in Altmann et al., 2018. Briefly, open reading frames (ORFs) TRS120 truncations (T1, T3) and BIN2 were

transferred by Gateway cloning into the GAL4 DNA-binding domain (DB) encoding Y2H vector pDEST-pPC97, and subsequently transformed into the yeast strain Y8930. These constructs were screened by yeast mating against a TRS120-T2 truncation and its phosphomutants TRS120-T2- SαD, SßD, SγD, SαßD and SαßγD fused to the Gal4 activation domain (AD) in the yeast strain Y8800. The constructs were generated in the lab but the screening for interactions between AD and DB was carried out by the collaborator's lab of Dr. Pascal Falter-Braun at the Helmholtz Zentrum, Munich. Interaction was assayed by growth on selective plates using the HIS3 reporter, and using 1mM 3-Amino-1,2,4-triazole (3-AT) to suppress background growth. All candidate interactions were verified by pairwise one-on-one mating in four independent experiments. Only pairs scoring positives in all four assays were considered as bona fide interaction partners.

3.20. *In vitro* kinase assays – sample preparation

Glutathione S-transferase (GST)-BIN2 (Li and Nam, 2002) and GST-T2-TRS120 phosphovariants were expressed in Escherichia coli (Rosetta-gami™ strain) under constant shaking for 20 hours at 25°C or 20 hours at 18°C, respectively. The expressed proteins were affinity purified with GST-tags. After sonication of the samples in 1x PBS, 1 mM PMSF, 1 mg/ml lysozyme and 1% Triton X-100, the bacterial cell rests were centrifuged for 30 min at 16,000 g. Supernatants were incubated for 2 hours with Glutathione Sepharose® 4 Fast Flow Beads (GE Healthcare) while rotating. After washing the samples five times, the GST tagged proteins were eluted with 10 mM glutathione and concentrated by ultra-filtration.

In vitro kinase assays with mass-spectrometry readout were performed to determine phosphorylation sites. For each reaction, 10µg of substrate (TRS120-T2) and different dilutions of the kinase (1:5, 1:10, 1:100) were incubated for 15, 30, and 120min in a kinase buffer (20 mM Tris HCl, 100 mM NaCl, 1 mM $MgCl_2$, 1 mM DTT, 1 mM ATP). For the negative controls, one sample with the highest kinase concentration and the longest incubation time was incubated in a kinase buffer without ATP. For the kinase dead control, the kinase was heat-inactivated

prior to the incubation with its substrate. To stop the reaction, samples were heated at 95°C for 5 min.

After the assay, the samples were sent to BayBioMS for further processing and MS analyses.

3.21. Statistical analysis and image processing

False discovery rates, determined with the standard two-tailed t-test, were set at a cutoff of 1%. Images taken with the Leica SP8 microscope were deconvolved using the built-in Huygens Scientific deconvolution software (www.leica-microsystems.com) operated in 2D. For consistency in quantitative analyses, we selected cortical root tip cells, at a height of 6-22 cells above the quiescent center in the root apical meristem. For particle count analysis, a Macro was written in ImageJ. This first allowed us to free hand draw around the cell of interest. This cell was then thresholded to select for the particles/puncta in the cytosol before performing the analysis of particle properties. Generally, four images per experiment were analyzed manually before applying the established parameters to the whole data set. Images were processed with Adobe photoshop (www.adobe.com) and GIMP (https://www.gimp.org), analyzed with Image J (https://imagej.nih.gov), and assembled with Inkscape (https://inkscape.org).

4. Results

4.1. Role of the TRAPPII complex and ECHIDNA in protein sorting at the TGN

In plant cells, major trafficking or sorting decisions of macromolecules occur at the trans-Golgi-network (TGN) or early endosome (EE). The TGN acts as a major hub for membrane trafficking during interphase and cytokinesis (Chow et al., 2008; Dettmer et al., 2006; Ravikumar et al., 2018). It has essential functions in exocytosis (Luo et al., 2015), endocytosis and protein sorting (Rosquete et al., 2018) as well as a number of specialized functions such as cell plate formation in dividing cells. In *Arabidopsis*, most of these functions are mediated by the Transport Protein Particle II (TRAPPII) protein complex (Qi & Zheng, 2011; Ravikumar et al., 2018; Rosquete et al., 2019; Rybak et al., 2014; Steiner, Rybak, et al., 2016) and ECHIDNA (ECH; Boutté et al., 2013; Gendre et al., 2011; McFarlane et al., 2013). Previous studies show that the *trappii* null mutants are seedling lethal and exhibit severe cytokinesis defects. This result is consistent with the role of the TGN in plant cell organization (Kalde et al., 2019; Ravikumar et al., 2018; Rybak et al., 2014; Steiner, Rybak, et al., 2016). ECH has been shown to be necessary for cell elongation and secretory vesicle formation in the cells (Boutté et al., 2013; Gendre et al., 2013, 2011; McFarlane et al., 2013). In spite of ECH and TRAPPII complex's important roles in trafficking at the TGN, little is known about the nature of their interaction, and how this interaction could be involved in making sure that their functions are performed efficiently.

4.1.1. TGN structure, endocytosis, cell elongation and cytokinesis are differentially impacted in *ech* and *trappii* mutants

Previous studies have already shown that the TGN structure in *ech* and *trappii* mutants are affected (Boutté et al., 2013; McFarlane et al., 2013; Qi & Zheng, 2011). I revisited this experiment with a quantitative analysis of the size and number of TGN punctae in interphase cells of *ech* and *trappii* mutants labeled with

TGN localizing markers VHAa1 and SYP61 fused with GFP and CFP respectively using high resolution CLSM (Figure 9). Already at first glance, I could observe aggregates of VHAa1:GFP compartments in the *trs120-4* mutants in contrast to *club-2* (Figure 9C). The quantitative analysis confirmed this observation. The average size of the VHAa1:GFP compartments in *trs120-4* mutants was significantly larger than those in the wild type. However, in *club-2* the opposite was observed. There was a decrease in the average size of VHAa1:GFP compartments in *club-2 in* comparison to the wild type (Figure 9B) .

Subsequently, while determining the localization dynamics of SYP61:CFP, which is a t-SNARE that colocalizes with VHAa1, the mutations displayed an opposite impact on the SYP61:CFP compartments; average particle size in *trappii* mutants was lower in comparison to those in the wild type (Figure 9F; $P=4e^{-11}$ for *club-2* and $4e^{-05}$ for *trs120-4*) while it was higher than wild type and formed aggregates in *ech* mutants (Figure 9F; P<0.05 for *ech*). This analysis thus indicated that the *ech* and *trappii* mutants might have a different impact on the TGN structure.

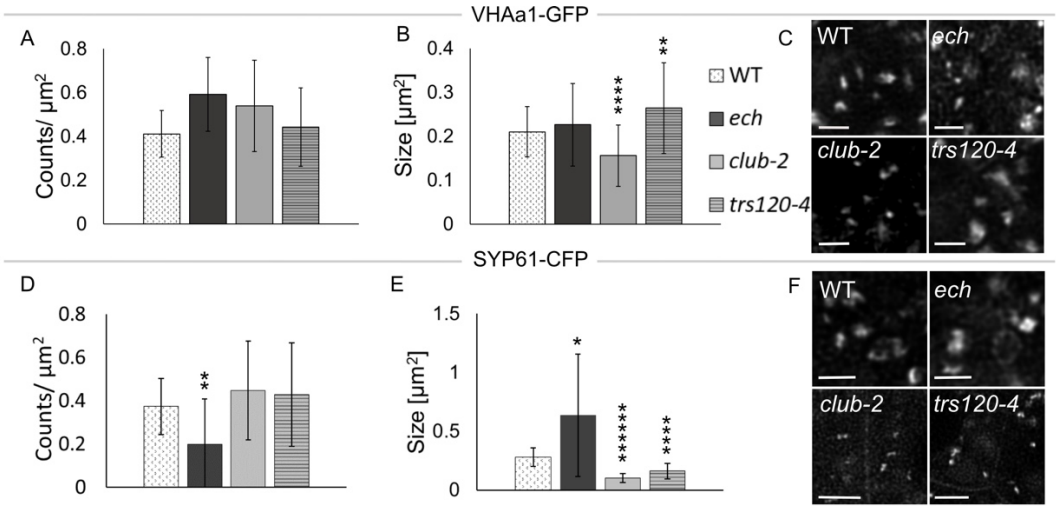

Figure 9: TGN structure is impacted in *ech* and *trappii* mutants.

Average particle or aggregate size (A, D) and representative deconvolved CLSM micrographs (C, F) for TGN markers in wild type, *ech*, *club-2 and trs120-4*. Data are mean±s.d. Student's two-tailed t-test: *P<0.05, **P<0.01, ****P<0.0001, *****P<0.00001. Scale bars: 1.5 µm. (A-C) Behavior of P_{VHAa1}::VHAa1-GFP-positive compartments. In *ech* mutants, particle or aggregate sizes were more variable than in the wild type. Particle size is decreased in *club-2* but particles aggregated in *trs120-4*; n=54 wild-type cells from 14 seedlings; n=37 *ech* cells from 10 seedlings; n=40 *club-2* cells from eight seedlings; n=57 *trs120-4* cells from 15 seedlings. (D-F) Behavior of P_{SYP61}::SYP61-CFP-

positive compartments. Particle counts were decreased in *ech* but unchanged in *trappii* mutants; conversely, particle size was increased in *ech* and decreased in *trappii*. n=33 wild-type cells from 10 seedlings; n=18 *ech* cells from six seedlings; n=26 *club-2* cells from eight seedlings; n=23 *trs120-4* cells from six seedlings. Image panel and caption adapted from Ravikumar et al., 2018.

Endocytosis is one of the basal functions of the TGN. Previous studies have already shown that endocytosis is not impaired in *trappii* mutants (Qi et al., 2011). By monitoring the rates of endocytosis in the cells of the mutants, I wanted to confirm this claim and compare it with that of the *ech* mutant. The experiment was carried out by performing a quantitative analysis of FM4-64 internalization dynamics (i.e., presence at the early endosome or TGN) at different time points in root tip cells. Endocytosis experiment for *trs120-4* mutants was carried out by Dr. Katarzyna Rybak, a doctoral candidate at Assaad lab. The results show that endocytosis is impaired in all mutants to a different degree. Endocytosis occurred at 14 to 18 min after FM4-64 application in the *ech* and *club-2* (Figure 10A) mutants showing that it was delayed in comparison to the wild type. But in *trs120-4* mutants it was severely impaired at all time points (Figure 10B). Results from the FM4-64 quantitative analysis show that *ech* and *club-2* display a slight delay in the rate of endocytosis in comparison to that in the wild type. However, in *trs120-4* mutants it was severely impaired in comparison to that in the wild type.

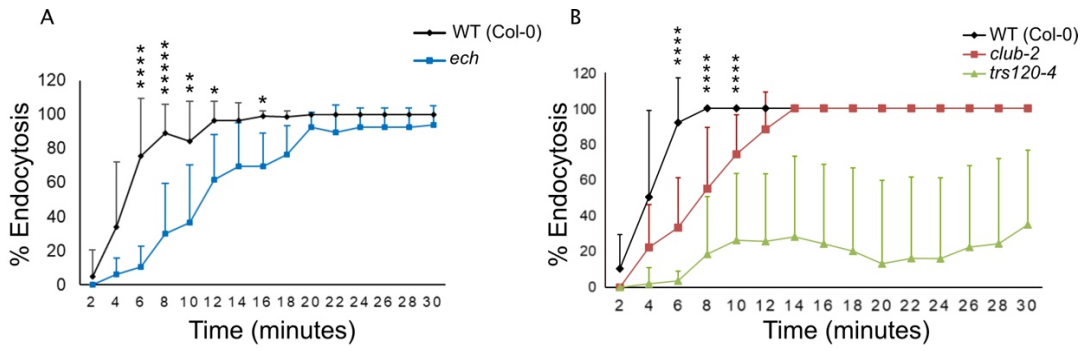

Figure 10: Rate of endocytosis in *ech* and *trappii*.

The rate is computed by the number of FM4-64-positive vesicles per cell at the given time points. Data are mean±s.d. Student's two-tailed t-test: *P<0.05, **P<0.01, ****P<0.0001, *****P<0.00001. (A) Endocytosis in *ech* mutants. n=116 cells from 14 wild-type seedlings, n=84 cells from eight *ech* seedlings. (B) Endocytosis in *trappii* mutants. n=225 cells from 16 wild-type seedlings, n=147 cells

from 10 *club-2* seedlings, n=111 cells from eight *trs120-4* seedlings. Image panel and caption adapted from Ravikumar et al., 2018.

In addition to the basal TGN functions, there are also various specialized TGN functions. I characterized two of the specialized TGN functions: cytokinesis, by quantifying the number of incomplete cell walls (cell wall stubs) and cell elongation, by measuring the length of the hypocotyls of the mutants imaged using scanning electron microscopy (SEM). The results revealed that the *ech* mutants were impaired in cell elongation but not in cytokinesis (Figure 11A). Conversely, *trappii* null mutants were cytokinesis defective but not impaired in cell elongation (Figure 11B). These results propose a partition in TGN functions among the different players.

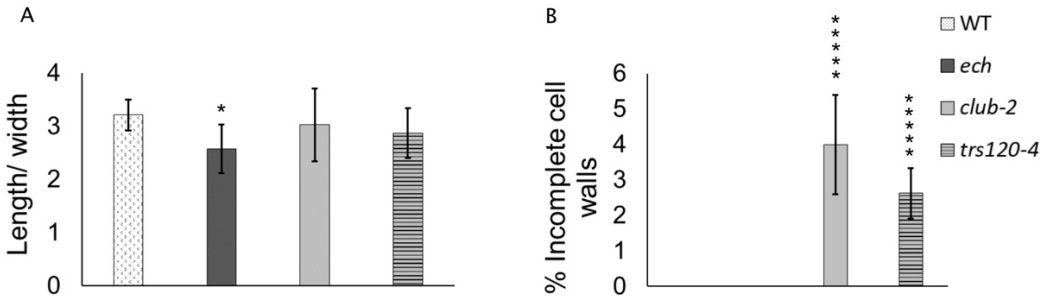

Figure 11: Cell elongation versus cytokinesis defects in *ech* and *trappii* hypocotyls.
The hypocotyls were imaged using environmental scanning electron microscopy. Data are mean±s.d. Student's two-tailed t-test *P<0.05, *****P<0.00001. n=80 cells from five wild-type seedlings, n=175 cells from seven *ech* seedlings, n=207 cells from nine *club-2* seedlings, n=162 cells from six *trs120-4* seedlings. (A). Cell elongation as measured by the length over the width of the hypocotyl cells. This is decreased in *ech* (P=0.02) but not in *trappii* mutants. (B). Cytokinesis defects as measured by the incidence of cell wall stubs or incomplete walls. These are detected in *trappii* mutants (P<10−04) but not in *ech*. Image panel and caption adapted from Ravikumar et al., 2018.

4.1.2. Plasma membrane and cell plate markers are mislocalized in *ech* and *trappii* mutants

To elucidate the role of ECH and TRAPPII in protein sorting at the TGN, I imaged two plasma membrane markers and two TGN markers in wild-type versus

mutant root tips. SYP121 and EXO84B, both fused to GFP, were the two plasma membrane markers chosen for this study since the Assaad lab has already monitored their localization dynamics in the *trappii* mutants (Rybak et al., 2014) but not in *ech*.

P_{SYP121}::SYP121:GFP (Collins et al., 2003) localizes to the plasma membrane in interphase cells and also to the cell plate throughout cytokinesis. The cell plate localization pattern is impaired in the *club-2* mutant (Rybak et al., 2014). In the *ech* mutants, I observed that although the plasma membrane and cell plate localization resembled the wild type, SYP121:GFP localized to additional compartments resembling vacuoles in both interphase and cytokinetic cells (Figure 12B, E). SYP121:GFP localization was the most impaired in *club-2* mutants (Figure 12C, E), it did not localize to the cell plate at all and displayed an aberrant localization pattern of SYP121:GFP positive endocompartments in the cytosol. In the other *trappii* mutant: *trs120-4*, SYP121:GFP displayed wild-type localization dynamics in cytokinetic cells, but had an increased abundance of endomembrane compartments in interphase cells in comparison to the wild type (Figure 12D, E).

P_{EXO84B}::EXO84B:GFP (Fendrych et al., 2010) is a subunit of the exocyst tethering complex that is absent at the cell plate during initiation, but later localizes to the cross wall after maturation (Fendrych et al., 2010; Rybak et al., 2014; Smertenko et al., 2017). The localization pattern of EXO84B:GFP in *ech* and *trs120-4* resembled that of the wild type localization. However, in *club-2* mutants (imaging data by Dr. Alexander Steiner), EXO84B:GFP only labeled elongated endomembrane compartments, and was completely absent at the cell plate (Figure 12F).

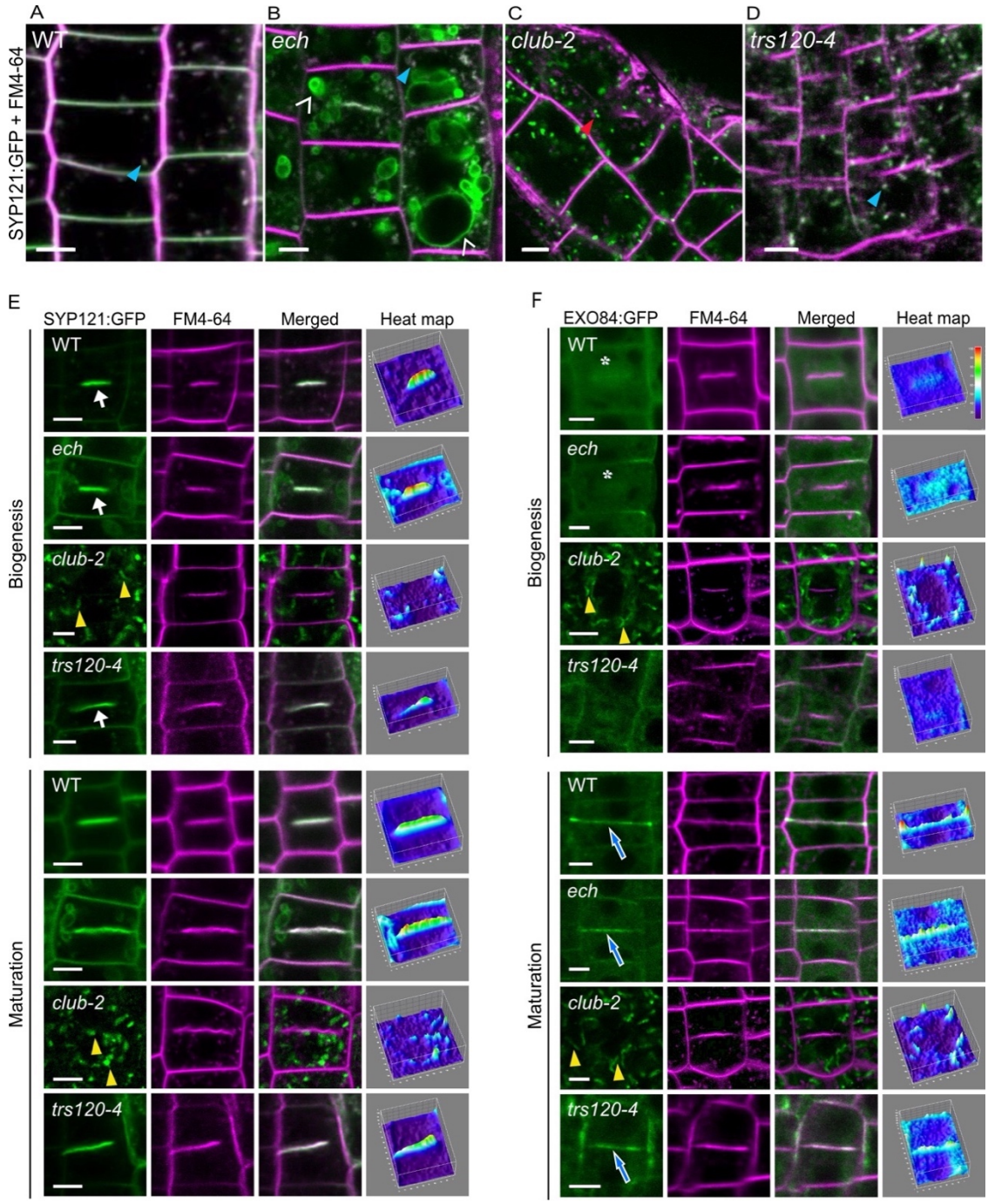

Figure 12: Sorting of plasma membrane markers in *ech* and *trappii* root tips.

Live imaging with GFP marker in green and FM4-64 in magenta. (A-D) P_{SYP121}::SYP121-GFP in non-dividing cells. SYP121-GFP-positive vesicles colocalize with FM4-64 in all backgrounds (blue arrowheads) with the exception of *club-2* (red arrowhead in C). There is mistargeting to vacuole-like structures in *ech* (white open arrowheads in B). n=38 wild-type, n=7 *ech*, n=10 *club-2* and n=11 *trs120-4* seedlings. (E,F) Imaging of cytokinetic cells. Surface plots are 3D heat maps depicting fluorescence intensity along the z-axis with a scale ranging from blue (low) to red (high). (E). P_{SYP121}:: SYP121-GFP. n=52 wild type, n=17 *ech*, n=12 *club-2*, n=28 *trs120-4* cytokinetic cells from at least ten seedlings. (F) P_{EXO84}::EXO84B-GFP. n=13 wild type, n=15 *ech*, n=11 *club-2*, n=10

trs120-4 cytokinetic cells from at least ten seedlings. White arrows indicate cell plates; yellow arrowheads indicate deviant vesicles in *club-2*. Asterisk indicates a diffuse cloud of GFP signal around the cell plate prior to insertion into the lateral wall. White-rimmed blue arrow indicates a cross wall. Scale bars: 5 µm. Image panel and caption adapted from Ravikumar et al., 2018.

In order to further understand protein sorting in the different mutant backgrounds, I next imaged two TGN markers, P_{VHAa1}::VHAa1:GFP and P_{SYP61}::SYP61:CFP in the cytokinetic cells of the mutant root tips. VHAa1:GFP (Dettmer et al., 2006) is a TGN marker, absent at the cell plate in the wild type (first panel in Figure 13). Interestingly, in 55% of the observed cell plates of the *ech* mutants (n= 18), VHAa1:GFP weakly labeled the cell plate showing a subtle deviation from the wild type. This deviation in the VHAa1:GFP localization pattern was much stronger in the *trappii* mutants, with an abnormally strong cell plate signal observed in 89% (n= 28) *club-2* and 72.2% (n= 43) *trs120-4* cell plates (Figure 13).

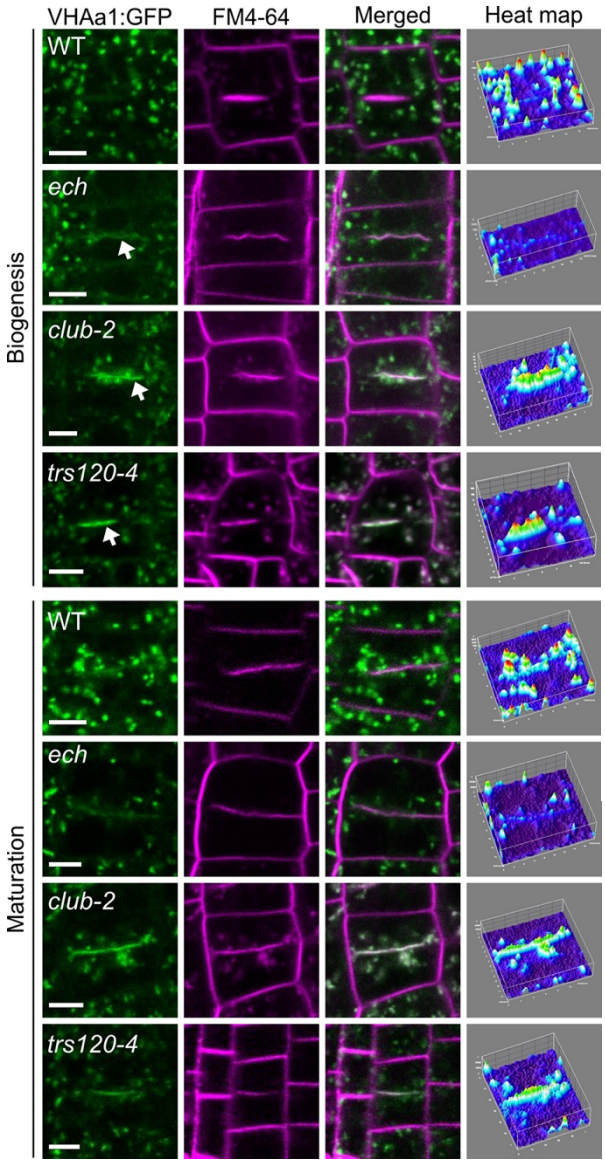

Figure 13: Sorting of a TGN marker in *ech* and *trappii* root tips.
Live imaging of dividing cells with P_{VHAa1}::VHAa1:GFP in green and FM4-64 in magenta. Note cell plate exclusion in the wild type versus ectopic localization to the cell plate, especially pronounced in *trappii* mutants. Surface plots are 3D heat maps depicting fluorescence intensity along the z-axis with a scale ranging from blue (low) to red (high). White arrows point to cell plate. At least ten seedlings were imaged per marker line. n = 46 wild type, n = 18 *ech*, n = 28 *club-2*, n = 43 *trs120-4* cytokinetic cells. Size bars = 5µm. Image panel and caption adapted from Ravikumar et al., 2018.

In contrast to VHAa1:GFP, which is excluded from the cell plate in the wild type, P_{SYP61}::SYP61:CFP (Drakakaki et al., 2012) is known to label the cell plate throughout cytokinesis and did not appear to be impaired in either *ech* or in *trappii* mutants (Figure 14B). However, just like in SYP121:GFP, the SYP61:CFP protein in *ech* mutants localized to additional compartments resembling vacuoles in both the interphase and cytokinetic cells (Figure 14A).

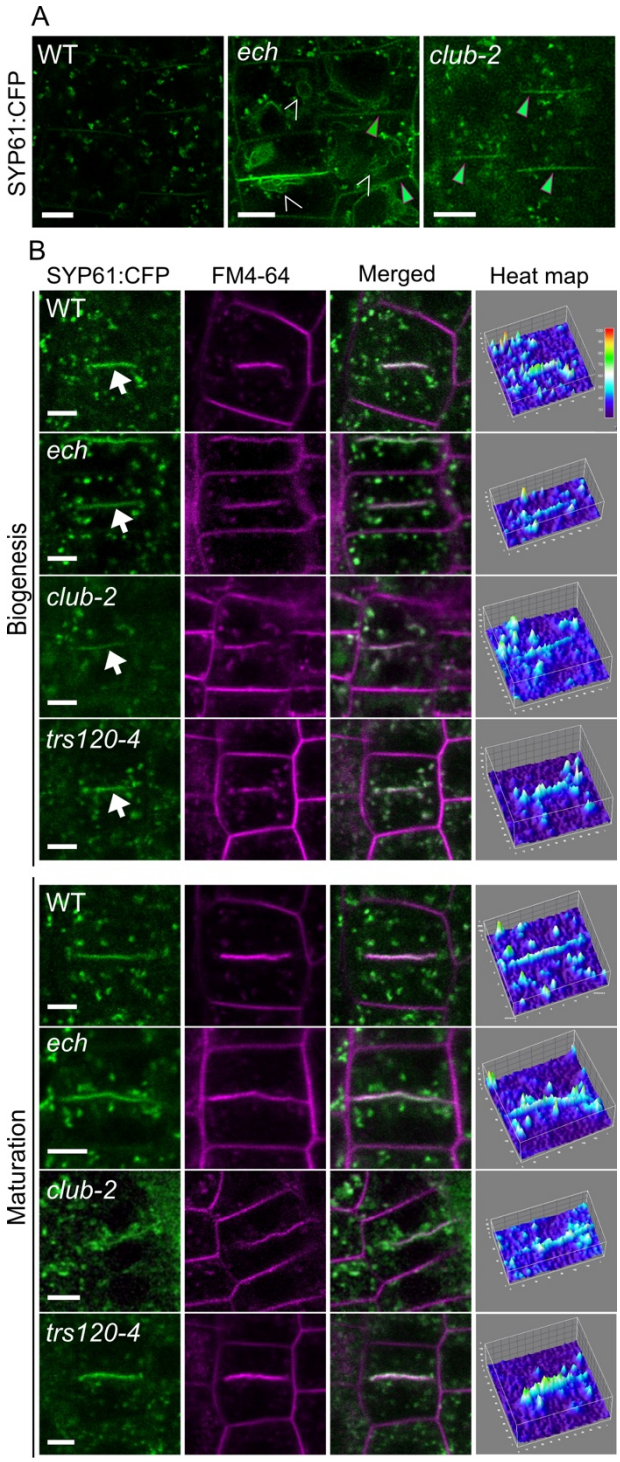

Figure 14: Sorting of the TGN marker P_{SYP61}::SYP61:CFP in *ech* and *trappii* root tips.

Live imaging with $P_{SYP61::}$SYP61:CFP marker in green and FM4-64 in magenta. (A). SYP61:CFP in non-dividing cells. SYP61:CFP is not localized to the plasma membrane in the WT but it is mislocalized to the plasma membrane in both *ech* and *club-2* (pink-rimmed green arrowheads). Note mistargeting to vacuole-like structures in *ech* (open arrowheads in middle panel). (B). Live imaging of P_{SYP61}::SYP61:CFP in dividing cells. Surface plots are 3D heat maps depicting fluorescence intensity along the z-axis with a scale ranging from blue (low) to red (high). White arrows point to cell plates. n = 10 wild-type, n = 8 *ech*, n = 4 *club-2*, n = 12 *trs120-4* cell plates. Size bars: 5 µm. Image panel and caption adapted from Ravikumar et al., 2018.

A cell plate marker: P_{KEULE}::KEULE:GFP (Steiner, Müller, et al., 2016) was imaged next. KEULE:GFP is a cytosolic marker that is sorted to the cell plate at the beginning of cytokinesis and labels it throughout mitosis, later localizing to the rapidly expanding leading edges of the cell plate at the disc phragmoplast stage (Steiner, Müller, et al., 2016). In both the *trappii* mutants, the KEULE:GFP

localization pattern differed from the wild type. In contrast to the plasma membrane markers, *trs120-4* mutants were severely impaired in targeting KEULE:GFP to the cell plate than *club-2* (Figure 15). In *ech*, the localization of KEULE:GFP to the cell plate was similar to the wild type, however, there was less cytosolic signal in the cells (Figure 15).

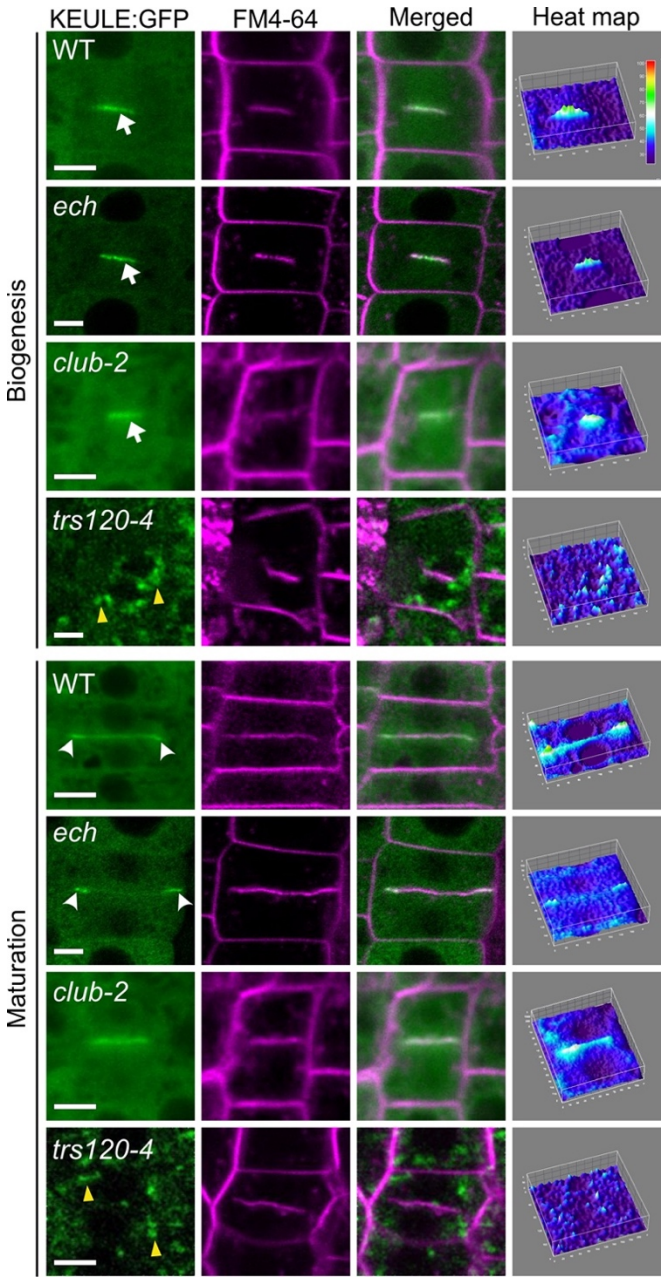

Figure 15: Sorting of a cell plate marker in *ech* and *trappii* root tips.

Live imaging of dividing cells with P_{KEU}::KEULE:GFP in green and FM4-64 in magenta. Surface plots are 3D heat maps depicting fluorescence intensity along the z-axis with a scale ranging from blue (low) to red (high). The localization dynamics of KEULE:GFP at the cell plate differed from the wild type in *trappii* but not in *ech* mutants, but there was less cytosolic signal in *ech* than in the wild type. Yellow arrowheads point to deviant vesicles in *trs120-4*. White arrows point to cell plate. Arrowheads point to the leading edges of the cell plate in the wild type and in *ech*. At least ten seedlings were imaged per marker line. n = 59 wild type, n = 32 *ech*, n = 46 *club-2*, n = 39 *trs120-4* cytokinetic cells. Size bars = 5µm. Image panel and caption adapted from Ravikumar et al., 2018.

In conclusion, firstly, the study shows that plasma membrane markers were mistargeted to different compartments in *ech* and *club-2*. I could observe

mislocalization of SYP61:CFP and SYP121:GFP (but not EXO84b:GFP) to compartments resembling vacuoles in *ech* but not in *trappii* mutant root tips. *club-2* mutants were more severely impaired in the targeting of plasma membrane markers than *trs120-4*. Secondly, TGN marker VHAa1:GFP severely deviated from the wild type in *trappii* mutants. And thirdly, protein sorting at the cell plate was impaired in *trappii* but not in *ech* mutants.

4.1.3. *ech trappii* double mutants show synergistic genetic interaction

The IP-MS data from the Assaad lab showed that there was no physical interaction between TRAPPII and ECH proteins. Also, the network interaction data (performed by the group of Pascal Falter-Braun) suggested that TRAPPII and ECH might be acting in two distinct yet adjacent pathways (Ravikumar et al., 2018). To elucidate whether these pathways were either partially redundant or completely independent, I performed double mutant analysis. If the pathways interacted independently, one would observe an additive double mutant phenotype. In case of either partial redundancy or overlap, a synthetically enhanced or synergistic (i.e., more than additive) double mutant phenotype is expected.

I first noticed almost tenfold increase of collapsed seeds among the progeny of plants homozygous for *ech* and segregating *club-2* null alleles, which is indicative of embryo lethality. I examined the embryo phenotypes in the siliques of plants segregating both the single and double mutant progeny (Figure 16). *ech* single mutants showed very weak embryo phenotypes up to heart stages, whereas *club-2* single mutants exhibited a few abnormal cell divisions throughout embryogenesis especially in the root apical meristem, at an average frequency of 11.8% (n=511 embryos). In the progeny of plants homozygous for *ech* and segregating *club-2* null alleles, I could observe a high frequency of unusually shaped embryos until the heart stage. The deviations were mostly in the basal region of the embryo and affected the root primordia (last column in Figure 16). Also, the embryos appeared radially swollen maybe because of reduced cell elongation. From the heart stage to the torpedo stage the number of double

mutants dropped drastically and I could observe no double mutant embryos at the torpedo stage (0% frequency, n= 130 torpedo stage mutants for the *ech club-2* double mutants). Taken together, from the observation of synergistically increased number of collapsed seeds, I concluded that the double mutants are embryo lethal, that collapsed by the late heart stage. In short, the combination of a viable *ech* allele with seedling lethal *club-2* allele gave rise to embryo lethality.

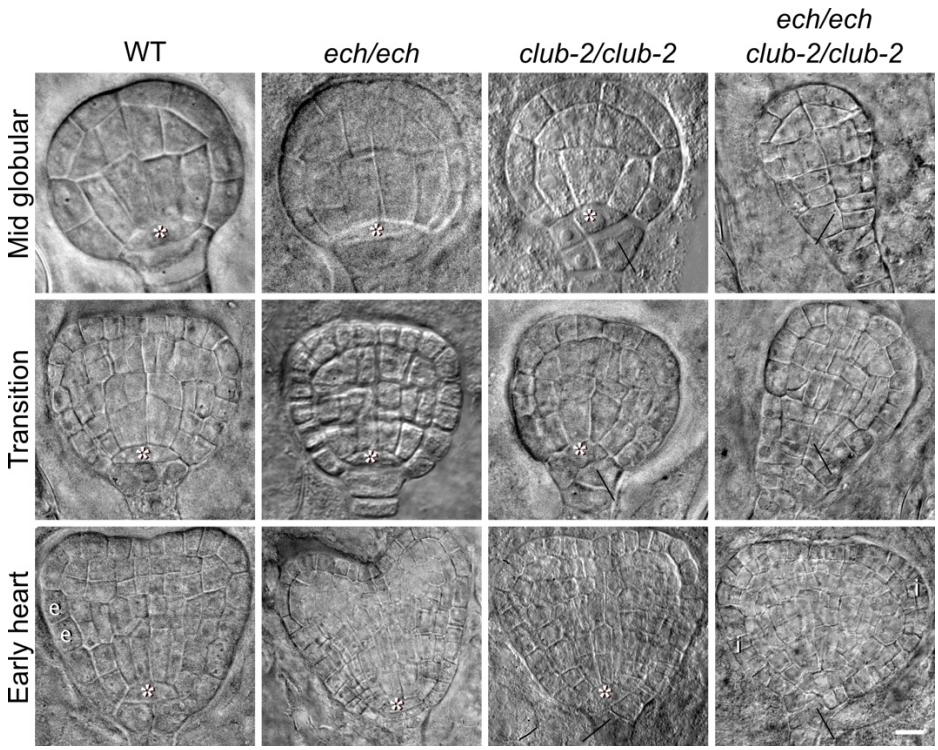

Figure 16: Embryogenesis in *ech* and *club-2* single and double mutants.
Null alleles used for both loci. Asterisk indicates the hypophysis or its progeny. Black arrows indicate aberrant cell division planes. Isodiametric cells and radial swelling occur in *ech club-2* heart stage double mutants (bottom right panel). e, elongated cell; i, isodiametric cell. n=157 embryos from three wild-type mother plants, n=123 embryos from three *ech* mother plants, n=511 embryos from six *club-2* mother plants, n=162 embryos from seven *ech club-2* mother plants. Scale bar: 10 µm. Image panel and caption adapted from Ravikumar et al., 2018.

To test which of the traits were synthetically enriched in the double mutants, we conducted a cellular analysis of single versus double mutant phenotypes. After a survey of 15 antibodies, Arabinogalactan proteins (AGP) glycans were found to be excellent markers for secretion. AGPs are assembled in the ER and Golgi and later are sorted to the cell wall through secretory vesicles (Nguema-Ona et al.,

2014). Immunostained root tip cells of null alleles of *ech* and *trappii* mutants showed that LM14 antibody, an AGP glycan labeled the cell walls. However, it failed to accumulate at the cell walls in *ech trs120-5* double mutants (Figure 17A). It is important to note here that the single mutant – *trs120-4*, is a null *trs120* allele. However, a hypomorphic *trs120* allele (*trs120-5*) was used for the double mutant. Therefore, the results signify a synergistic enrichment in secretion in the double mutants. In addition to this, the double mutants exhibited isodiametric cells in the elongation zone of the root (experiment conducted by Mr. Nils Kalbfuss, a student at Assaad lab, SEM imaging was done in collaboration with Dr. Wanner at LMU). I confirmed this observation, by carrying out a quantitative analysis of cell length vs width in the elongation zone of root tip cells labelled with FM4-64 in homozygous *ech* mutants, hypomorphic *trs120-5* mutants and the *ech trs120-5* double mutants. This data confirmed the primary observation and revealed that cell elongation was also abnormally impaired in the double mutants (Figure 17B). In conclusion, there was a synthetic enhancement of the secretion defect and of cell elongation in the double mutant embryos or seedlings.

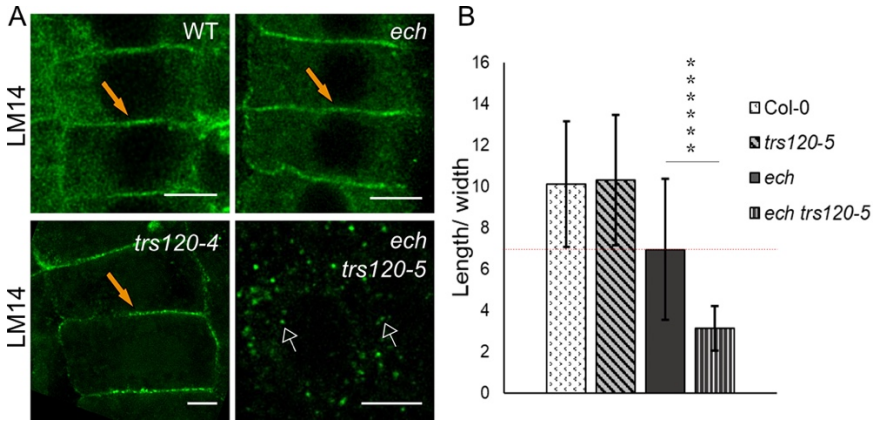

Figure 17: Double mutant analysis between *ech* and *trappii*.

(A). Antibody staining of root tips with LM14 antibody against AGP glycans. The polysaccharide is secreted to the cell surface (orange arrows) in the wild type and null single mutants, but it accumulates in intracellular vesicles (open arrows) in the *ech trs120*-5 double mutant. n=8 wild-type seedlings; n=6 *ech* seedlings; n=7 *trs120-4* seedlings; n=6 *ech trs120-5* seedlings. Scale bars: 5 µm. (B). Cell elongation in the root tip of single versus double mutants. Cell elongation is affected in *ech*-null but not in *trs120-5* hypomorphic alleles; it is synthetically (i.e., more than additively) enhanced in the *ech trs120-5* double mutant. Data are mean±s.d. Student's two-tailed t-test. ******$P<e^{-29}$. Ten seedlings were analyzed per genotype. n=41 wild type, n=40 *ech*, n=30

trs120-5 and n=59 *ech trs120-5* cells. Image panel and caption adapted from Ravikumar et al., 2018.

Next, I wanted to ascertain whether the proteins were dependent on each other with respect to their localization patterns. Therefore, I monitored and quantified the localization dynamics of TRAPPII in *ech* and vice versa. Firstly, P_{TRS120}::TRS120:GFP (Rybak et al., 2014) marker demonstrated normal cell plate localization dynamics in *ech* mutants (Figure 18A). Secondly, the quantification data also revealed that the number and appearance of TRS120:GFP positive endocompartments were identical between *ech* and the wild type in interphase cells (Figure 18B). Correspondingly, the localization pattern of ECH was unaffected by *trappii* mutation (Figure 18E, F. G; Ravikumar *et al.,* 2018). All things considered, the data suggests that ECHIDNA and TRAPPII might act in distinct pathways that are able to compensate for each other with regard to essential TGN functions such as secretion and cell elongation.

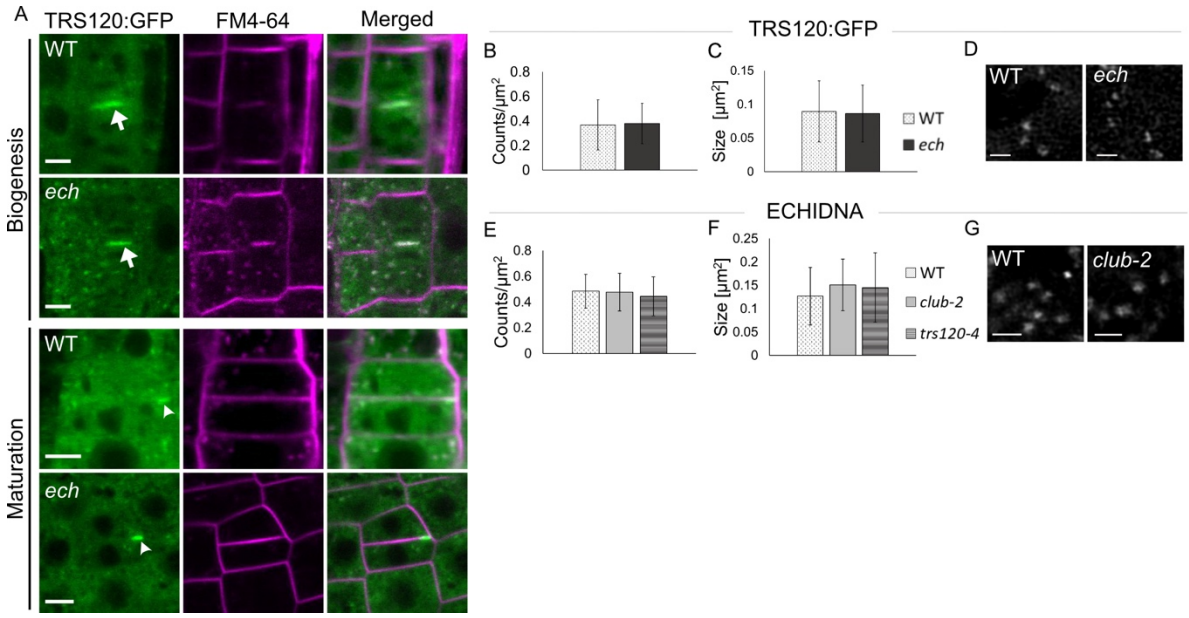

Figure 18: Behavior of TRS120-GFP in *ech* and of ECHIDNA in *trappii* mutants.

(A). Live imaging of P_{TRS120}::TRS120-GFP in wild-type and *ech* root tip cells. The mutant and wild-type localization dynamics are similar. Two partial and two complete time lapses were performed. Scale bars: 5 µm. (B-G) Comparison of normalized particle counts/cell area (B, E), average size of particles or aggregates (C, F) and representative CLSM deconvolved images (D, G) for TRS120-GFP live (B, C) (n=28 wild-type cells from seven seedlings; n=29 *ech* cells from eight seedlings) or ECHIDNA antibody (E-G) signal in segregating wild type and mutants (n=35 cells from five wild-type seedlings, n=52 cells from 19 *club-2* seedlings, n=64 cells from 12 *trs120-4* seedlings). Interphase cells were chosen for analysis. Single cells were selected as region of interest for the experiment. Data are mean±s.d. Student's two-tailed t-test. Scale bars: 1.5 µm. Image panel and caption adapted from Ravikumar et al., 2018.

4.2. TRS33 is a subunit of the TRAPPII complex and is required for its membrane association

The *Arabidopsis* TRAPPII complex localizes to the TGN/EE and is involved in specialized TGN functions (Ravikumar et al., 2018; Rybak et al., 2014; Steiner, Rybak, et al., 2016; Thellmann et al., 2010). In spite of its significantly important biological role, little information is known about its topology. Additionally, it is still unclear whether it more closely resembles yeast or metazoan orthologous complexes with respect to its subunit composition.

4.2.1. A synergistic interaction of the double mutant *trs33-1 club-2* link them functionally

To determine the link between the TRAPPII-specific subunits and the shared subunits of the complex, I carried out double mutant analysis between a shared subunit and a TRAPPII-specific allele. For this study, I chose AtTRS33, which is known to be a shared subunit of the TRAPPII and TRAPPIII complex in yeast and metazoans (Lipatova, Majumdar, & Segev, 2016; Thomas et al., 2018) and has been shown to be necessary for the TRAPPII assembly in yeast (Tokarev et al., 2009) and *Aspergillus* (Pinar et al., 2019). Previous work in the lab has already characterized a null insertion allele, *trs33-1* (Thellmann et al., 2010). This was crossed to a null allele of the TRAPPII-specific subunit CLUB/AtTRS130 (termed as *club-2*; Jaber *et al.*, 2010). The F2 generation of the cross did not have any seedlings that were double homozygous for null mutants of these genes, this implied that the *club-2 trs33-1* double mutants are either gametophytic or embryo lethal. Embryo phenotypes were then monitored to verify whether they were indeed embryo lethal.

The putative double mutant embryos showed aberrant embryo development in comparison to the single mutants, they remained globular even during the later stages, unable to acquire the heart shaped form and finally collapsing by the late heart stage (Figure 19A). The number of putative double mutants drastically

decreased from 8 to 15% at the globular (n = 234) and heart (n = 327; Figure 19B, C) stages to 0% by the torpedo stage (n = 155; ; Figure 19B, C). Since *trs33-1* and *club-2* have weak to moderate seedling lethality (Jaber et al., 2010; Thellmann et al., 2010), an additive phenotype would mean a strong seedling lethality but not an embryo lethal phenotype. Thus, the result of the double mutant analysis points to a synergistic genetic interaction (Guarente, 1993; Pérez-Pérez, Candela, & Micol, 2009). Taken together, the genetic interaction results suggests that there is a functional link between AtTRS33 and CLUB/ AtTRS130.

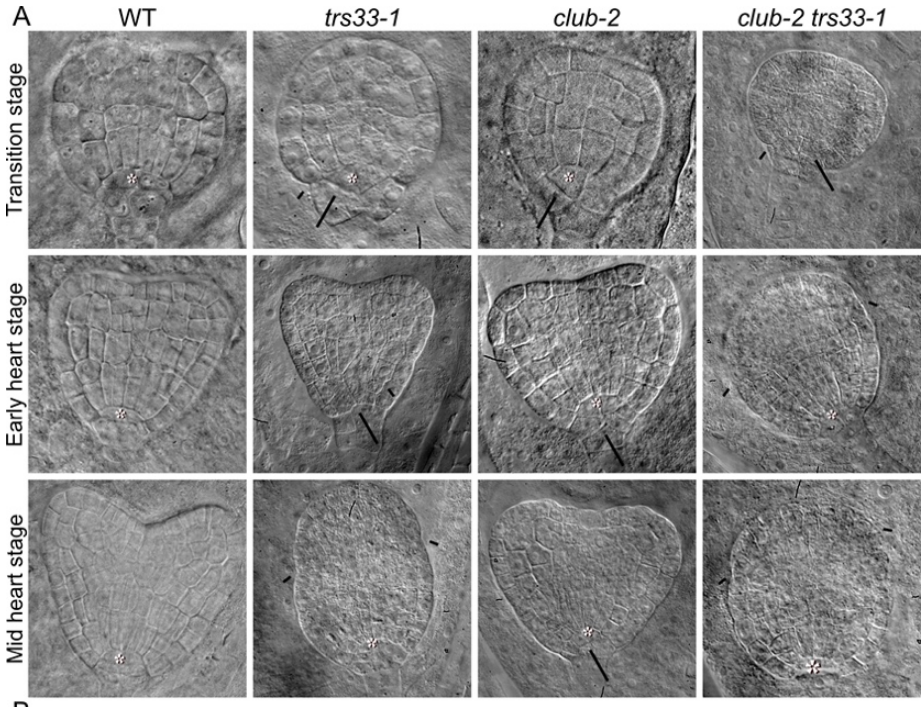

B

		WT looking	*club-2*	*trs33-1*	*club-2trs33-1*	Total
Col–0	Heart	67	0	0	0	67
	Torpedo	49	0	0	0	49
club-2	Heart	169	29	0	0	198
	Torpedo	47	7	0	0	54
trs33-1	Heart	86	0	18	0	104
	Torpedo	58	0	7	0	65
trs33-1 club-2	Heart	240	20	31	36	327
	Torpedo	122	14	19	0	155

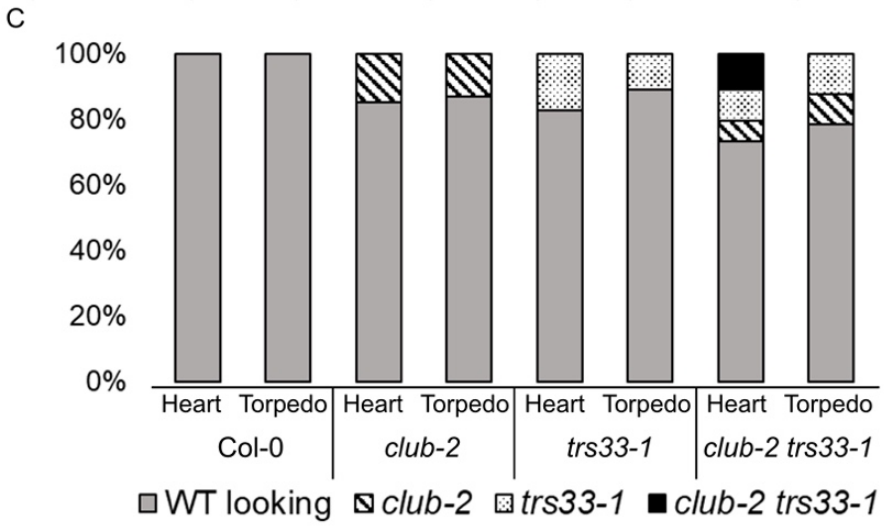

Figure 19: Double mutant analysis between *trs33-1* and *club-2*.

(A). Embryogenesis in *trs33-1* and *club-2* single and double mutants. Null alleles were used for both loci. Asterisk points to the hypophysis or to its progeny. Black arrows: aberrant division plane. Blue arrowheads: aberrant cell shape. Note the aberrant cell division and deformed shape of *trs33-*

1 club-2 heart stage double mutants (bottom right panel). We detected 11% (n = 327) heart stage but 0% torpedo stage (n = 155 torpedo embryos in total; see Figure S2) putative double mutant embryos from mother plants segregating both *trs33-1* and *club-2*. n = 157 embryos from three wild-type mother plants, n = 219 embryos from three *trs33-1* mother plants, n = 511 embryos from six *club-2* mother plants, n = 870 embryos from seven *trs33-1 club-2* mother plants. (B). Incidence of *club-2 trs33-1* putative double mutant phenotypes. The table lists the number of embryos for each genotype at heart and torpedo stages. n = 3 wild-type mother plants; n = 6 *club-2* mother plants; n = 3 *trs33-1* mother plants; n = 7 *trs33-1 club2* mother plants. (C). Incidence (%) as a graph. Siliques of wild type (Col-0), *club-2* and *trs33-1* single mutants, and plants segregating both *club-2* and *trs33-1* were analyzed for embryo phenotypes. Single mutant embryos were observed at all stages. In contrast, putative double mutants (black fill) were observed until the heart but not at the torpedo stage. Image panel and caption adapted from Kalde et al., 2019.

4.2.2. *trs33-1* mutants are necessary for the membrane localization of TRS120:GFP

TRS33 is a shared TRAPPII and TRAPPIII complex subunit identified in yeast and metazoans (Lipatova et al., 2016; Thomas et al., 2018; Tokarev et al., 2009). In *Arabidopsis*, AtTRS33 has been implicated in cytokinesis and was identified in the TRAPPII interactome (Kalde et al., 2019; Rybak et al., 2014; Thellmann et al., 2010). However, in *Arabidopsis* the functional link of AtTRS33 to the TRAPPII complex is still unclear. Therefore, I next assessed the effect of the *trs33-1* mutation on the localization dynamics of the TRAPPII-specific subunit AtTRS120. As with previous studies, in the wild type background, TRS120:GFP localized to the cytosol, TGN endocompartments in interphase cells (Figure 20A) and to the cell plate in cytokinetic cells (Figure 20B, C), reorganizing to the leading edges during maturation (Figure 20C). However, in the *trs33-1* mutant background, only cytosolic TRS120:GFP signal was present but TGN endocompartments were completely absent in interphase cells (Figure 20A). In cytokinetic cells, the TRS120:GFP signal was present as a diffuse cytosolic cloud around the cell plate and during maturation it re-organized to the leading edges in the same diffused manner with very weak cell plate signal (Figure 20B, C, D). These results suggests that AtTRS33 is necessary for the proper localization dynamics of AtTRS120 during cytokinesis and also for its membrane association.

Along with the double mutant analysis, this data ascertains a functional link between AtTRS33 and AtTRS120 in the *Arabidopsis* TRAPPII complex.

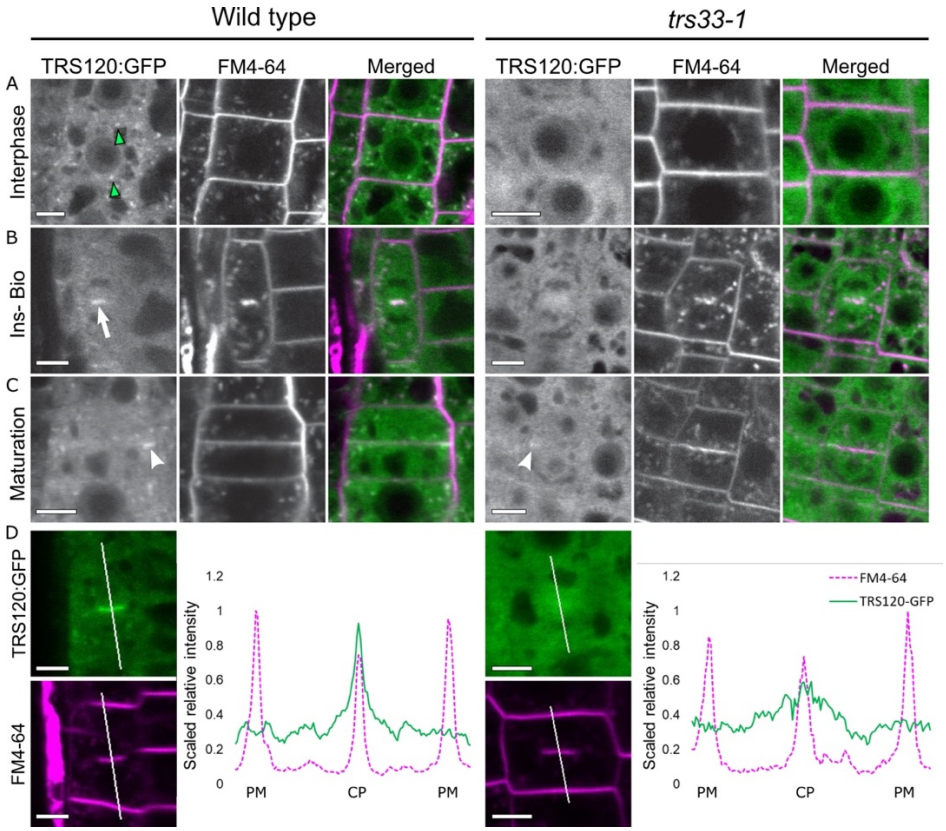

Figure 20: TRS33 is required for normal subcellular localization of TRS120:GFP.
Live imaging of TRS120:GFP (green) and FM4-64 (magenta) in roots of P_{TRS120}::TRS120:GFP plants. (A). Cells at interphase show TRS120:GFP enriched at endomembrane compartments (green arrowheads) in the wild type, but not in *trs33-1*, where only a cytosolic haze can be seen. (B). During early stages of cytokinesis (Ins- Bio or cell plate initiation and biogenesis), TRS120:GFP is enriched at the cell plate (white arrow) in the wild type, but not in *trs33-1*. (C). During late stages of cytokinesis (cell plate maturation), TRS120:GFP reorganizes to the leading edges of the cell plate (white arrowhead) in the wild type. By contrast, only a weak and relatively diffuse TRS120:GFP signal can be detected at the leading edges of the cell plate in the *trs33-1* mutant (white arrowhead). (D). Line graphs depicting scaled relative fluorescence intensities. A sharp peak is seen at the cell plate (CP) in the wild type (red arrowhead), but not in *trs33-1*. PM, plasma membrane. At least 10 seedlings were imaged per marker line. n 5 8 for wild type, n 5 7 *trs33-1* for cytokinetic cells. Scale bars= 5 µm. Image panel and caption adapted from Kalde et al., 2019.

4.3. The TRAPPII complex acts as a putative Rab GEF

In *Arabidopsis*, the Rab-A GTPases form a clade of Rab GTPases that act primarily at the cell edges and at the TGN (Elliott et al., 2020; Rutherford & Moore, 2002). The Rab-A5 subclade of Rab-A GTPases are localized to the TGN in *Arabidopsis* and are known to label the cell plates in cytokinetic cells. They were also shown to mark the geometric edges of the cells i.e., where two faces meet, signifying an important spatial domain in the cells (Kirchhelle et al., 2016). The Rab-A5c GTPases were also reported to be essential for growth anisotropy of cells and to help control the direction of growth in lateral roots independently of cellulose microtubule orientation (Kirchhelle et al., 2016; Kirchhelle, Garcia-Gonzalez, Irani, Jérusalem, & Moore, 2019) . I wanted to verify if the localization of the Rab-A5c GTPases is dependent on the TRAPPII complex.

4.3.1. The edge localization pattern of YFP:RAB-A5c is defective in *trappii* mutants

I observed the localization dynamics of Rab-A5c GTPase in the immunostained root tip cells of the wild-type and *trappii* mutants that were crossed with a $P_{Rab\text{-}A5c}$::YFP:Rab-A5c (Kirchhelle et al., 2016) marker and labeled with a GFP antibody. In the wild type cells, YFP:Rab-A5c labeled the cytosol and were clearly marking the geometric edges of the cells. However, in both the *trappii* mutants, the edge localization of YFP:Rab-A5c was abolished (Figure 21). This interesting observation suggests that the TRAPPII complex might be necessary for the proper membrane association of the Rab-A5c GTPases.

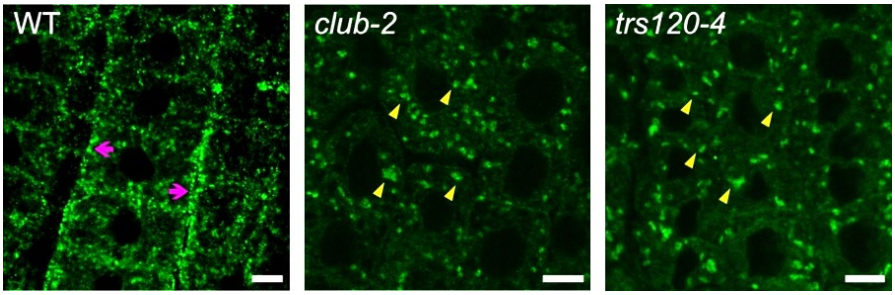

Figure 21: Localization dynamics of P_{A5c}::YFP:Rab-A5c in the wild type and *trappii* mutants root tips.

Immunostained cells with YFP:Rab-A5c in green. The edge localized is abolished in both *trappii* mutants. Yellow arrowheads point to aberrant localization of YFP:Rab-A5c in the cytosol of the *trappii* mutants. Note the absence of YFP:Rab-A5c at the cell edges of the *trappii* mutants. Magenta arrow points to edge localized YFP:Rab-A5c in the wild type root tips. n = 10 seedlings for wild type; n = 8 seedlings for *club-2*; n = 5 seedlings for *trs120-4.* Size bars = 5 µm.

4.3.2. The localization of YFP:RAB-A2a in *trappii* mutants show cell plate re-localization defects

Previous studies have shown that the TRAPPII complex and RAB-A2a GTPases play a role during cytokinesis (Chow et al., 2008; Qi et al., 2011; Rybak et al., 2014). I wanted to verify these results and determine their localization dynamics during cell plate initiation and maturation. To this extent, live-cell imaging of root tip cells with P_{a2a}::YFP:RAB-A2a marker (Chow et al., 2008; Kalde et al., 2019; Figure 24A, B) as well as with P_{TRS120}::TRS120:GFP (Rybak et al., 2014; Figure 22) was carried out during cytokinesis. Both the markers localized at the cell plate during cell plate initiation and later also re-organized to the leading edges of the cell plate during maturation (Kalde et al., 2019).

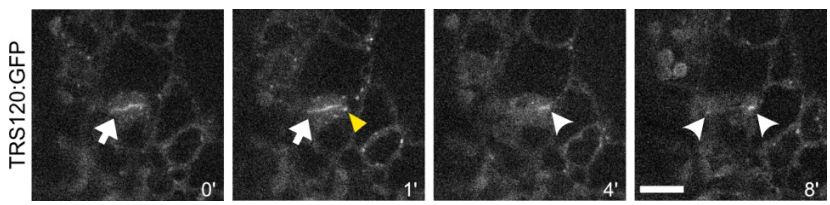

Figure 22: Localization pattern of P_{TRS120}::TRS120:GFP.

Spinning disk confocal microscopy of root tips. TRS120:GFP. Time lapses are shown, with minutes indicated in the right panel. Maximum intensity projections of 4D imaging data. White arrows point to cell plates. White arrow heads point to the leading edges of the CP. Endosomal compartments

in the cytosol are labeled by yellow arrowheads. n = 10 hypocotyls, 7 root tips and 3 petioles. Size bars = 10µm.

I then determined the YFP:RAB-A2a localization dynamics in the null *trappii* specific alleles. In seedling-lethal null *trappii* mutants, even though YFP:RAB-A2a retained membrane association and was present at the cell surface, it additionally labeled endosomal (or FM4-64 positive compartments) compartments present next to the cell plate and during maturation, YFP:RAB-A2a failed to reorganize to the leading edges of the cell plate (Figure 23A, B, Figure 24B and Figure 27A, B). The data shows that YFP:RAB-A2a does not require the TRAPPII complex for its initial recruitment to the membranes, but is necessary later for its re-organization during cell plate expansion. In conclusion, both YFP:RAB-A2a and TRS120:mCherry are present at the cell plate and colocalize with each other during cytokinesis and the localization dynamics of YFP:RAB- A2a depend on TRAPPII function.

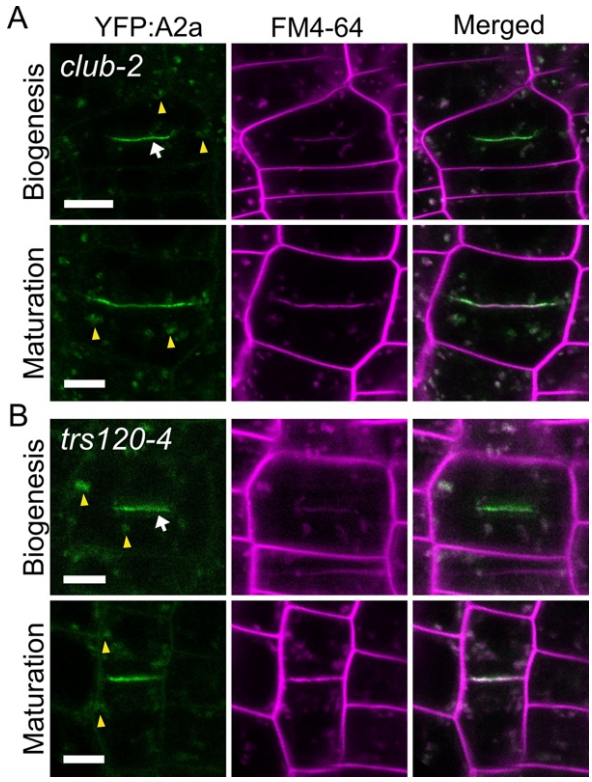

Figure 23: The behavior of YFP:RAB-A2a variants in *trappii* root tips.

Live imaging with YFP marker in green and FM4-64 in magenta. (A, B). P_{A2a}::YFP:RAB-A2a does not completely reorganize to the leading edges of the cell plate in both *trappii* mutants during cell plate maturation. n = 35 cytokinetic cells for *club-2*; n =20 cytokinetic cells for *trs120-4*; at least 20 seedlings were imaged per line. White arrows point to cell plates. Endosomal compartments in the cytosol are labeled by yellow arrowheads. Biogenesis and maturation refer to the cell plate at different cytokinesis stages. At least 10 seedlings were imaged per marker line. Size bars = 5 µm. Image panel and caption adapted from Kalde et al., 2019.

4.3.3. The localization pattern of YFP:RAB-A2a CA and DN variants in *trappii* mutants is perturbed

In yeast and metazoans, the TRAPPII complex is well studied for its role as a Rab-GEF (Morozova et al., 2006; Riedel et al., 2018). I wanted to test whether this holds true in *Arabidopsis* as well. I hypothesized that the TRAPPII complex might act as an upstream GEF for RAB-A2a because of its dependance on the TRAPPII complex for its proper localization at the cell edges and also during cytokinesis (4.3.1; 4.3.2). To test this hypothesis, I determined the localization dynamics of the dominant negative (DN) and constitutively active (CA) RAB-A2a variants, in wild-type versus *trappii* (*trs33-1*) mutant backgrounds and performed

quantitative analysis for signal intensity at the cell plate vs the leading edges, for the signal intensity at the cell plate vs the plasma membrane and also for the numbers of cells that showed either total, partial or no re-localization of RABA2a:YFP and its variants to the leading edges. The RAB-A2a variants are expressed under their native promoter and fused to YFP. They have been previously described by Chow et al. 2008, for convenience purposes they were termed as YFP:A2a-DN (GDP-bound) and YFP:A2a-CA (GTP-bound).

As an initial experiment, I quantified the localization dynamics of YFP:RAB-A2a in the *trs33-1* mutant root tips. YFP:A2a labeled the cell plate of the cytokinetic cells in the mutants (Figure 24A). However, unlike the other *trappii* mutants (4.3.2), *trs33-1* showed at least partial re-localization of the YFP:A2a signal to the leading edges of the cell plate (occurring at a frequency of 70.58%; Figure 24A, B and Figure 27B) during cell plate expansion and maturation.

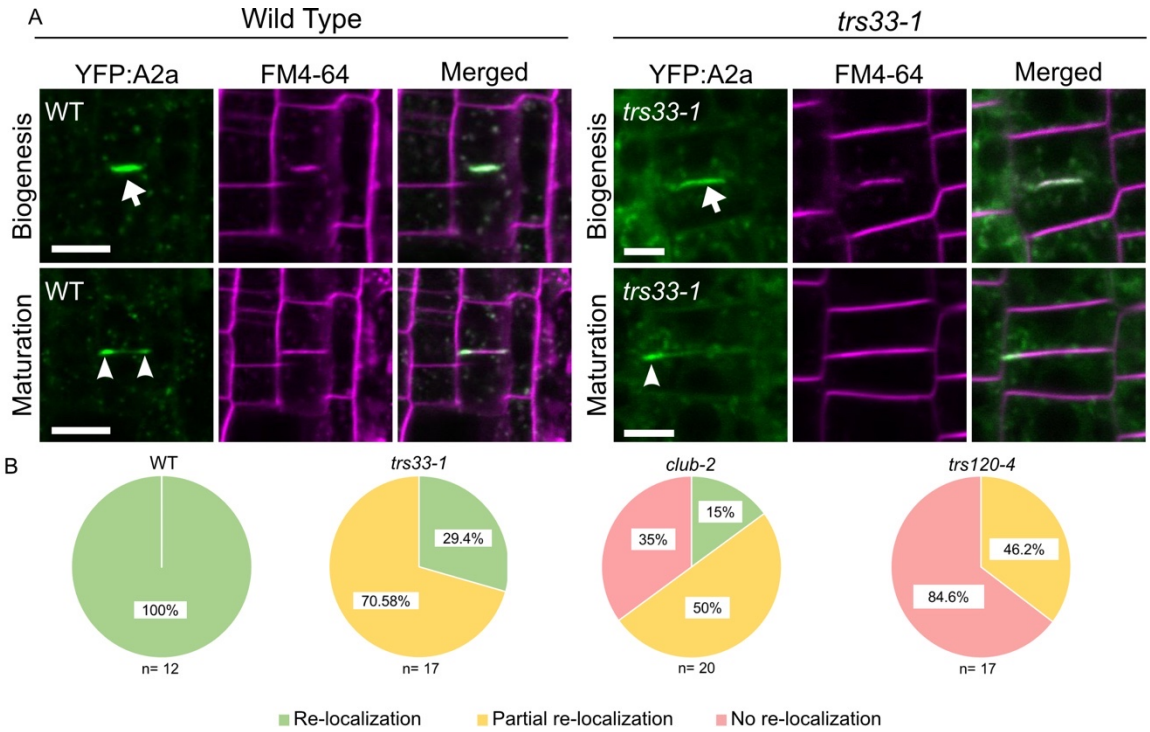

Figure 24: Sorting of YFP:RAB-A2a in *trs33-1* root tips.

(A). Live imaging of P_{A2a}::YFP:RAB-A2a (YFP:A2a, in green) in wild type and *trs33-1* backgrounds. Membranes are stained with FM4-64 (magenta). YFP:A2a is present at the cell plate during the anaphase-to telophase transition and reorganizes to the leading edges at the end of cytokinesis. This is seen in both the wild type and in *trs33-1*. The incidence of untethered endosomal

compartments in the vicinity of the cell plate is higher in *trs33-1* than in the wild type. White arrows point to cell plate. White arrow heads point to the leading edges of the CP. Biogenesis and Maturation refer to the cell plate at different cytokinesis stages. At least ten seedlings were imaged per marker line. n = 8 wild type, n = 16 *trs33-1* cytokinetic cells. Size bars = 5µm. (B). Pie charts depicting incidence of fully (green) or partially (yellow) re-localized signal, or cell plates with no re-localization (pink). n=12, 17, 20 and 17 expanding cell plates in WT, *trs33-1*, *club-2* and *trs120-4*, respectively. At least 20 seedlings were imaged per line. Image panel and caption adapted from Kalde et al., 2019.

Localization dynamics observed in live imaging and later quantification of the data showed that the YFP:A2a-DN is recruited to the cell plate in the wild type and later partially re-localized to the leading edges of the cell plate during maturation (at a frequency of 69.2% total re-localization and 53.8% of partial re-localization; Figure 25A, B and Figure 27A, B). Even though one would expect GDP-bound Rabs to remain cytosolic and not associated to membranes, my observation is compatible with previous studies showing that dominant-negative Rab GTPase mutants can retain membrane localization, and that YFP:A2a-DN localizes to the cell plate (Asaoka et al., 2013; Chow et al., 2008). Interestingly, in *trs33-1* mutants, even though the cell plate was weakly labeled, there were a large number of YFP:A2a-DN-labelled endocompartments, forming a cloud of punctae in the vicinity of the cell plate (Figure 25A). This localization pattern was similar to a previous observation of KNOLLE-positive cytokinetic compartments in *trappii* mutants (Jaber et al., 2010; Rybak et al., 2014; Thellmann et al., 2010). Almost no re-localization of the cell plate to the leading edges was observed during cell plate maturation in the *trs33-1* mutants (at a frequency of 12.5% partial re-localization and 87.5% no re-localization; Figure 25B; Figure 27B). Another interesting observation was the decreased cell plate intensity versus plasma membrane intensity in comparison to the wild type ($p<0.00005$; Figure 27C). The results suggest a synthetic enhancement of the YFP:A2a-DN localization phenotype in *trappii*.

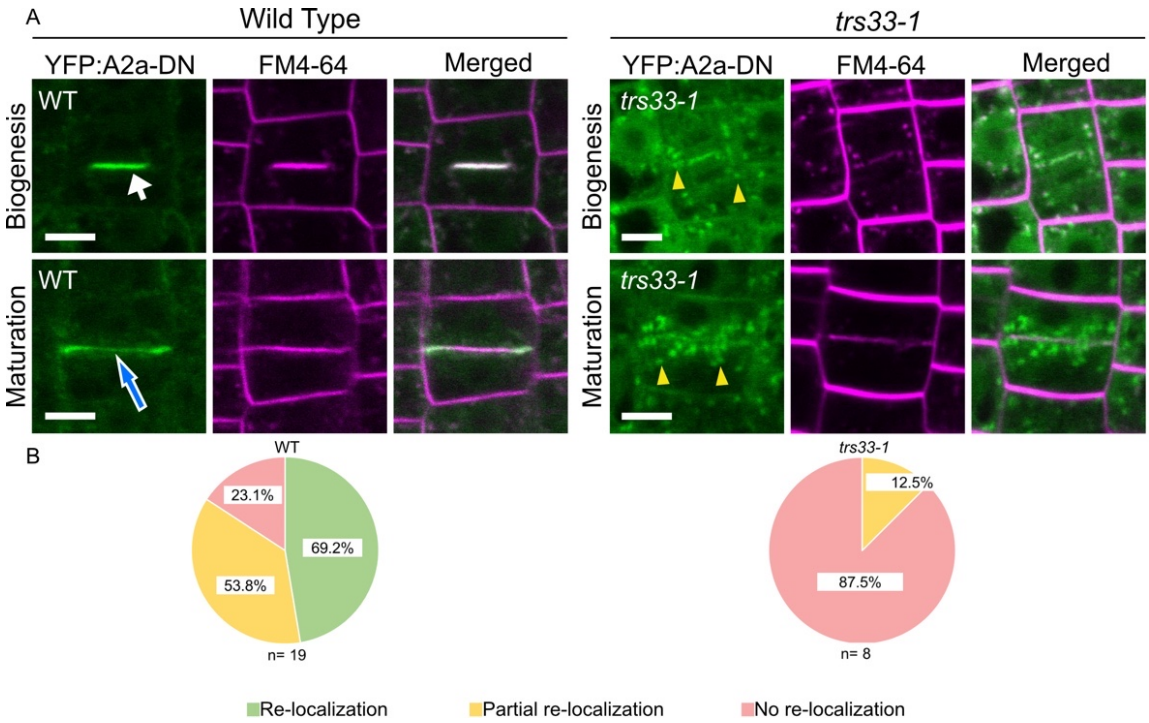

Figure 25: Sorting of YFP:RAB-A2a-DN, a GDP bound variants in *trs33-1* root tips.

Live imaging of YFP:RAB-A2a-DN (YFP:A2a-DN, in green) expressed from the RAB-A2a native promoter in wild type and *trs33-1* backgrounds. (A). of P_{A2a}::YFP:A2a-DN (GDP-bound) labels the cell plate but, in contrast to YFP:A2a (WT), fails to reorganize to the leading edges of the cell plate in WT root tips. In *trs33-1*, YFP:A2a-DN weakly labels the CP and predominantly localizes to endosomal compartments around the cell plate (yellow arrowheads). Thus, *trs33-1* synthetically enhances the YFP:A2a-DN localization phenotype. White arrows point to cell plate and the white-rimmed blue arrow to a cross wall. Biogenesis and Maturation refer to the cell plate at different cytokinesis stages. At least ten seedlings were imaged per marker line. n = 10 wild type, n = 6 *trs33-1* cytokinetic cells. Size bars=5µm. (B). Pie charts depicting incidence of fully (green) or partially (yellow) re-localized signal, or cell plates with no re-localization (pink). n = 19 and 8 expanding cell plates in WT and *trs33-1*, respectively. At least 20 seedlings were imaged per line. Image panel and caption adapted from Kalde et al., 2019.

The GTP-bound YFP:A2a-CA labelled wild-type cell plates in a more uniform manner than YFP:RAB-A2a (Figure 26A). It also stably labeled the plasma membrane of the cytokinetic cells, which was not observed in either YFP:RAB-A2a or YFP:A2a-DN (Figure 24A; Figure 25A; Figure 26A, B). Therefore, the cell plate to plasma membrane intensity was almost equal and the ratio was roughly 1.0 (Figure 27C). However, the opposite was true in the *trs33-1* mutants and also in *trs120-4* mutants (Kalde et al., 2019). The cell plate labeled more strongly than the plasma membrane (Figure 26A, B and Figure 27C). This result points to a

partial suppression of the YFP:A2a-CA localization phenotype. Here, in order to understand the results, it is important to consider the TRAPPII complex as a GEF. In the absence of a GEF, one would expect an increase in the number of GDP-bond Rab pools and a decrease in GTP-bound Rab pools. However, since TRAPPII is not the only protein that is responsible for the proper localization of Rabs (as shown before in 4.3.1), we can therefore presume enhancement and (at least partial) suppression phenotype of GDP bound and GTP bound YFP:A2a respectively, in the *trappii* mutants. YFP:A2a-CA is more correctly localized the cell plate in the *trappii* mutants than in the wild type, which infers a partial suppression phenotype. A complete suppression phenotype would show a complete re-localization of the YFP:A2a-CA signal to the leading edges of the cell plate in the *trappii* mutants, which is not what I observed in my imaging experiments.

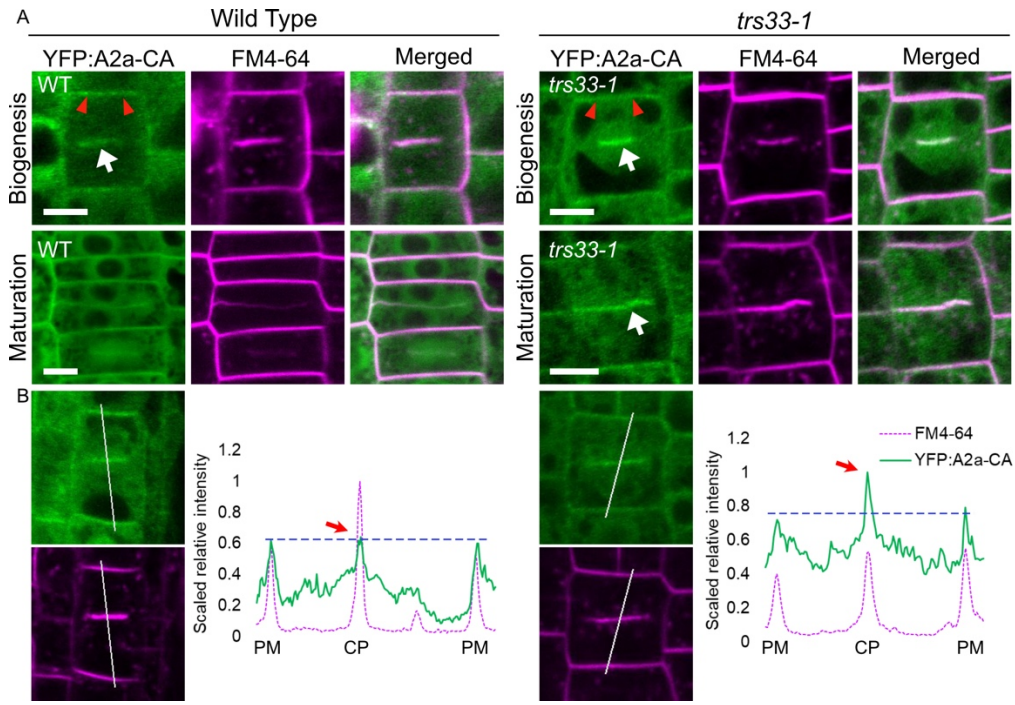

Figure 26: Sorting of YFP: RAB-A2a-CA, a GTP bound variants in *trs33-1* root tips.

Live imaging of YFP: RAB-A2a-CA (YFP:A2a-CA, in green) expressed from the RAB-A2a native promoter in wild type and *trs33-1* backgrounds. Membranes are stained with FM4-64 (magenta). (A). P_{A2a}::YFP:A2a-CA (GTP-bound) only weakly labels the cell plates of WT root tips and ectopically localizes to the plasma membrane (red arrowheads). In contrast, in the *trs33-1* mutants, it has a stronger signal at the cell plate and a weaker ectopic signal. n = 8 wild type, n = 10 *trs33-1* cytokinetic cells. (B). Line graphs depicting scaled relative fluorescence intensities of

P_{A2a}::YFP:A2a-CA. Even peaks of maximal intensity (red arrows) are seen at the CP in both the wild-type and in *trs33-1*, but in *trs33-1* the intensity relative to the ectopic plasma membrane signal is higher. Thus, *trs33- 1* partially suppresses the YFP:A2a-CA localization phenotype. White arrows point to cell plate. CP: cell plate. PM: plasma membrane. Biogenesis and Maturation refer to the cell plate at different cytokinesis stages. At least ten seedlings were imaged per marker line. Size bars = 5µm. Image panel and caption adapted from Kalde et al., 2019.

The localization data clearly show that the mutations in the *trappii* complex subunits firstly, although initially show normal cell plate localization, cause defects in the relocalization of YFP:A2a signal to the leading edges of the cell plate (Figure 27A, B). Secondly, they cause enhancement of the GDP-bound YFP:A2a-DN localization phenotype and partial suppression of the GTP-bound YFP:A2a-CA localization phenotype (Figure 27B, C), which provides very convincing genetic evidence that TRAPPII functions upstream of RAB-A2a. Therefore, these results along with the known function of the TRAPPII complex in yeast and metazoans, strongly suggest that the TRAPPII complex might act as a putative GEF for Rab-A GTPases in *Arabidopsis*.

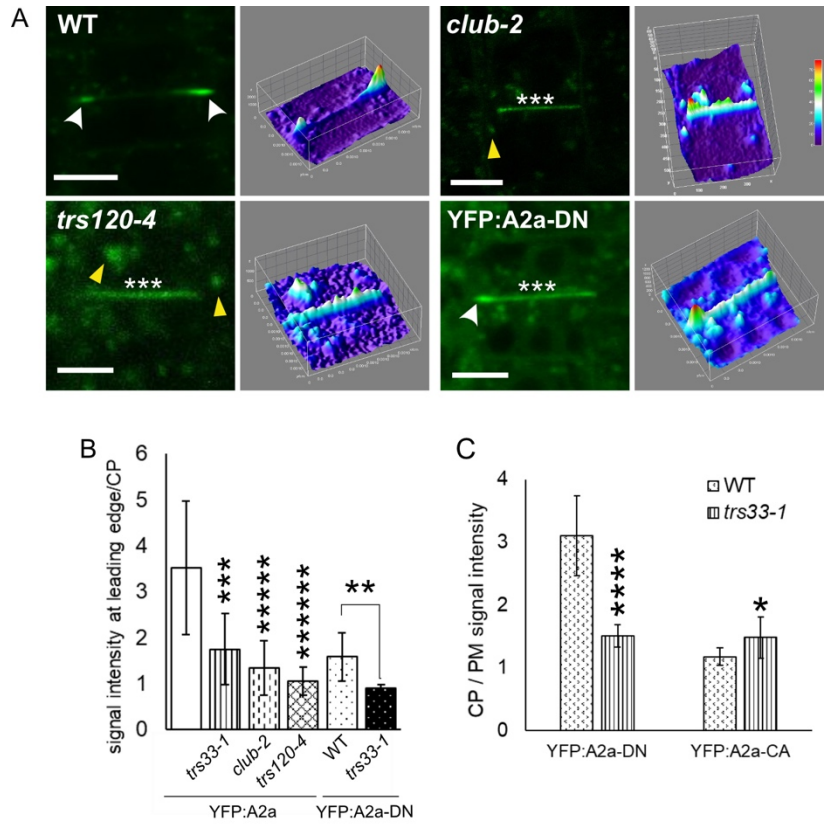

Figure 27: The behavior of YFP: RAB-A2a, -DN and -CA in wild-type versus *trappii* root tips. Live imaging with YFP marker in green. (A). Left: P_{A2a}::YFP:A2a in wild-type versus mutant backgrounds and P_{A2a}::YFP:A2a-DN (GDP-bound) in wild-type. Right: 3D heat maps of YFP:A2a depicting fluorescence intensity along the z axis with a scale ranging from blue (low) to red (high). YFP:A2a does not completely reorganize to the leading edges of the cell plate in *trappii* mutants and nor does YFP:A2a-DN fully reorganize to the leading edges of the cell plate in WT root tips. White arrow heads point to the leading edges of the CP and yellow arrow heads to aberrant endosomal compartments. Asterisks indicate aberrant YFP:A2a or YFP:A2a-DN at the center of the cell plate. (B). Ratio of signal intensity at the leading edges versus the center of the cell plate (CP). This is significantly decreased for *trappii*-specific and *trs33-1* mutants. There is also a significant decrease for P_{A2a}::YFP:A2a-DN in *trs33-1* versus wild-type backgrounds. * P < 0.02; ** P < 0.01; *** P< 0.001; **** P < 0.0001; ***** P<0.000001. (C). Ratio of signal intensity at the cell plate (CP) versus the plasma membrane (PM). This is significantly decreased for P_{A2a}::YFP:A2a-DN in *trs33-1* (****: P < 0.0001). Conversely, this is significantly increased for P_{A2a}::YFP:A2a-CA in *trs33-1* (*: P < 0.02). Cell cycle stage: expansion to maturation. Size bars = 5µm. Image panel and caption adapted from Kalde et al., 2019.

4.4. Post-translational modification and regulation of the TRAPPII complex

4.4.1. The TRAPPII complex is a target of shaggy-like kinases

While trying to understand the regulation of the TRAPPII complex under different environmental conditions, Assaad lab identified BIN2, a shaggy-like kinase (AtSK) as the only interactor of the TRS120$^{499-1187}$ (or TRS120-T2) truncated moiety in a large scale Y2H screen with 2400 different pair-wise tests of diverse kinases with TRAPPII complex subunits. This points to a specific and robust interaction between the two partners. When investigated *in silico* for GSK3 target sites on AtTRS120, we could identify three putative sites - S923, S971 and S1165, which were termed as α, β and γ respectively. These are conserved among higher plants and reside in the plant-specific moiety of AtTRS120.

To elucidate the mechanism of interaction between AtTRS120 and BIN2, site directed mutations were generated on all the three putative AtSK sites in TRS120-T2 and TRS120:GFP, to non-phosphorylatable alanine residues (S to A) or constitutively phosphorylated (also called phosphomimetic) aspartate residues (S to D). The point mutations were cloned as cDNA sequences for expression in yeast and bacteria (TRS120-T2 and TRS120-T2 SβD construct for Y2H was generated by Dr. Alexander Steiner, a postdoctoral fellow in the lab). In Y2H screens (performed by Dr. Melina Altmann in the lab of our collaborator Dr. Pascal Braun at Helmholtz Zentrum, Munich), the BIN2-AtTRS120 interaction, but not TRAPPII complex interactions, was abolished when all three sites were mutated (Figure 28).

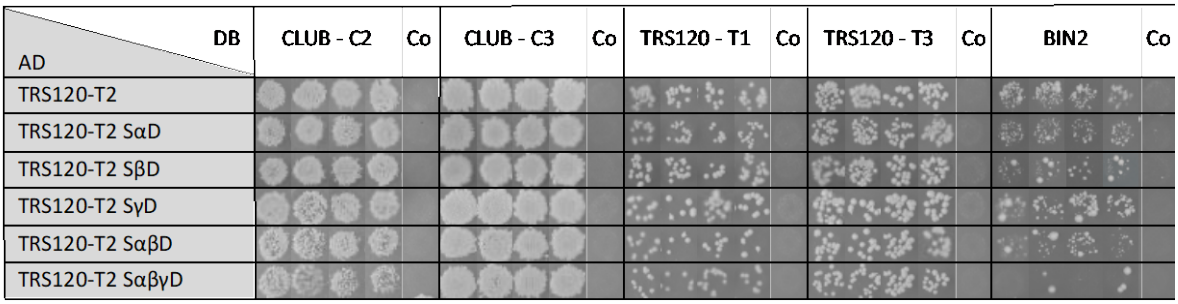

Figure 28: Y2H assay for testing TRAPPII-Shaggy-like kinase interactions.

Yeast two-hybrid assays of interactions between BIN2 and TRAPPII truncations (CLUB-C2, CLUB-C3, TRS120-T1, TRS120-T3; Fig. S3A), as positive controls, fused to the GAL4 DNA-binding domain (DB) and TRS120-T2 truncation and its phosphomutants TRS120-T2- SαD, SßD, SγD, SαßD and SαßγD fused to the Gal4 activation domain (AD). The panels are from different plates. For the control only one representative example is shown (Co). The results show interactions between BIN2 and AtTRS120-T2 wild-type and phosphovariants; there was, however, no interaction if all three target sites were phosphomimetic. As negative control, the BIN2-DB construct was tested with the empty AD vector. This interaction was verified by pairwise one-on-one mating in four independent replicate experiments. Image panel by Dr. Melina Altmann.

Next, kinase assay with mass spectrometry readouts were performed from purified proteins of the different kinases from the AtSK family and TRS120-T2 as the substrate. The kinase assay was performed in the Assaad lab (kinase assays of one SK11 and one BIL2 kinase replicate were performed by Ms. Miriam Abele), and the mass spec run and analysis were performed at the BayBioMS facility at the TUM. The results showed that indeed the AtSKs phosphorylated the substrate on the three sites in a time and concentration (of the kinase) dependent manner. We could also observe from these results that mostly all kinases phosphorylated and preferred the TRS120-γ site (Figure 29).

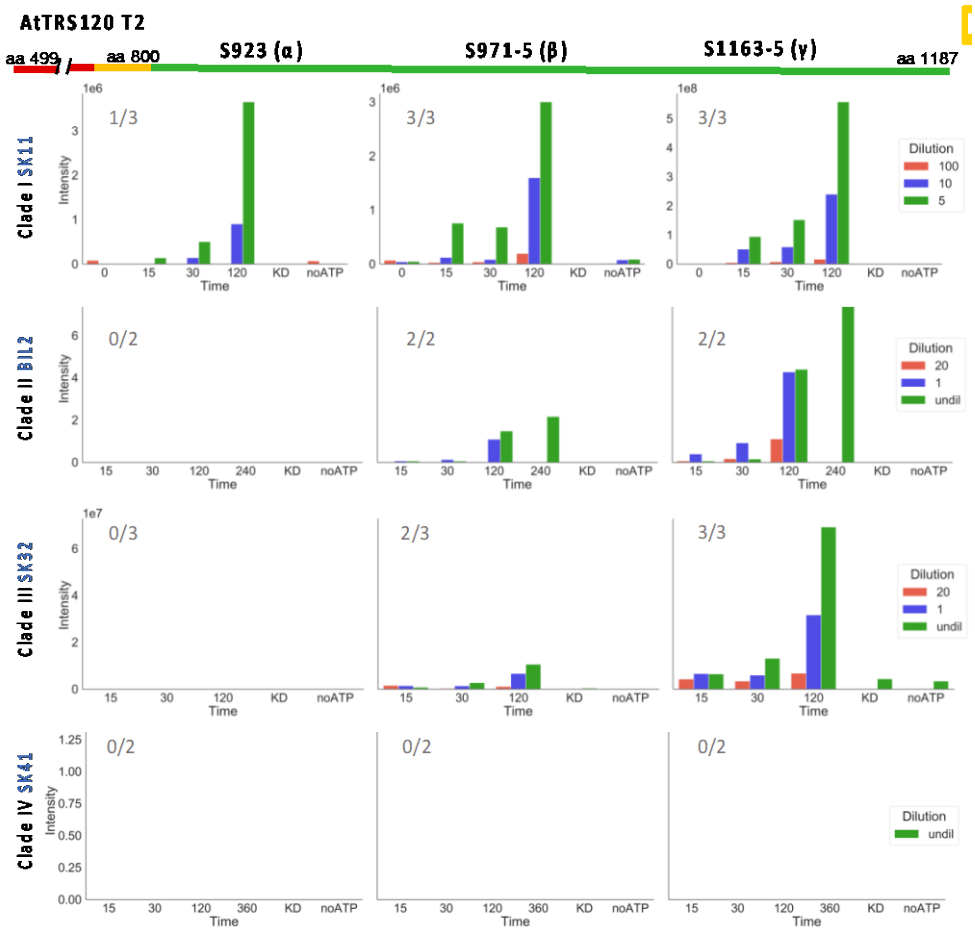

Figure 29: Kinase assay for testing TRAPPII-Shaggy-like kinase interactions.
AtTRS120-T2 has highly (red) and moderately (orange) conserved sequences, as well as plant-specific sequences (green). Three GSK3 consensus sites (referred to as α, β, γ) can be found in the plant-specific T2 domain. For the kinase assay, one member of each shaggy-like kinase clade was used with the TRS120-T2 truncation as substrate. AtSKs in clades I-III differentially phosphorylate the substrate at three GSK3 consensus sites (with a preference for the γ site) in a time-dependent and concentration-dependent manner. A clade IV AtSK did not phosphorylate at all. Samples incubated for 120 minutes in a kinase buffer without ATP, or samples with kinase that was heat inactivated, served as negative controls. The numbers in grey in each plot denote the number of times the phosphorylation event was seen in the given number of independent replicates. Image panel and captions by Miriam abele.

Three lines of evidence confirm that TRAPPII is a target of AtSKs. Firstly, the large Y2H screen showed that BIN2 and AtTRS120 was the only binary interaction amongst various kinases. Secondly, Y2H screen with the phosphomimetic variants revealed that BIN2-AtTRS120 interaction was not conserved anymore when all three putative AtSK target sites were mutated. And thirdly, kinase assay

with mass spec readout confirmed a time and concentration dependent interaction of AtTRS120 with the various members of the AtSK kinase clade. Taken together, these results strongly indicate that a specific and robust interaction exists between the TRAPPII and AtSK kinases.

4.4.2. The phosphorylation status of the TRAPPII complex affects its localization pattern and membrane association

Site directed mutations at the AtTRS120 AtSK phosphosites introduced into genomic sequences were fused with GFP and were transformed into the segregating *trs120-4* mutant line (these constructs were generated by Dr. Alexander Steiner). The transformed lines were termed as phosphovariants. Previous studies have shown that in the wild-type, TRAPPII complex resides in the cytosol, at the TGN endocompartments and at the cell plate (Ravikumar *et al.,* 2018; Rybak *et al.,* 2014; Figure 30A). The phosphovariants also exhibited similar localization patterns. However, the impact of the phosphorylation status in the phosphovariants affected AtTRS120 membrane association. The phosphomimetic lines differed in their localization pattern in comparison to the non-phosphorylatable lines. The former was more membrane associated, with lower cytosolic signal in comparison to the latter (Figure 30A, B). The differences in the localization dynamics between the phosphovariants point to the specificity of the AtTRS120 phosphorylation status in regulating AtTRS120 localization and its membrane association.

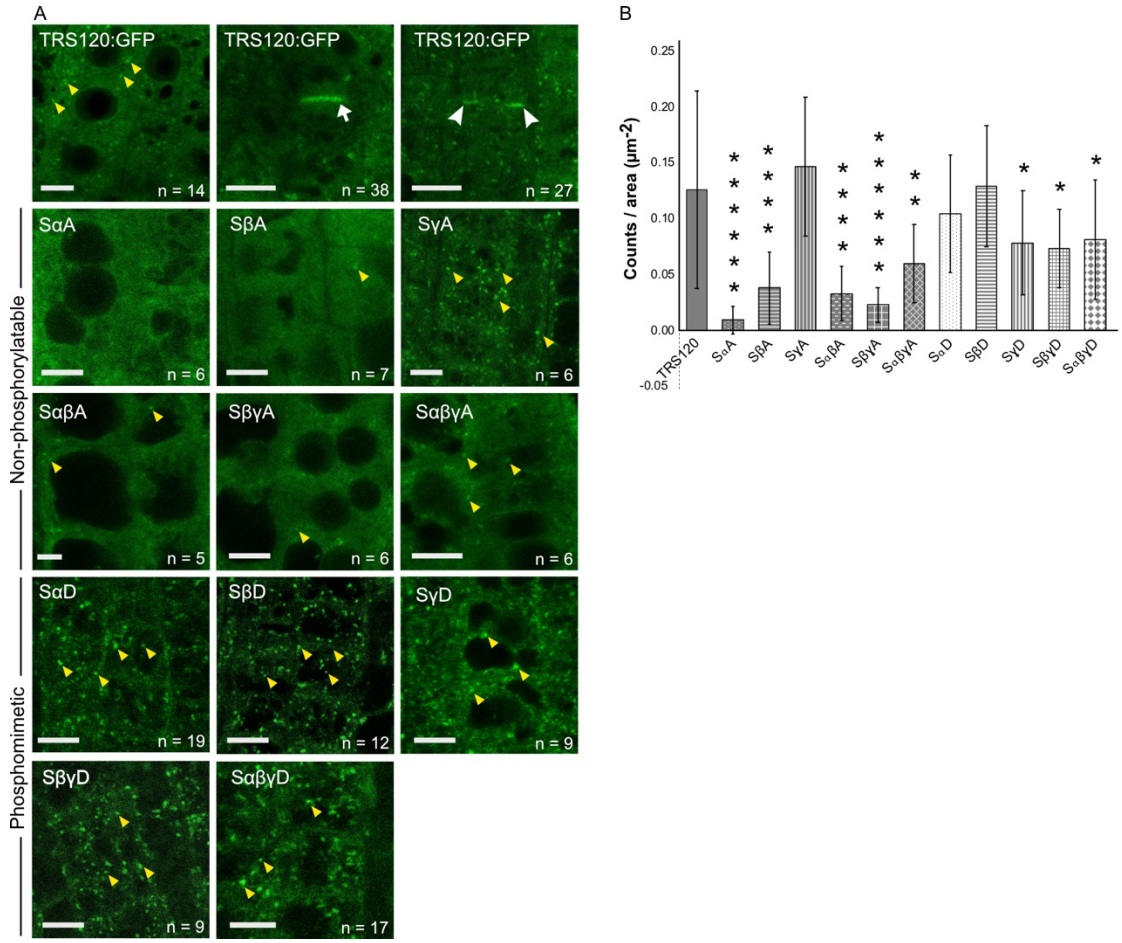

Figure 30: Localization of TRS120 phosphovariants

(A). CLSM of of P_{TRS120}::TRS120:GFP phosphovariants in root tip cells of light grown seedlings. Sample numbers are indicated on the bottom right, refer to number of root tips imaged. Different phosphovariants are shown; note the absence of cytosolic signal and atypical appearance of P_{TRS120}::TRS120-SαβD:GFP in the bottom left panel, localizing to PPB (blue arrow) and phragmoplast (reddish orange arrow). Yellow arrowheads point to endomembrane compartments, white arrow to the cell plate, white arrowheads to the leading edge of the expanding cell plate. Size bars=5µm (B). Quantification of the localization pattern of TRS120:GFP phosphovariants. Comparison of particle counts/cell area for the wild type TRS120 vs its phosphovariants. Data are mean±s.d. Student's two-tailed t-test: *P<0.05, **P<0.01, ****P<0.0001, ******P<0.000001, #P<0.00000001. Sample numbers: n= at least 16 cells from at least 4 seedlings.

5. Discussion

5.1. TRAPPII and ECHIDNA act independently in protein sorting at the TGN

The TRAPPII complex and ECHIDNA (ECH) are both TGN localized proteins, playing major roles in protein sorting at the TGN. A previous study revealed that both a TRAPPII subunit (AtTRS120) and ECH were present in the proteome of SYP61. SYP61 is a SNARE at the TGN, involved in exocytic trafficking and transport of cell wall components to the plasma membrane (Drakakaki et al., 2012). TRAPPII complex is required for cell plate formation and localizes to the cell plate throughout cytokinesis. It is shown to be involved in exocytosis (Jaber et al., 2010; Qi et al., 2011; Ravikumar et al., 2017; Rybak et al., 2014; Thellmann et al., 2010). ECH on the other hand, is involved in the secretion of cell wall polysaccharides and cell elongation (Gendre et al., 2013, 2011). A recent study found that ECH also plays a role in seed coloration in terms of flavonoid accumulation in the vacuole of seed coat cells and protein trafficking to the vacuole (Ichino, Maeda, Hara-Nishimura, & Shimada, 2020). This is in agreement with Gendre *et al.*, 2011, where altered appearance of vacuoles along with aggregation of vacuoles could be observed in *ech* mutants. And also with McFarlane *et al.*, 2013 where it was shown that pectin, a polysaccharide that is normally secreted to the apical surface of the seed coat cells, abnormally accumulated in post-Golgi vesicles, vacuoles and ER derived bodies.

These reports suggest distinct roles of the TRAPPII complex and ECH at the TGN. Since both the TRAPPII complex and ECH reside at the TGN and are required for protein sorting at the TGN, we hypothesized that they might interact with each other and might act in concert to execute the different functions at the TGN. Interestingly, ECH and TRS120 co-localized to the same structures in interphase cells (Ravikumar et al., 2018). However, ECH protein could not be detected in the immunoprecipitates with CLUB:GFP or TRS120:GFP carried out previously in the lab (Rybak et al., 2014). The next step was therefore to determine the relationship

between ECH and the TRAPPII complex, whether they are dependent on each other at all or are involved in completely different pathways while carrying out their functions at the TGN.

To explore this, I first investigated whether the fundamental functions of the TGN, as well as the TGN structure and integrity is altered in the null *ech* and *trappii* mutants. Earlier reports have indicated that the TGN structure is indeed affected in both the *ech* and *trappii* mutants through the use of data from transmission electron microscopy (TEM) (Boutté et al., 2013; Gendre et al., 2011; McFarlane et al., 2013; Qi et al., 2011). Our TEM micrographs (experiments were performed by Dr. Alexander Steiner a former postdoctoral fellow in Assaad lab) imaged at the lab of Prof. Gerhard Wanner at the LMU, Munich, confirmed these findings for the *trappii* alleles (Ravikumar et al., 2018). The quantitative analyses further confirmed these claims and showed that the *ech* and *trappii* mutants affect the TGN structure differently. The rate of endocytosis, which is one of the basal functions of the TGN, was also more impaired in the *trs120-4* mutants than in *ech* or *club-2* mutants.

More interestingly, specialized TGN functions such as cytokinesis and cell elongation were also differentially impacted in the *ech* and *trappii* mutants. The localization dynamics of various markers also showed disparity in the mutants. Plasma membrane markers were mislocalized to compartments resembling vacuoles in *ech* mutants and *club-2* showed severe defects in the trafficking of the plasma membrane markers. VHAa1, which is a TGN marker, was mislocalized to the cell plate in the *trappii* mutants and protein sorting at the cell plate was also impaired in the *trappii* mutants but not in *ech*. Taken together, these results point to differences in the impact to the TGN structure and function in the two mutants at least to different extents and indicate a division of different TGN functions among the proteins.

The IP-MS and Y2H data showed no evidence of a physical interaction between the TRAPPII complex and ECH or other ECH interacting partners such as YIP4a/b (Gendre et al., 2013; Ravikumar et al., 2018). Additionally, a network interaction

analysis (performed by the group of Pascal Falter-Braun) was performed, in which the core-TRAPP subunits and ECHIDNA, together with their binary interactors were projected onto the *Arabidopsis* Interactome map (*Arabidopsis* Interactome Mapping Consortium, 2011). This analysis provided a network level verification that ECH and TRAPP associated with or belonged to different communities (Ravikumar et al., 2018).

All of these observations suggested that they might act in two separate pathways (Ravikumar et al., 2018). To test this hypothesis, I conducted double mutant analysis with the null alleles of *ech* and *club-2* to ascertain if they might be at least partially redundant or if they indeed act in two distinct and independent pathways. Embryo lethality of the double mutants indicated that ECH and TRAPPII displayed a synergistic genetic interaction. Synergy often suggests that the two proteins function in parallel pathways and also proposes that ECH and TRAPPII are at least partially functionally redundant (Pérez-Pérez et al., 2009). This result was again reinforced in the double mutants of *ech trs120-5; trs120-5* is a hypomorphic allele of *AtTRS120*. Initially, cell elongation defects were observed in the SEM imaging data of hypocotyls of these double mutants (experiment performed by Mr. Nils Kalbfuss, Master's student in Assaad lab, SEM imaging done in collaboration with Dr. Gerhard Wanner at LMU, Ravikumar et al. 2018), where the cells appeared isodiametric. To confirm this observation, I carried out quantitative measurements of the ratio of length vs breadth of the root cells in the elongation zone, the results revealed synthetically enhanced cell elongation defects in the double mutants of *ech trs120-5.* In addition to this, secretory defects could be observed in these double mutants in immunostained root tips with an AGP antibody. AGP glycans are cell wall polysaccharides (Nguema-Ona et al., 2014) and are routinely used as markers for secretion. LM14, an AGP antibody, labeled the cell walls in the null alleles of *ech* and *trs120-4* single mutants, but failed to do so for the double mutant *ech trs120-5*, just to note again that *trs120-5* is a hypomorphic allele of *AtTRS120*. Here it is also important to be aware that the secretion of proteins or polysaccharides to the plasma membrane can be via various routes or pathways. Previous works have shown that ECH and TRAPPII are responsible for sorting of specific set proteins but not for others. For example,

PIN2 and AUX1 polarity is affected in the *trappii* mutants but not in *ech* mutants (Gendre, Jonsson, Boutté, & Bhalerao, 2015; Qi et al., 2011; Qi & Zheng, 2011; Rybak et al., 2014) and the trafficking of AUX2 is impaired in *ech* (Boutté et al., 2013). Therefore, a probable explanation for this synergistic interaction is that ECH and TRAPPII are involved in different but overlapping routes to the plasma membrane, and thus, secretion of certain proteins is compromised in the double mutants, as seen for AGP glycans.

Finally, an analysis of physical, network and genetic interactions strongly suggests that ECH and TRAPPII overlap for the basal TGN functions such as exocytosis but also have distinct specialized TGN functions such as cell plate formation (which was impaired in *trappii* but not in *ech*) and cell elongation (which was defective in *ech* but not in *trappii*). We could observe considerable variation in localization or association patterns of the *ech* and *trappii* mutants in relation to both TGN structure and function (Table 23). Both the proteins were also observed to be not dependent on each other for their localization pattern in the cells (Ravikumar et al., 2018). Two parallel pathways, which are able to take over certain basal functions in the absence of either player might be the reason as to why null *trappii or ech* alleles survive until or past the seedling stage but not the double mutants. These results add to the robustness of TGN fundamental basal functions and also reveal the dynamic organizational capabilities of the TGN.

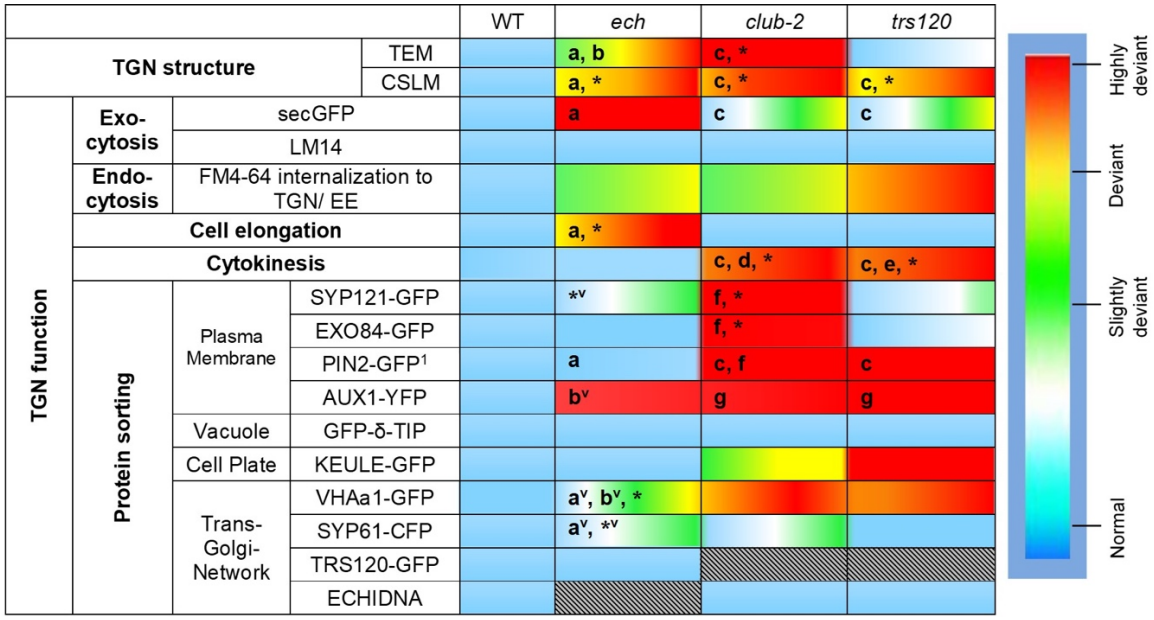

Table 23: TGN structure and function in *ech* and *trappii*.

The heat map depicts the extent of deviation from the wild type (see scale), with gradients representing the range of phenotypes observed. Grey rectangles with lines indicate that this data point does not apply. The data summarize the observations of this study, unless otherwise specified. (a) Gendre et al. 2011; (b) Boutté et al. 2013; (c) Qi et al. 2011; (d) Jaber et al. 2010; e: Thellmann et al. 2010; f: Rybak et al. 2014; g: Qi and Zheng 2011. Asterisk indicates also reported in this study. [1]Immunostaining for *ech*, live imaging of GFP marker for *trappii*. [v] indicates the vacuolar mislocalization of marker, seen specifically in *ech* mutants. Table and caption adapted from Ravikumar et al., 2018.

5.2. Role of the AtTRS33 subunit in the TRAPPII complex function

The function, topology and subunit composition of the TRAPP complexes has been well characterized in the yeast, mammalian and drosophila systems. Until recently, the TRAPP complexes in the *Aspergillus* system were uncharacterized. But a study by Pinar et al. 2015 demonstrated that the TRAPPII subunits associated with Rab-E GTPases in *A. nidulans*. Using *in vivo* localization data and *in vitro* Rab nucleotide exchange assays, they also illustrated its function as a Rab-E GEF and showed that it plays a role at the transition from Golgi-to-post Golgi identity. A consecutive study from the group revealed the modularity of the TRAPP complexes and their subunit composition, resembling those of metazoans to a greater extent than of the yeast system (Pinar et al., 2019). In Bet5-S agarose purifications coupled with MS/MS analysis, they identified the presence of TRAPPII and TRAPPIII subunits: Trs120, Trs130, Tac17, TRAPPC11, 12 and 13 along with other shared TRAPP subunits including an additional subunit labeled as Trs65. However, from literature we know that Trs65 and TRAPPC13 are orthologs. Trs65 was first identified in yeast; later, an ortholog of Trs65 was identified in metazoans and annotated as TRAPPC13 (Ramírez-Peinado et al., 2017; Reiling et al., 2013; Sacher, Barrowman, Schieltz, Yates Iii, & Ferro-Novick, 2000). Recently, TRAPPC13 subunit was shown to be a part of the TRAPPIII complex in metazoans as opposed to yeast, where Trs65 is a TRAPPII-specific subunit (Riedel et al., 2018). It was therefore confusing to see them (Trs65 and TRAPPC13) annotated as two different subunits of the TRAPP complexes and also assigned to different complexes in *A. nidulans*: Trs65 as a part of TRAPPII complex and TRAPPC13 as a part of TRAPPIII complex. The study described the Trs65 subunit to be necessary for the dimerization and assembly of the TRAPPII complex, which is similar to the yeast as well as in this thesis. A search on the AspGD search engine of the pull-down product of Bet5-S: TRAPPC13 (AN4358), revealed that it contains a TRAPPC13 related domain (Interpro IPR010378). When searched for the Trs65 subunit (AN1248) on the same search engine, it is defined to be a component of the TRAPPII complex, annotated by Pinar *et al.*, 2015. In Pinar *et al.*, 2015, the molecular weight of Trs65 of *A. nidulans* was indicated to be the same as that of the yeast (63KDa). The

weight of TRAPPC13 is 36.7KDa in *A. nidulans* while that in metazoans was 46.5 KDa (A5PLN9). This disparity might be because the identified Trs65 and TRAPPC13 subunits in *A. nidulans* might perhaps be paralogs of the TRAPPC13 subunit having similar but not identical functions.

Another concern in the study is the presence of the (TRAPPII-complex specific subunit) Trs65 band, although unlabeled, seen on the SDS-PAGE of (TRAPPIII-complex specific subunit) Trs85-S purified TRAPPs. The purified products are described to be associated with core/shared subunit plus TRAPPIII-specific subunits. However, the intensity of the Trs65 band is stronger than the labeled TRAPPIII-specific - TRAPPC11 band. Additionally, its intensity is almost as the same intensity as the Trs23 band on the gel. However, MS/MS analysis of the Trs85-S-purified TRAPPs could not detect Trs65. The negative staining electron microscopy data of TRAPPIII complex could not identify TRAPPIII subunits – TRAPPC11, 12 and 13. This could be because of low abundance of the TRAPPIII complex observed in cells, almost half of that of the TRAPPII complex. However, there is no adequate *in vivo* verification for the results presented. Since it was indicated that Trs65 along with Trs33 is necessary for the dimerization and assembly of the TRAPPII complex onto the core/shared subunits but not its stability, I have assigned it as a TRAPPII-specific subunit (green in Table 24). The TRAPPC13 subunit has been assigned as a TRAPPIII-specific subunit (orange in Table 24) as proposed by the authors.

The *Arabidopsis* TRAPPII complex was first identified in a screen for cytokinesis-defective mutants. Positional cloning of the *club* mutant identified in the screen verified CLUB as a homolog of the yeast Trs130 TRAPPII complex-specific subunit (Jaber et al., 2010). Consecutively, it was shown that another TRAPPII complex subunit, AtTRS120 is required for cell plate biogenesis and formation (Ravikumar et al., 2018; Rybak et al., 2014; Thellmann et al., 2010). In the recently published Kalde et al., 2019 paper from the lab, IP-MS data revealed all 13 subunits of the TRAPP complex co-purifying with CLUB and Rab-A2a GTPases, showing that homologues of all the TRAPP subunits of yeast and metazoans are present in plants. The results of the differential IP-MS, also suggested that

Arabidopsis has at least two TRAPP complexes: TRAPPII and TRAPPIII, involved in diverse cellular functions (Kalde et al., 2019).

To better understand the topology of the TRAPPII complex in *Arabidopsis* and further confirm the differential IP-MS results, I carried out double mutant analysis. I investigated the double mutants of a AtTRS33 allele (*trs33-1* null mutant, Thellmann et al., 2010) identified as part of the TRAPPII complex in the differential IP-MS data and a CLUB allele (*club-2* null mutant, Jaber et al., 2010) previously identified as a TRAPPII-specific subunit. The double mutants were embryo lethal, unable to form heart shape embryos during the later stages of embryo development and finally collapsing as large globular shaped embryos. They were synergistically enhanced, suggesting that the two proteins are part of one multi-protein complex (Guarente, 1993; Pérez-Pérez et al., 2009). The result of the genetic interaction reveals a functional link between a TRAPPII complex-specific subunit and a shared subunit. Interestingly, experiments in other systems have yielded similar results. In yeast and human cells it was shown that Trs33 and Trs65 subunits are necessary for the association of the TRAPPII complex with its core/ shared subunits ((Tokarev et al., 2009)). Experiments in *A. nidulans* yielded similar results, revealing that Trs33 is involved in the assembly of TRAPPII-specific subcomplex onto the core TRAPP (Pinar et al., 2019). It can therefore be implied that AtTRS33 is indeed a part of the TRAPPII complex in *Arabidopsis*, in line with both yeast, metazoans and *Aspergillus*. This result was also supported by the yeast two-hybrid analyses (performed by Dr. Melina Altmann from the lab of our collaborator Dr. Pascal Falter Braun), that was positive for a binary interaction between AtTRS33 and AtTRS20/AtTCA17/TRAPPC2L, a TRAPPII complex-specific subunit in yeast (Kalde et al., 2019).

In support of my double mutant analysis, I could also show that the absence of AtTRS33 affected the localization pattern of AtTRS120, a TRAPPII complex-specific subunit, rendering it cytosolic and unable to associate to membranes. Earlier works in yeast also corroborated this observation; loss in the Trs33 subunit displayed defects in TRAPPII complex assembly. Additionally, diffused Trs130:GFP puncta could be observed in the cells of the *trs33* mutants (Tokarev

et al., 2009). The observation that AtTRS33 is required for the membrane association of AtTRS120 further confirms the claim that AtTRS33 is a necessary part of the TRAPPII complex in *Arabidopsis*. Taking this one step further, it also suggests that a fully assembled TRAPPII complex is necessary for its membrane association.

Taken together along with my results, this suggests that the function of TRS33 is conserved across kingdoms. The *Arabidopsis* TRAPPII interactome is vast and mostly unexplored, and it does contain a plant-specific TRS65 orthologue (Kalde et al., 2019). However, it is yet to be determined whether AtTRS65 might also help build or stabilize the TRAPPII complex like in the yeast system and also if AtTRS33 and AtTRS65 are functionally redundant in terms of TRAPPII complex assembly. A double mutant analysis between AtTRS33 and AtTRS65 might provide more clues regarding their interaction dynamics.

Recently, AtTRS33 was reported to be necessary for apical meristematic growth in *Arabidopsis* and was shown to be involved in cell growth and organization (J. Zhang et al., 2020); the results of the study propose a functional divergence of the AtTRS33 protein and also offers scope for further characterization of this protein along with other TRAPP subunits in plants.

Table 24: TRAPP subunits and their different compositions in eukaryotes.

Yeast TRAPP		Metazoan TRAPP		*Arabidopsis* TRAPP			*Aspergillus* TRAPP		
Subunit	Weight (KDa)	Subunit	Weight (KDa)	AGI	Subunit	Weight (KDa)	AspGD	Subunit	Weight (KDa)
Bet5	18	TRAPPC1	17	At1g51160	BET5	18.9	AN8828	Bet5	18
Trs20	20	TRAPPC2	16	At1g80500@*	TRS20*	15	AN11500	Trs20#	20
Bet3(2x)	22	TRAPPC3	20	At5g54750	BET3	22	AN9086	Bet3	22
Trs23	23	TRAPPC4	24	At5g02280	TRS23	16	ASPND_04634	Trs23	25
Trs31	29	TRAPPC5	21	At5g58030	TRS31	21.8	AN6825	Trs31	32
Trs33#	31	TRAPPC6 (A, B)	19, 15	At3g05000	TRS33#	19.5	AN10826	Trs33#	31
Tca17	17	TRAPPC2L	16	At2g20930@	TCA17	15.6	ASPND_03640	Tca17	19
Trs120	120	TRAPPC9	140	At5g11040	TRS120	129.6	AN6533	TRS120	148
Trs130	130	TRAPPC10	142	At5g54440	CLUB	140.6	AN1038	Trs130	128
-	-	-	-	-	-	-	AN1248	Trs65# (?)	63
Trs65#	65	TRAPPC13	46.5	At2g47960*	TRS65*	49.2	AN4358	TRAPPC13 (?)	36.7
Trs85	85	TRAPPC8	161	At5g16280	TRS85	143.5	AN7311	Trs85	81.6
-	-	TRAPPC11	129	At5g65950*	TRAPPC11*	132.2	AN1374	TRAPPC11	141.8
-	-	TRAPPC12	79	At4g39820*	TRAPPC12*	46.3	AN4930	TRAPPC12	49.2

Shared subunits are colored in blue, TRAPPII-specific subunits in green and TRAPPIII-specific in orange. In *Aspergillus*, the probable presence of low amounts of the TRAPPI complex consisting of the core hetero-heptamer subunits is colored in pink. The Tca17 subunit in *Aspergillus* is a part of the TRAPPI, TRAPPII and TRAPPIII complexes and is colored in violet (Pinar et al., 2019). Molecular weights of yeast and metazoan TRAPP subunits obtained from Scrivens et al. 2011. Molecular weights of *Arabidopsis* TRAPP subunits obtained from the *Arabidopsis* information resource (TAIR). Molecular weights of *Aspergillus* TRAPP subunits obtained from AspGD, Pinar et al., 2015 and Pinar et al., 2019. 2x = 2 copies of Bet3 (Thomas et al. 2019). # = necessary subunits for assembly of TRAPPII-specific subcomplex onto core TRAPP to generate TRAPPII. (A, B) two homologues of TRAPPC6 is present in the humans (Borner et al., 2014). @= Reannotation of TRAPPC2/C2L subunits, only one of which has been previously described by Thellmann et al. 2010. *= TRAPP subunits not previously recognized in plant genomes. (?) = ambiguously annotated subunits in *Aspergillus*.

5.3. The TRAPPII complex is a putative Rab GEF

Rab GEFs act upstream of Rab GTPases. Since GEFs are involved in the activation and subsequent stabilization of Rab substrates on membranes, they are implicated as the primary determinants of Rab localization. The GEFs preferentially bind to inactive, GDP-bound Rab GTPases and are involved in the removal of GDP. This then allows GTP to bind, activating the Rab GTPases. The GTP-bound, activated Rab GTPases then recruit a diverse local network of Rab effectors to the membrane where they are localized. Rab effectors usually include downstream tethering proteins, for membrane-membrane recognition, and also GEFs for the next Rab GTPase in the trafficking pathway, thereby forming a Rab cascade.

Using elegant time-resolved microscopy and kymograph data, a recent study in the *Aspergillus* system reported the mechanism of TRAPPII complex recruitment to the TGN and its function as a GEF for Rab11 GTPases (Pinar & Penãlva, 2020). The study also disproved the previously claimed 'TRAPP conversion theory' from TRAPPI to TRAPPII. Using 3D movie and kymograph analyses, the authors demonstrated that a core subunit (Bet3) as well as a TRAPPII-specific subunit (TRS120) colocalize at the TGN over time, appearing and dispersing simultaneously, implying that they are present at the same time point of the cisternal cycle and not turning up in a sequential manner. However, a concern with the study is the lack of other lines of evidence. Maybe a control experiment showing colocalization dynamics between two other subunits (a shared subunit and a TRAPPII-specific subunit) to test whether this remains true could deeply enhance the results.

In *Arabidopsis*, it is still ambiguous whether the TRAPP complex has GEF activity. Previous studies have shown that the TRAPPII complex colocalizes and is also functionally linked to Rab-A GTPases. Additionally, it was demonstrated that the expression of a constitutively active Rab-A1 but not a Rab-D2 subclade, partially rescues the phenotype of a *trs130* null allele (Qi et al., 2011; Qi & Zheng, 2011). Although the nature of this link is still unclear, to some extent, it strengthens

the hypothesis that the TRAPPII complex acts upstream of Rab-A GTPases, most probably as a GEF, inferring from the yeast and metazoans systems. Furthermore, the TGN localization of TRAPPII components and its involvement in the biogenesis of cell plates, which is a Rab-A compartment, makes TRAPPII a favorable candidate for a Rab-A GEF in plants (Naramoto et al., 2014; Qi et al., 2011; Qi & Zheng, 2011; Ravikumar et al., 2018, 2017; Rybak et al., 2014).

I wanted to tackle this hypothesis, by determining localization phenotypes of a Rab-A marker (Rab-A5c) in *trappii* mutants, as well as the localization pattern of the Rab-A2a GDP/GTP locked variants in the *trappii* mutants. Interestingly, the edge localization pattern of the Rab-A5c marker observed in the wild type was completely abolished in both the mutants; suggesting that in the absence of TRAPPII, Rab-A5c is unable to correctly localize to its target membrane compartments. It is known that GEFs are involved in the correct spatial transport of Rabs to their target membranes. A study reported that mis-targeting specific Rab GEFs causes mis-localization of their associated Rab GTPases (Blümer et al., 2013). Therefore, the edge localization defect of the Rab-A5c observed in the *trappii* mutants suggests that the TRAPPII complex might act as an upstream Rab-A GEF.

Kalde et al. 2019 described the localization dynamics of the YFP:A2a marker in relation to a TRS120:mCherry marker during cytokinesis. Both the markers are present at the cell plate throughout cytokinesis and also re-organize to the leading edges of the cell plate during telophase. And my results of the YFP:A2a marker localization in the *trappii* mutants (*trs120-4*, *club-2* and *trs33-1*) showed that the localization dynamics of YFP:RAB-A2a depended on TRAPPII function. It revealed that even though TRAPPII is not required for the initial recruitment of Rab-A2a to the membranes and also the cell plate, it is required later for the re-organization of Rab-A2a to the leading edges of the cell plate.

The localization dynamics of the dominant negative (DN) and constitutively active (CA) RAB-A2a variants, in wild-type versus *trappii* (*trs33-1*) mutant backgrounds and the quantitative analysis for relative signal intensities clearly showed that the

mutations in the *trappii* complex subunits causes an enhancement of the GDP-bound YFP:A2a-DN localization phenotype and a partial suppression of the GTP-bound YFP:A2a-CA localization.

The quantitative IP-MS data in Kalde et al. 2019 suggested that at least two TRAPP complexes exist in plants, based on their affinity towards GDP-bound vs GTP-bound Rab-A2a variants. The first group that bound preferentially to GDP-bound RabA2a, consisted of homologues of all metazoan TRAPPII subunits, including formerly undetected AtTRS20/TCA17/TRAPPC2(L) homologue and AtTRS33. A second set of *Arabidopsis* TRAPP subunits failed to interact with the GDP-bound form of RAB-A2a. Among these was AtTRS65/TRAPPC13, which is not a component of yeast TRAPPII but of metazoan TRAPPIII (Kim et al., 2016; Riedel et al., 2018). These subunits preferentially bound to the vacuolar RAB-G3f Rab GTPase suggesting a role in vacuolar trafficking. Also, interestingly, the components of the TRAPPII complex favorably associated with a GDP-bound mutant of RAB-A2a instead of with wild-type or GTP- bound RAB-A2a. The results of the differential IP-MS in the research article, support the hypothesis that firstly, *Arabidopsis* has multiple TRAPP complexes, that are involved in diverse cellular functions. Secondly, along with my own live-cell imaging data and quantitative analyses, provides further proof that the TRAPPII complex acts upstream of the Rab-A GTPases, most likely as a Rab-A GEF because of its affinity towards the GDP-bound RAB-A2a mutants.

Given the previous claim that functionally links TRAPPII and Rab-A1 GTPases (Qi & Zheng, 2011) and my results showing that TRAPPII potentially acts upstream of both Rab-A5c and Rab-A2a, it is tempting to speculate that the TRAPPII complex acts as an universal GEF for all six Rab-A subclades. However, since Rab-A GTPase is highly expanded in plants compared to yeast or metazoans, there is a possibility that other unidentified GEFs are also involved in the activation of Rab-A GTPases. Interestingly, it was recently reported that in metazoans, Parcas protein acted as a GEF for Rab-11 in addition to the TRAPPII complex (Riedel et al., 2018). Even though the *Arabidopsis* genome does not code for a

Parcas homologue, it will be interesting to see whether other additional Rab GEFs for the Rab-A clade are present in plants.

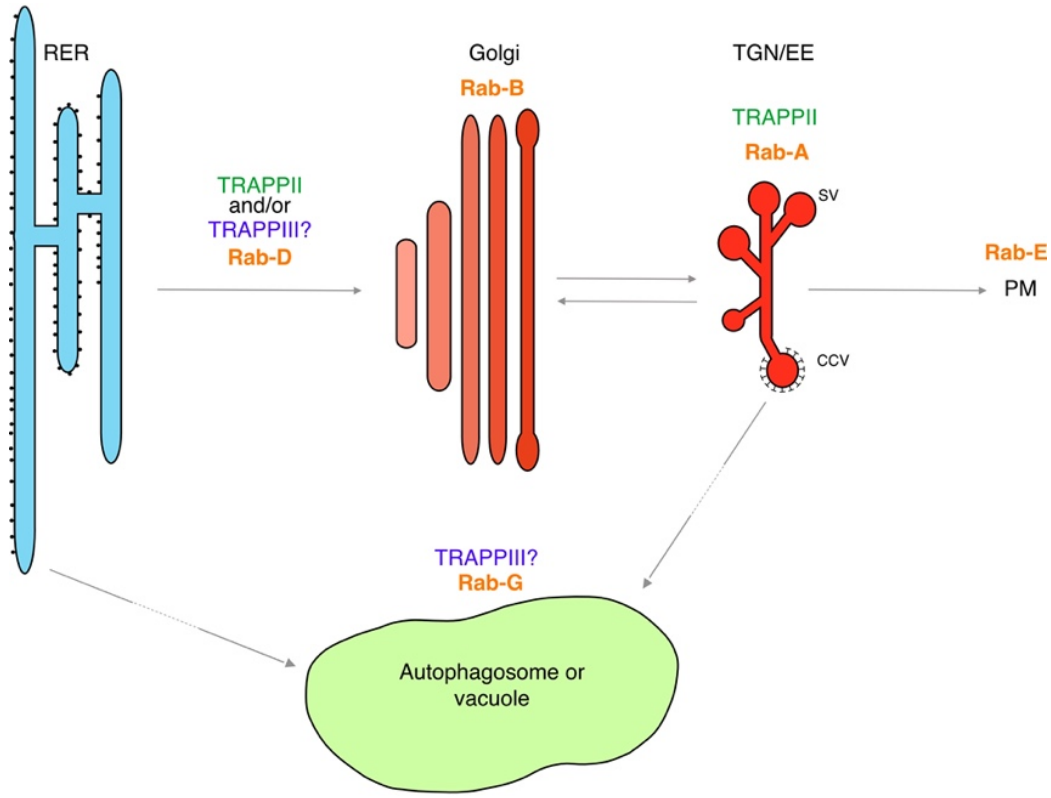

Figure 31: TRAPP complexes and Rab GTPases in membrane trafficking.
In plants, TRAPPII resides at the TGN/EE and is a putative GEF for the Rab-A clade of Ypt31/Rab11 orthologues. Rab clades identified in TRAPPII immunoprecipitation-mass spectrometry (IP-MS, Kalde et al., 2019) are D, B, A and E and these are on a biosynthetic trafficking route. Rab-F or Rab-G clades were not robustly identified in the CLUB/AtTRS130 interactome (Kalde et al., 2019). The study also postulated the existence of a plant TRAPPIII complex that resembles metazoan TRAPPIII. Based on preferential binding to the vacuolar Rab-G, which is required for autophagy (Elliott et al., 2020) and on orthology, TRAPPIII is tentatively placed on an autophagy and/or vacuolar trafficking route. Whether *Arabidopsis* TRAPPII or III plays a role in ER/Golgi traffic remains to be determined. The dashed arrows depict late endosomes/multivesicular bodies along post-Golgi trafficking routes. RER: rough endoplasmic reticulum; TGN: trans-Golgi network; SV: secretory vesicles; CCV: clathrin coated vesicles; PM: plasma membrane. Illustration adapted from Miriam abele (Kalde et al., 2019).

5.4. TRAPPII complex is post-translationally regulated by a specific phosphocode

While a lot of focus in previous studies has been on understanding the functions of the TRAPPII complex in yeast, metazoans, *Aspergillus* and plants, not much emphasis is placed on the post-translational regulation of this protein complex. It is important that membrane dynamics are tightly regulated both spatially and temporally during cytokinesis, since even tiny delays or mislocalizations during cytokinesis have been shown to have drastic effects (Normand & King, 2010; Thiele et al., 2009).

Since not much was known about the functional regulation of the TRAPPII complex, one of the objectives of my thesis was to determine if/how the TRAPPII complex might be regulated by upstream signal transduction pathways. The first interesting observation or link was the robust and specific binary interaction of the BIN2 GSK3 kinase with AtTRS120 subunit of the TRAPPII complex during the lab's large Y2H screening. BIN2-AtTRS120 interaction was exclusive, in that, it was the only kinase to interact with any of the subunits of the TRAPPII complex. Time and concentration dependent increase in the intensity of phosphorylation of the AtTRS120 substrate by the different GSK3 kinases in the *in vitro* kinase assay further verified this interaction. Also, the three phospho-sites identified from the kinase assay overlapped with those from the *in-silico* data (Assaad, unpublished). Y2H results showing BIN2 binding to all, except the triple phosphomimetic mutants, suggests a certain coordination for this interaction.

When the *trs120-4* mutant segregating plants were transformed with different phosphovariant constructs, we could already observe from the segregation analysis (conducted by Miriam Abele, a student in the Assaad lab) that it was not possible to obtain homozygous line for both the phosphovariant constructs and *trs120-4* mutant background for many of the phosphovariant lines. One of the reasons could be that the plants are not viable if the wild-type AtTRS120 is absent, since the phosphovariant constructs are unable to carry out the normal functions

in the cells. We could however obtain, hemizygous lines and this is what we used for further experiments.

AtTRS120 has three GSK3 target sites, which translates into eight differential phosphorylation combinations. The impact of the phosphorylation status affected its membrane localization dynamics in the cells as well as its affinity towards the BIN2 kinase as observed in the Y2H experiments. These results strongly suggest that AtTRS120 is regulated by a specific phosphocode, which in turn might be guiding its membrane associations and also maybe confers specificity to the AtTRS120 interaction partners.

The TRAPPII complex has two distinct molecular or membrane related functions: it acts as a tethering factor and as a Rab-GEF. As a tethering factor, the TRAPPII complex is physically involved in tethering vesicles to the cell plate; the cell plate biogenesis defects observed in *club-2* and *trs120-4* null *trappii* alleles. (Jaber et al. 2010; Rybak et al. 2014; Thellmann et al. 2010) provide evidence for an active tethering role for the TRAPPII complex (Ravikumar et al., 2017). My observations as well as previous studies have also shown that the TRAPPII complex is required for the spatiotemporal regulation of membrane traffic (Ravikumar et al., 2018; Rybak et al., 2014) and have provided indirect *in vivo* evidence that the TRAPPII complex acts as a Rab-A GEF (Kalde et al., 2019; Qi & Zheng, 2011). The dual role of TRAPPII as a tethering factor would provide a scaffold for its GEF activity to fine tune trafficking both spatially and temporally. It is possible that the specificity of the TRAPPII complex's putative GEF activity could be regulated by phosphorylation via GSK3 kinases. However, this hypothesis needs to be tested by future experiments. Performing Rab GEF assays on Rab-A GTPases with different AtTRS120 phosphovariant lines could be a good start to test this hypothesis.

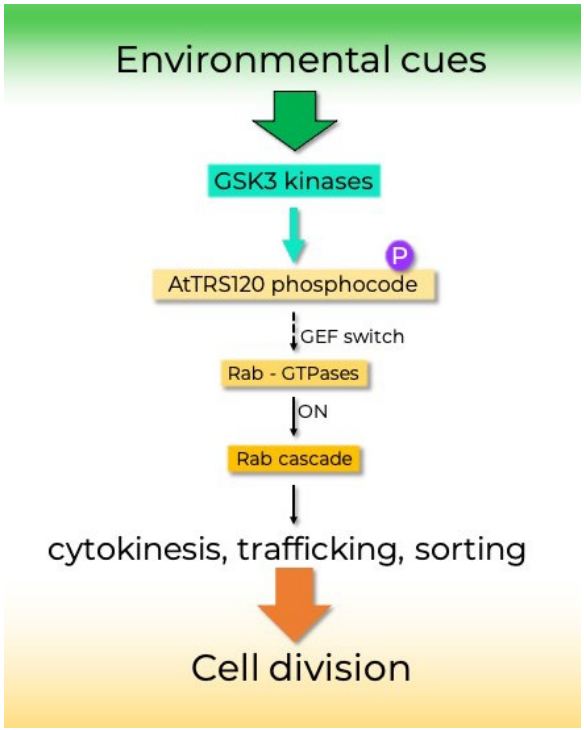

Figure 32: A specific phosphocode of AtTRS120 affects its interactome.

This study demonstrates the phospho-regulation of the AtTRS120 subunit of TRAPPII complex by GSK3 kinases, which are in turn activated under distinct environmental signals. A specific phosphocode of the AtTRS120 affects its interactome, driving its membrane dynamics. The dotted line is the speculative function of the AtTRS120 phosphorylation status affecting its membrane related GEF activity on Rab GTPases.

6. Conclusions and Outlook

As a preliminary goal, the current study aimed to better understand the versatile functions of the TGN resident proteins: TRAPPII complex and ECHIDNA (ECH) and how they regulate their functions. Double mutant analysis carried out to determine the genetic interaction between TRAPPII complex and ECH revealed that they interact synergistically. A synergistic interaction usually means that the two proteins act as members of a protein complex, or that they are functionally redundant. In this case, the latter is more probable since physical interaction data carried out in the Assaad lab was negative for TRAPPII and ECH as well as other ECH interacting proteins – YIP4a/ YIP4b. Interestingly, the double mutants also exhibited severe secretory and cell elongation defects, which was otherwise absent in the single mutants. The localization dynamics of ECH in *trappii* mutants and vice versa was not affected. However, the localization dynamics of the different markers were differentially impacted in the null mutants of the proteins. Both TRAPPII and ECH affected the TGN structure differentially. Additionally, specialized TGN functions such as cell plate biogenesis and cell elongation were revealed to have a distinct effect in the *ech* and *trappii* mutants. The quantitative and localization analyses, as well as the double mutant phenotypes highlight the divergent role of ECH and the TRAPPII complex in dividing cells. However, while they may have partially redundant or overlapping functions at the TGN in interphase cells, ECH and TRAPPII are also non-redundant in their specialized functions.

My research made evident that a TRAPP complex subunit AtTRS33 was a part of the TRAPPII complex in plants, similar to other eukaryotes. I could establish that AtTRS33 was functionally linked to a TRAPPII-specific subunit using double mutant analysis. Importantly, in the absence of AtTRS33, the TRAPPII complex failed to localize to membranes. This result highlighted the importance of AtTRS33 for its membrane association and also hints towards AtTRS33 playing a vital role in TRAPPII complex assembly in plants. Future investigations to explore potential plant-specific functions of AtTRS33 would be interesting.

The current study also brought to light, the putative role of the TRAPPII complex as a Rab-A GEF in plants. Utilizing live imaging and subsequent quantitative analyses of relative signal intensities of the different Rab-A2a GTPase mutant versions, I could show that the TRAPPII complex might perhaps be acting upstream of the Rab-A GTPases. Along with the imaging analyses , quantitative IP-MS data in Kalde et al. 2019 provided further proof that the TRAPPII complex acts upstream of the Rab-A GTPases, most likely as a Rab-A GEF because of its affinity towards the GDP-bound RAB-A2a mutants. Given the previous claim that functionally linked TRAPPII and Rab-A1 GTPases (Qi & Zheng, 2011) and my results showing that TRAPPII potentially acts upstream of Rab-A GTPases, it is tempting to speculate that the TRAPPII complex acts as an universal GEF for all six Rab-A subclades, however this needs further verification.

In the last part of the work, we established that a Shaggy-like kinase (GSK3) phosphorylates AtTRS120 on specific target sites and explored the impact of this phosphorylation event. Y2H data revealed that BIN2 kinase is unable to bind to AtTRS120 when all three target sites are phosphorylated suggesting that the TRAPPII complex might perhaps undergo structural changes when phosphorylated. I also demonstrated that the various phosphovariants lines had an impact on the localization dynamics of AtTRS120. The data suggests that AtTRS120 is regulated by a distinct phosphocode determining its membrane association.

Future experiments to firstly, decipher whether a specific AtTRS120 phosphocode/s is/are involved in switching the TRAPPII complex to regulate membrane dynamics as a Rab GEF vs a tethering complex would be the next significant step.

Secondly, since the GSK3 kinases are known to mostly phosphorylate substrates that are primed by a previous kinase, identifying the priming kinases, if any, for AtTRS120 will be very interesting. The interactome data of the various AtTRS120 phosphovariant lines (Assaad et al., unpublished) could provide some clues about

putative priming kinases. To verify these clues, one could perform *in vitro* kinase assays, which will also lead to identifying the priming sites on AtTRS120.

Thirdly, since we could not obtain homozygous AtTRS120 phosphovariant lines for most of the phosphovariant combinations and the fact that the localization dynamics of the phosphorylatable line differed from the that of the non-phosphorylatable lines, it is tempting to hypothesize that the formation of the TRAPPII complex might also be affected by the phosphorylation status of AtTRS120. Live-cell imaging of the AtTRS120 phosphovariant lines in conjunction with the different readily available membrane markers at the Assaad lab to determine whether the puncta detected in the AtTRS120 phosphovariant lines are indeed present at the TGN could provide some preliminary confirmation. Additionally, determining the localization dynamics of the AtTRS120 phosphovariant lines in the *trappii* mutant backgrounds could present a enhanced understanding of the regulatory mechanism of the TRAPPII complex formation and function.

Finally, it would be of interest to determine if perhaps the CLUB subunit is also regulated by a phosphocode and to interpret its regulatory mechanism(s).

Taken together, this study delves deep into understanding the diverse functions of the TRAPPII complex at the TGN, its post-translational regulation and finally, how the phosphorylation status affects the TRAPPII complex's localization dynamics during cell division. Finally, by providing a unique connection between the cellular membrane trafficking machinery and the GSK3 kinases, the work once again highlights that precision is highly important during protein and membrane trafficking for proper plant growth and development.

7. References

Aridor, M., & Traub, L. M. (2002). Cargo selection in vesicular transport: The making and breaking of a coat. *Traffic*, Vol. 3, pp. 537–546. https://doi.org/10.1034/j.1600-0854.2002.30804.x

Aridor, M., Weissman, J., Bannykh, S., Nuoffer, C., & Balch, W. E. (1998). Cargo selection by the COPII budding machinery during export from the ER. *Journal of Cell Biology*, *141*(1), 61–70. https://doi.org/10.1083/jcb.141.1.61

Asaoka, R., Uemura, T., Ito, J., Fujimoto, M., Ito, E., Ueda, T., & Nakano, A. (2013). Arabidopsis RABA1 GTPases are involved in transport between the *trans* -Golgi network and the plasma membrane, and are required for salinity stress tolerance. *The Plant Journal*, *73*(2), 240–249. https://doi.org/10.1111/tpj.12023

Barlowe, C. (2003). Signals for COPII-dependent export from the ER: What's the ticket out? *Trends in Cell Biology*, Vol. 13, pp. 295–300. https://doi.org/10.1016/S0962-8924(03)00082-5

Barr, F. A. (2013). Rab GTPases and membrane identity: Causal or inconsequential? *Journal of Cell Biology*, Vol. 202, pp. 191–199. https://doi.org/10.1083/jcb.201306010

Bassik, M. C., Kampmann, M., Lebbink, R. J., Wang, S., Hein, M. Y., Poser, I., … Weissman, J. S. (2013). A Systematic Mammalian Genetic Interaction Map Reveals Pathways Underlying Ricin Susceptibility. *Cell*, *152*, 909–922. https://doi.org/10.1016/j.cell.2013.01.030

Blümer, J., Rey, J., Dehmelt, L., Maze, T., Wu, Y. W., Bastiaens, P., … Itzen, A. (2013). RabGEFs are a major determinant for specific Rab membrane targeting. *Journal of Cell Biology*, *200*(3), 287–300. https://doi.org/10.1083/jcb.201209113

Borner, G. H. H., Hein, M. Y., Hirst, J., Edgar, J. R., Mann, M., & Robinson, M. S. (2014). Fractionation profiling: A fast and versatile approach for mapping vesicle proteomes and protein-protein interactions. *Molecular Biology of the Cell*, *25*(20), 3178–3194. https://doi.org/10.1091/mbc.E14-07-1198

Boutté, Y., Jonsson, K., McFarlane, H. E., Johnson, E., Gendre, D., Swarup, R.,

… Bhalerao, R. P. (2013). ECHIDNA-mediated post-Golgi trafficking of auxin carriers for differential cell elongation. *Proceedings of the National Academy of Sciences of the United States of America*, *110*(40), 16259–16264. https://doi.org/10.1073/pnas.1309057110

Cai, H., Zhang, Y., Pypaert, M., Walker, L., & Ferro-Novick, S. (2005). Mutants in trs120 disrupt traffic from the early endosome to the late Golgi. *The Journal of Cell Biology*, *171*(5), 823–833. https://doi.org/10.1083/jcb.200505145

Cai, Y., Chin, H. F., Lazarova, D., Menon, S., Fu, C., Cai, H., … Reinisch, K. M. (2008). The structural basis for activation of the Rab Ypt1p by the TRAPP membrane tethering complexes. *Cell*, *133*(7), 1202–1213. Retrieved from https://doi.org/10.1016/j.cell.2008.04.049

Chow, C.-M., Neto, H., Foucart, C., & Moore, I. (2008). Rab-A2 and Rab-A3 GTPases define a trans-golgi endosomal membrane domain in Arabidopsis that contributes substantially to the cell plate. *The Plant Cell*, *20*(1), 101–123. https://doi.org/10.1105/tpc.107.052001

Clough, S. J., & Bent, A. F. (1998). Floral dip: a simplified method for Agrobacterium -mediated transformation of Arabidopsis thaliana. *The Plant Journal*, *16*(6), 735–743. https://doi.org/10.1046/J.1365-313X.1998.00343.X

Clouse, S. D. (2011). Brassinosteroids. *The Arabidopsis Book*, *9*, e0151. https://doi.org/10.1199/tab.0151

Collins, N. C., Thordal-Christensen, H., Lipka, V., Bau, S., Kombrink, E., Qiu, J.-L., … Schulze-Lefert, P. (2003). SNARE-protein-mediated disease resistance at the plant cell wall. *Nature*, *425*(6961), 973–977. https://doi.org/10.1038/nature02076

Dajani, R., Fraser, E., Roe, S. M., Young, N., Good, V., Dale, T. C., & Pearl, L. H. (2001). Crystal structure of glycogen synthase kinase 3β: Structural basis for phosphate-primed substrate specificity and autoinhibition. *Cell*, *105*(6), 721–732. https://doi.org/10.1016/S0092-8674(01)00374-9

Del Conte-Zerial, P., Brusch, L., Rink, J. C., Collinet, C., Kalaidzidis, Y., Zerial, M., & Deutsch, A. (2008). Membrane identity and GTPase cascades regulated by toggle and cut-out switches. *Molecular Systems Biology*, *4*. https://doi.org/10.1038/msb.2008.45

Dettmer, J., Hong-Hermesdorf, A., Stierhof, Y.-D., & Schumacher, K. (2006). Vacuolar H+-ATPase activity is required for endocytic and secretory trafficking in Arabidopsis. *The Plant Cell*, *18*(3), 715–730. https://doi.org/10.1105/tpc.105.037978

Drakakaki, G., van de Ven, W., Pan, S., Miao, Y., Wang, J., Keinath, N. F., … Raikhel, N. (2012). Isolation and proteomic analysis of the SYP61 compartment reveal its role in exocytic trafficking in Arabidopsis. *Cell Research*, *22*(2), 413–424. https://doi.org/10.1038/cr.2011.129

Elliott, L., Moore, I., & Kirchhelle, C. (2020). Spatio-temporal control of post-Golgi exocytic trafficking in plants. *Journal of Cell Science*, *133*, 1–12. https://doi.org/10.1242/jcs.237065

Fan, X., Yang, C., Klisch, D., Ferguson, A., Bhaellero, R. P., Niu, X., & Wilson, Z. A. (2014). ECHIDNA Protein Impacts on Male Fertility in Arabidopsis by Mediating trans-Golgi Network Secretory Trafficking during Anther and Pollen Development. *PLANT PHYSIOLOGY*, *164*, 1338–1349. https://doi.org/10.1104/pp.113.227769

Fendrych, M., Synek, L., Pecenková, T., Toupalová, H., Cole, R., Drdová, E., … Zársky, V. (2010). The Arabidopsis exocyst complex is involved in cytokinesis and cell plate maturation. *The Plant Cell*, *22*(9), 3053–3065. https://doi.org/10.1105/tpc.110.074351

Frame, S., Cohen, P., & Biondi, R. M. (2001). A common phosphate binding site explains the unique substrate specificity of GSK3 and its inactivation by phosphorylation. *Molecular Cell*, *7*(6), 1321–1327. https://doi.org/10.1016/S1097-2765(01)00253-2

Garcia, V. J., Xu, S. L., Ravikumar, R., Wang, W., Elliott, L., Gonzalez, E., … Wang, Z. Y. (2020). TRIPP Is a plant-specific component of the arabidopsis TRAPPII membrane trafficking complex with important roles in plant development. *The Plant Cell*, *32*(7), 2424–2443. https://doi.org/10.1105/tpc.20.00044

Gendre, D., Jonsson, K., Boutté, Y., & Bhalerao, R. P. (2015). Journey to the cell surface—the central role of the trans-Golgi network in plants. *Protoplasma*, *252*(2), 385–398. https://doi.org/10.1007/s00709-014-0693-1

Gendre, D., McFarlane, H. E., Johnson, E., Mouille, G., Sjödin, A., Oh, J., …

Bhalerao, R. P. (2013). Trans-Golgi network localized ECHIDNA/Ypt interacting protein complex is required for the secretion of cell wall polysaccharides in Arabidopsis. *The Plant Cell*, *25*(7), 2633–2646. https://doi.org/10.1105/tpc.113.112482

Gendre, D., Oh, J., Boutté, Y., Best, J. G., Samuels, L., Nilsson, R., … Bhalerao, R. P. (2011). Conserved Arabidopsis ECHIDNA protein mediates trans-Golgi-network trafficking and cell elongation. *Proceedings of the National Academy of Sciences of the United States of America*, *108*(19), 8048–8053. https://doi.org/10.1073/pnas.1018371108

Griffiths, G., & Simons, K. (1986). The trans Golgi network: Sorting at the exit site of the Golgi complex. *Science*, *234*(4775), 438–443. https://doi.org/10.1126/science.2945253

Grosshans, B. L., Ortiz, D., & Novick, P. (2006). Rabs and their effectors: Achieving specificity in membrane traffic. *Proceedings of the National Academy of Sciences of the United States of America*, Vol. 103, pp. 11821–11827. https://doi.org/10.1073/pnas.0601617103

Guarente, L. (1993). Synthetic enhancement in gene interaction: a genetic tool come of age. *Trends in Genetics*, *9*(10), 362–366. https://doi.org/10.1016/0168-9525(93)90042-G

Hua, Z., & Graham, T. R. (2003). Requirement for Neo1p in Retrograde Transport from the Golgi Complex to the Endoplasmic Reticulum. *Molecular Biology of the Cell*, *14*(12), 4971–4983. https://doi.org/10.1091/mbc.E03-07-0463

Ichino, T., Maeda, K., Hara-Nishimura, I., & Shimada, T. (2020). Arabidopsis ECHIDNA protein is involved in seed coloration, protein trafficking to vacuoles, and vacuolar biogenesis. *Journal of Experimental Botany*, *71*(14), 3999–4009. https://doi.org/10.1093/jxb/eraa147

Jaber, E., Thiele, K., Kindzierski, V., Loderer, C., Rybak, K., Jürgens, G., … Assaad, F. F. (2010). A putative TRAPPII tethering factor is required for cell plate assembly during cytokinesis in Arabidopsis. *The New Phytologist*, *187*(3), 751–763. https://doi.org/10.1111/j.1469-8137.2010.03331.x

Jenkins, M. L., Harris, N. J., Dalwadi, U., Fleming, K. D., Ziemianowicz, D. S., Rafiei, A., … Burke, J. E. (2020). The substrate specificity of the human TRAPPII complex's Rab-guanine nucleotide exchange factor activity.

Communications Biology, *3*(1), 1–12. https://doi.org/10.1038/s42003-020-01459-2

Jonak, C., & Hirt, H. (2002). Glycogen synthase kinase 3/SHAGGY-like kinases in plants: an emerging family with novel functions. *Trends in Plant Science*, *7*(10), 457–461. Retrieved from https://doi.org/10.1016/S1360-1385(02)02331-2

Kalde, M., Elliott, L., Ravikumar, R., Rybak, K., Altmann, M., Klaeger, S., … Assaad, F. F. (2019). Interactions between Transport Protein Particle (TRAPP) complexes and Rab GTPases in Arabidopsis. *The Plant Journal*, *100*(2), 279–297. https://doi.org/10.1111/tpj.14442

Kim, J. J., Lipatova, Z., Majumdar, U., & Segev, N. (2016). Regulation of Golgi Cisternal Progression by Ypt/Rab GTPases. *Developmental Cell*, *22*(364), 440–452. https://doi.org/10.1016/j.devcel.2016.01.016

Kim, J. J., Lipatova, Z., & Segev, N. (2016). TRAPP Complexes in Secretion and Autophagy. *Frontiers in Cell and Developmental Biology*, *4*, 20. https://doi.org/10.3389/fcell.2016.00020

Kim, Y.-G., Raunser, S., Munger, C., Wagner, J., Song, Y.-L., Cygler, M., … Sacher, M. (2006). The Architecture of the Multisubunit TRAPP I Complex Suggests a Model for Vesicle Tethering. *Cell*, *127*, 817–830. https://doi.org/10.1016/j.cell.2006.09.029

Kirchhelle, C., Chow, C. M., Foucart, C., Neto, H., Stierhof, Y. D., Kalde, M., … Moore, I. (2016). The Specification of Geometric Edges by a Plant Rab GTPase Is an Essential Cell-Patterning Principle During Organogenesis in Arabidopsis. *Developmental Cell*, *36*(4), 386–400. https://doi.org/10.1016/j.devcel.2016.01.020

Kirchhelle, C., Garcia-Gonzalez, D., Irani, N. G., Jérusalem, A., & Moore, I. (2019). Two mechanisms regulate directional cell growth in Arabidopsis lateral roots. *ELife*, *8*. https://doi.org/10.7554/eLife.47988

Kotzer, A. M., Brandizzi, F., Neumann, U., Paris, N., Moore, I., & Hawes, C. (2004). AtRabF2b (Ara7) acts on the vacuolar trafficking pathway in tobacco leaf epidermal cells. *Journal of Cell Science*, *117*(26), 6377–6389. https://doi.org/10.1242/jcs.01564

Koumandou, L., Dacks, J. B., Coulson, R. M., & Field, M. C. (2007). Control

systems for membrane fusion in the ancestral eukaryote; evolution of tethering complexes and SM proteins. *BMC Evolutionary Biology*, *7*(7). https://doi.org/10.1186/1471-2148-7-29

Kwon, S. Il, Cho, H. J., Kim, S. R., & Park, O. K. (2013). The rab GTPase rabG3b positively regulates autophagy and immunity-associated hypersensitive cell death in Arabidopsis. *Plant Physiology*, *161*(4), 1722–1736. https://doi.org/10.1104/pp.112.208108

Lamb, C. A., Nühlen, S., Judith, D., Frith, D., Snijders, A. P., Behrends, C., & Tooze, S. A. (2016). TBC1D14 regulates autophagy via the TRAPP complex and ATG9 traffic. *The EMBO Journal*, *35*(3), 281–301. https://doi.org/10.15252/embj.201592695

Lazar, T., Götte, M., & Gallwitz, D. (1997). Ventricular transport: How many Ypt/Rab GTPases make a eukaryotic cell? *Trends in Biochemical Sciences*, Vol. 22, pp. 468–472. https://doi.org/10.1016/S0968-0004(97)01150-X

Lipatova, Z., Hain, A. U., Nazarko, V. Y., & Segev, N. (2015). Ypt/Rab GTPases: Principles Learned from Yeast. *Critical Reviews in Biochemistry and Molecular Biology*, *50*, 203–211. https://doi.org/10.3109/10409238.2015.1014023

Lipatova, Z., Majumdar, U., & Segev, N. (2016). Trs33-Containing TRAPP IV: A Novel Autophagy-Specific Ypt1 GEF. *Genetics*, *204*, 1117–1128. https://doi.org/10.1534/genetics.116.194910

Luo, Y., Scholl, S., Doering, A., Zhang, Y., Irani, N. G., Di Rubbo, S., … Russinova, E. (2015). V-ATPase activity in the TGN/EE is required for exocytosis and recycling in Arabidopsis. *Nature Plants*, *1*(7), 1–10. https://doi.org/10.1038/nplants.2015.94

Lynch-Day, M. A., Bhandari, D., Menon, S., Huang, J., Cai, H., Bartholomew, C. R., … William Wickner, by T. (2010). Trs85 directs a Ypt1 GEF, TRAPPIII, to the phagophore to promote autophagy. *Proceedings of the National Academy of Sciences*, *107*(17), 7811–7816. https://doi.org/10.1073/pnas.1000063107

Markgraf, D. F., Peplowska, K., & Ungermann, C. (2007). Rab cascades and tethering factors in the endomembrane system. *FEBS Letters*, Vol. 581, pp. 2125–2130. https://doi.org/10.1016/j.febslet.2007.01.090

McFarlane, H. E., Watanabe, Y., Gendre, D., Carruthers, K., Levesque-Tremblay,

G., Haughn, G. W., … Samuels, L. (2013). Cell Wall Polysaccharides are Mislocalized to the Vacuole in echidna Mutants. *Plant and Cell Physiology*, *54*(11), 1867–1880. https://doi.org/10.1093/pcp/pct129

Morozova, N., Liang, Y., Tokarev, A. A., Chen, S. H., Cox, R., Andrejic, J., … Segev, N. (2006). TRAPPII subunits are required for the specificity switch of a Ypt–Rab GEF. *Nature Cell Biology*, *8*(11), 1263–1269. https://doi.org/10.1038/ncb1489

Naramoto, S., Nodzy ski, T., Dainobu, T., Takatsuka, H., Okada, T., Friml, J., & Fukuda, H. (2014). VAN4 Encodes a Putative TRS120 That is Required for Normal Cell Growth and Vein Development in Arabidopsis. *Plant and Cell Physiology*, *55*(4), 750–763. https://doi.org/10.1093/pcp/pcu012

Nguema-Ona, E., Vicré-Gibouin, M., Gotté, M., Plancot, B., Lerouge, P., Bardor, M., & Driouich, A. (2014, October 2). Cell wall O-glycoproteins and N-glycoproteins: Aspects of biosynthesis and function. *Frontiers in Plant Science*, Vol. 5, pp. 1–12. https://doi.org/10.3389/fpls.2014.00499

Normand, G., & King, R. W. (2010). Understanding cytokinesis failure. *Advances in Experimental Medicine and Biology*, *675*, 27–55. https://doi.org/10.1007/978-1-4419-6199-0_3

Novick, P., Medkova, M., Dong, G., Hutagalung, A., Reinisch, K., & Grosshans, B. (2006). Interactions between Rabs, tethers, SNAREs and their regulators in exocytosis. *Biochemical Society Transactions*, *34*(5), 683–686. https://doi.org/10.1042/BST0340683

Olkkonen, V. M., & Stenmark, H. (1997). Role of Rab GTPases in membrane traffic. *International Review of Cytology*, Vol. 176, pp. 1–85. https://doi.org/10.1016/s0074-7696(08)61608-3

Pérez-Pérez, J. M., Candela, H., & Micol, J. L. (2009). Understanding synergy in genetic interactions. *Trends in Genetics*, Vol. 25, pp. 368–376. https://doi.org/10.1016/j.tig.2009.06.004

Pinar, M., Arias-Palomo, E., de los Ríos, V., Arst, H. N., & Peñalva, M. A. (2019). Characterization of Aspergillus nidulans TRAPPs uncovers unprecedented similarities between fungi and metazoans and reveals the modular assembly of TRAPPII. *PLOS Genetics*, *15*(12), e1008557. https://doi.org/10.1371/journal.pgen.1008557

Pinar, M., Arst, H. N., Pantazopoulou, A., Tagua, V. G., De Los Ríos, V., Rodríguez-Salarichs, J., … Peñalva, M. A. (2015). TRAPPII regulates exocytic Golgi exit by mediating nucleotide exchange on the Ypt31 ortholog RabERAB11. *Proceedings of the National Academy of Sciences of the United States of America*, *112*(14), 4346–4351. https://doi.org/10.1073/pnas.1419168112

Pinar, M., & Penãlva, M. A. (2020). En bloc TGN recruitment of Aspergillus TRAPPII reveals TRAPP maturation as unlikely to drive RAB1-to-RAB11 transition. *Journal of Cell Science*, *133*(10). https://doi.org/10.1242/jcs.241141

Qi, X., Kaneda, M., Chen, J., Geitmann, A., & Zheng, H. (2011). A specific role for Arabidopsis TRAPPII in post-Golgi trafficking that is crucial for cytokinesis and cell polarity. *The Plant Journal : For Cell and Molecular Biology*, *68*(2), 234–248. https://doi.org/10.1111/j.1365-313X.2011.04681.x

Qi, X., & Zheng, H. (2011). Arabidopsis TRAPPII is functionally linked to Rab-A, but not Rab-D in polar protein trafficking in trans-Golgi network. *Plant Signaling and Behavior*, *6*(11), 1679–1683. https://doi.org/10.4161/psb.6.11.17915

Ramírez-Peinado, S., Ignashkova, T. I., van Raam, B. J., Baumann, J., Sennott, E. L., Gendarme, M., … Reiling, J. H. (2017). TRAPPC13 modulates autophagy and the response to Golgi stress. *Journal of Cell Science*, *130*(14), 2251–2265. https://doi.org/10.1242/jcs.199521

Ravikumar, R., Kalbfuß, N., Gendre, D., Steiner, A., Altmann, M., Altmann, S., … Assaad, F. F. (2018). Independent yet overlapping pathways ensure the robustness and responsiveness of trans-Golgi network functions in Arabidopsis. *Development*, *145*(21), dev169201. https://doi.org/10.1242/dev.169201

Ravikumar, R., Steiner, A., & Assaad, F. F. (2017). Multisubunit tethering complexes in higher plants. *Current Opinion in Plant Biology*, Vol. 40, pp. 97–105. https://doi.org/10.1016/j.pbi.2017.08.009

Reiling, J. H., Olive, A. J., Sanyal, S., Carette, J. E., Brummelkamp, T. R., Ploegh, H. L., … Sabatini, D. M. (2013). A Creb3–arf4 Signalling Pathway Mediates the Response to Golgi Stress and Susceptibility to Pathogens. *Nature Cell*

Biology, *15*(12), 1473–1485. https://doi.org/10.1038/ncb2865

Riedel, F., Galindo, A., Muschalik, N., & Munro, S. (2018). The two TRAPP complexes of metazoans have distinct roles and act on different Rab GTPases. *Journal of Cell Biology*, *217*(2), 601–617. https://doi.org/10.1083/jcb.201705068

Rosquete, M. R., Davis, D. J., & Drakakaki, G. (2018). The plant trans-golgi network: Not just a matter of distinction. *Plant Physiology*, Vol. 176, pp. 187–198. https://doi.org/10.1104/pp.17.01239

Rosquete, M. R., Worden, N., Ren, G., Sinclair, R. M., Pfleger, S., Salemi, M., … Drakakaki, G. (2019). AtTRAPPC11/ROG2: A role for TRAPPs in maintenance of the plant trans-golgi network/early endosome organization and function. *Plant Cell*, *31*(8), 1879–1898. https://doi.org/10.1105/tpc.19.00110

Rutherford, S., & Moore, I. (2002). The Arabidopsis Rab GTPase family: Another enigma variation. *Current Opinion in Plant Biology*, Vol. 5, pp. 518–528. https://doi.org/10.1016/S1369-5266(02)00307-2

Rybak, K., Steiner, A., Synek, L., Klaeger, S., Kulich, I., Facher, E., … Assaad, F. F. (2014). Plant cytokinesis is orchestrated by the sequential action of the TRAPPII and exocyst tethering complexes. *Developmental Cell*, *29*(5), 607–620. https://doi.org/10.1016/j.devcel.2014.04.029

Sacher, M., Barrowman, J., Schieltz, D., Yates Iii, J. R., & Ferro-Novick, S. (2000). Identification and characterization of five new subunits of TRAPP. *European Journal of Cell Biology*, *79*, 71–80. Retrieved from doi:10.1078/S0171-9335(04)70009-6

Sacher, M., Shahrzad, N., Kamel, H., & Milev, M. P. (2019). TRAPPopathies: An emerging set of disorders linked to variations in the genes encoding transport protein particle (TRAPP)-associated proteins. *Traffic*, Vol. 20. https://doi.org/10.1111/tra.12615

Scrivens, P. J., Noueihed, B., Shahrzad, N., Hul, S., Brunet, S., & Sacher, M. (2011). C4orf41 and TTC-15 are mammalian TRAPP components with a role at an early stage in ER-to-Golgi trafficking. *Molecular Biology of the Cell*, *22*(12), 2083–2093. https://doi.org/10.1091/mbc.E10-11-0873

Segev, N. (2001). Ypt/Rab GTPases: Regulators of Protein Trafficking. *Science*

Signaling, *2001*(100), re11. https://doi.org/10.1126/stke.2001.100.re11

Siniossoglou, S., & Pelham, H. R. B. (2001). An effector of Ypt6p binds the SNARE Tlg1p and mediated selective fusion of vesicles with late Golgi membranes. *The EMBO Journal*, *20*(21), 5991–5998. Retrieved from https://www.ncbi.nlm.nih.gov/pmc/articles/PMC125711/pdf/cde603.pdf

Smertenko, A., Assaad, F., Baluška, F., Bezanilla, M., Buschmann, H., Drakakaki, G., … Žárský, V. (2017). Plant Cytokinesis: Terminology for Structures and Processes. *Trends in Cell Biology*, *27*(12), 885–894. https://doi.org/10.1016/j.tcb.2017.08.008

Söllner, T., Bennett, M. K., Whiteheart, S. W., Scheller, R. H., & Rothman, J. E. (1993). A protein assembly-disassembly pathway in vitro that may correspond to sequential steps of synaptic vesicle docking, activation, and fusion. *Cell*, *75*(3), 409–418. https://doi.org/10.1016/0092-8674(93)90376-2

Steiner, A., Müller, L., Rybak, K., Vodermaier, V., Facher, E., Thellmann, M., … Assaad, F. F. (2016). The Membrane-Associated Sec1/Munc18 KEULE is Required for Phragmoplast Microtubule Reorganization during Cytokinesis in Arabidopsis. *Molecular Plant*, *9*(4), 528–540. https://doi.org/10.1016/j.molp.2015.12.005

Steiner, A., Rybak, K., Altmann, M., McFarlane, H. E., Klaeger, S., Nguyen, N., … Assaad, F. F. (2016). Cell cycle-regulated PLEIADE/AtMAP65-3 links membrane and microtubule dynamics during plant cytokinesis. *The Plant Journal*, *88*(4), 531–541. https://doi.org/10.1111/tpj.13275

Surkont, J., & Pereira-Leal, J. B. (2016). Are There Rab GTPases in Archaea? *Molecular Biology and Evolution*, *33*(7), 1833–1842. https://doi.org/10.1093/molbev/msw061

Sztul, E., & Lupashin, V. (2006). Role of tethering factors in secretory membrane traffic. *American Journal of Physiology - Cell Physiology*, Vol. 290, pp. C11–C26. https://doi.org/10.1152/ajpcell.00293.2005

Tan, D., Cai, Y., Wang, J., Zhang, J., Menon, S., Chou, H. T., … Walz, T. (2013). The EM structure of the TRAPPIII complex leads to the identification of a requirement for COPII vesicles on the macroautophagy pathway. *Proceedings of the National Academy of Sciences of the United States of America*, *110*(48), 19432–19437. https://doi.org/10.1073/pnas.1316356110

Taussig, D., Lipatova, Z., & Segev, N. (2014). Trs20 is required for TRAPP III complex assembly at the PAS and its function in autophagy. *Traffic*, *15*(3), 327–337. https://doi.org/10.1111/tra.12145

Ter Haar, E., Coll, J. T., Austen, D. A., Hsiao, H. M., Swenson, L., & Jain, J. (2001). Structure of GSK3β reveals a primed phosphorylation mechanism. *Nature Structural Biology*, *8*(7), 593–596. https://doi.org/10.1038/89624

Thellmann, M., Rybak, K., Thiele, K., Wanner, G., & Assaad, F. F. (2010). Tethering factors required for cytokinesis in Arabidopsis. *Plant Physiology*, *154*(2), 720–732. https://doi.org/10.1104/pp.110.154286

Thiele, K., Wanner, G., Kindzierski, V., Jürgens, G., Mayer, U., Pachl, F., & Assaad, F. F. (2009). The timely deposition of callose is essential for cytokinesis in Arabidopsis. *Plant Journal*, *58*(1), 13–26. https://doi.org/10.1111/j.1365-313X.2008.03760.x

Thomas, L. L., Joiner, A. M. N., & Fromme, J. C. (2018). The TRA PPI II complex activates the GTPase Ypt1 (Rab1) in the secretory pathway. *Journal of Cell Biology*, *217*(1). https://doi.org/10.1083/jcb.201705214

Thomas, L. L., van der Vegt, S. A., & Fromme, J. C. (2019). A Steric Gating Mechanism Dictates the Substrate Specificity of a Rab-GEF. *Developmental Cell*, *48*(1), 100-114.e9. https://doi.org/10.1016/j.devcel.2018.11.013

Tokarev, A. A., Taussig, D., Sundaram, G., Lipatova, Z., Liang, Y., Mulholland, J. W., & Segev, N. (2009). TRAPP II Complex Assembly Requires Trs33 or Trs65. *Traffic*, *10*(12), 1831–1844. https://doi.org/10.1111/j.1600-0854.2009.00988.x

Ueda, T., Yamaguchi, M., Uchimiya, H., & Nakano, A. (2001). Ara6, a plant-unique novel type Rab GTPase, functions in the endocytic pathway of Arabidopsis thaliana. *EMBO Journal*, *20*(17), 4730–4741. https://doi.org/10.1093/emboj/20.17.4730

Wang, Z. Y., Zhu, J. Y., & Sae-Seaw, J. (2013). Brassinosteroid signaling. *Development*, *140*(8), 1615–1620. https://doi.org/10.1242/dev.060590

Yip, C. K., Berscheminski, J., & Walz, T. (2010). Molecular architecture of the TRAPPII complex and implications for vesicle tethering. *Nature Structural & Molecular Biology*, *17*(11), 1298–1304. https://doi.org/10.1038/nsmb.1914

Zerial, M., & McBride, H. (2001). Rab proteins as membrane organizers. *Nature*

Reviews Molecular Cell Biology, Vol. 2, pp. 107–117. https://doi.org/10.1038/35052055

Zhang, C., Bowzard, J. B., Greene, M., Anido, A., Stearns, K., & Kahn, R. A. (2002). Genetic interactions link ARF1, YPT31/32 and TRS130. *Yeast*, *19*(12), 1075–1086. https://doi.org/10.1002/yea.903

Zhang, J., Chen, J., Wang, L., Zhao, S., Wang, W., Li, J., … Lu, M. (2020). An essential role for Arabidopsis Trs33 in cell growth and organization in plant apical meristems. *Plant Cell Reports*, *39*(3), 381–391. https://doi.org/10.1007/s00299-019-02497-9

Zhao, S., Li, C. M., Luo, X. M., Ka, G., Siu, Y., Gan, W. J., … Yu, S. (2017). Mammalian TRAPPIII Complex positively modulates the recruitment of Sec13/31 onto COPII vesicles. *Scientific Reports*, *7*, 1–12. https://doi.org/10.1038/srep43207

Zhen, Y., & Stenmark, H. (2015). Cellular functions of Rab GTPases at a glance. *Journal of Cell Science*, *128*(17), 3171–3176. https://doi.org/10.1242/jcs.166074

Zheng, H., Camacho, L., Wee, E., Batoko, H., Legen, J., Leaver, C. J., … Moore, I. (2005). A Rab-E GTPase mutant acts downstream of the Rab-D subclass in biosynthetic membrane traffic to the plasma membrane in tobacco leaf epidermis. *Plant Cell*, *17*(7), 2020–2036. https://doi.org/10.1105/tpc.105.031112

Zou, S., Chen, Y., Liu, Y., Segev, N., Yu, S., Liu, Y., … Xie, Z. (2013). Trs130 participates in autophagy through GTPases Ypt31/32 in Saccharomyces cerevisiae. *Traffic*, *14*(2), 233–246. https://doi.org/10.1111/tra.12024

1.